DEPARTMENT OF MECHANICAL ENGINEERING & MECHANICS
COLLEGE OF ENGINEERING & TECHNOLOGY
OLD DOMINION UNIVERSITY
NORFOLK, VIRGINIA 23529

RADIATIVE INTERACTIONS IN CHEMICALLY REACTING SUPERSONIC INTERNAL FLOWS

By

S. N. Tiwari, Principal Investigator

and

R. Chandrasekhar

Progress Report
For the period ended December 31, 1990

Prepared for
National Aeronautics and Space Administration
Langley Research Center
Hampton, Virginia 23665-5225

Under
Research Grant NAG-1-423
Drs. J.P. Drummond and A. Kumar, Technical Monitor
FLDMD-Theoretical Flow Physics Branch

April 1991

Old Dominion University Research Foundation

Old Dominion University Research Foundation is a not-for-profit corporation closely affiliated with Old Dominion University and serves as the University's fiscal and administrative agent for sponsored programs.

Any questions or comments concerning the material contained in this report should be addressed to:

Executive Director
Old Dominion University Research Foundation
P. O. Box 6369
Norfolk, Virginia 23508-0369

Telephone: (804) 683-4293
Fax Number: (804) 683-5290

DEPARTMENT OF MECHANICAL ENGINEERING & MECHANICS
COLLEGE OF ENGINEERING & TECHNOLOGY
OLD DOMINION UNIVERSITY
NORFOLK, VIRGINIA 23529

**RADIATIVE INTERACTIONS IN CHEMICALLY REACTING
SUPERSONIC INTERNAL FLOWS**

By

S. N. Tiwari, Principal Investigator

and

R. Chandrasekhar

Progress Report
For the period ended December 31, 1990

April 1991

FOREWORD

This is a progress report on the research project, "Analysis and Computation of Internal Flow Field in a Scramjet Engine," for the period ended January 14, 1991. Special attention during this period was directed to investigate "Radiative Interactions in Chemically Reacting Supersonic Internal Flows." The work was supported by the NASA Langley Research Center (Theoretical Flow Physics Branch of the Fluid Mechanics Division) through the grant NAG-1-423. The grant was monitored by Drs. J.P. Drummond and A. Kumar of FLDMD-Theoretical Flow Physics Branch.

RADIATIVE INTERACTIONS IN CHEMICALLY REACTING SUPERSONIC INTERNAL FLOWS

S. N. Tiwari and R. Chandrasekhar

Department of Mechanical Engineering and Mechanics

Old Dominion University, Norfolk, VA 23529-0247

ABSTRACT

The two-dimensional, elliptic Navier-Stokes equations are used to investigate supersonic flows with finite-rate chemistry and radiation, for hydrogen-air systems. The chemistry source term in the species equation is treated implicitly to alleviate the stiffness associated with fast reactions. The explicit, unsplit MacCormack finite-difference scheme is used to advance the governing equations in time, until convergence is achieved. The specific problem considered is the premixed flow in a channel with a ten-degree compression ramp. Three different chemistry models are used, accounting for increasing number of reactions and participating species. Two chemistry models assume nitrogen as inert, while the third model accounts for nitrogen reactions and NO_x formation. The tangent slab approximation is used in the radiative flux formulation. A pseudo-gray model is used to represent the absorption-emission characteristics of the participating species. Results obtained for specific conditions indicate that the radiative interactions vary substantially, depending on reactions involving HO_2 and NO species, and that this can have a significant influence on the flowfield.

TABLE OF CONTENTS

NOMENCLATURE

A *band absorptance*, m^{-1}

A_o *band width parameter*, m^{-1}

C_j *concentration of the jth species*, $kg - mole/m^3$

C_p *constant pressure specific heat*, $J/kg - K$

C_o *correlation parameter*, $(N/m^2)^{-1}m^{-1}$

E *total internal energy*

e_ω *Planck's function*

f_j *mass fraction of jth species*

H *total enthalpy*, J/kg

h *static enthalpy*, J/kg

k *thermal conductivity*

k_b *backward rate constant*

k_f *forward rate constant*

P *pressure*, N/m^2

P_j *partial pressure of jth species*

q_R *total radiative flux*

R *gas constant*

S *integrated band intensity*, $(N/m^2)^{-1}m^{-2}$

T *temperature*, K

u, v *velocity in $x -$ and $y -$ directions*, m/s

w_j *production rate of jth species*, $kg/m^3 - s$

x, y *physical coordinates*

γ *ratio of specific heats*

κ_p *Planck mean absorption coefficient*

λ *second coefficient of viscosity, wavelength*

μ *dynamic viscosity*, $kg/m - s$

ξ, η *computational coordinates*

ρ *density*

σ *Stefan − Boltzmann constant*

τ *shear stress*

ϕ *equivalence ratio*

ω *wave number*, m^{-1}

INTRODUCTION

In recent years there has been a renewed interest in the development of a hypersonic transatmospheric aerospace vehicle capable of flying at sub-orbital speeds. A hydrogen-fueled supersonic combustion ramjet (scramjet) engine is a strong candidate for propelling such a vehicle. For a better understanding of the complex flowfield in different regions of the engine, both experimental and computational techniques are employed. Several computer programs have been developed [1–4] and applied to gain more insight into the problem involving the flow in the various sections of the scramjet module.

The combustion of hydrogen and air in the scramjet combustor results in absorbing-emitting gases such as water vapor and hydroxyl radicals. Existence of such gases makes the study of radiation heat transfer an important issue. There are several models available in the literature to represent the absorption-emission characteristics of molecular gases [5–10]. One- and two-dimensional radiative heat transfer equations for various flow and combustion related problems are available [11–19]. In earlier studies [16,18,19], both pseudo-gray and nongray gas models were employed to evaluate radiative heat transfer for chemically reacting supersonic flow. Results of both models were compared and the pseudo-gray model was found to be computationally more efficient.

Considerable work has been carried out in the past decade to model the chemical kinetic mechanism of the hydrogen-air system. A most complete model would involve some 60 reaction paths [20], rendering numerical solution very difficult, if not impossible. A two-step chemistry model, has been used for computing supersonic combustion [4, 16, 18, 19]. This model has only four species and two reaction paths, and is useful for preliminary studies. However, there are several limitations to this model, such as ignition-phase inaccuracy (i.e. a much shorter ignition delay) and also, overprediction of flame temperature and longer reaction times. Recent improvements in this area include a 8–species, 14–reaction model [21] and a 9–species, 18–reaction model [2, 22]. While none of these aforementioned models account

1

for nitrogen reactions (assuming nitrogen as inert), recent developments in this area include a 15–species, 35–reaction model which accounts for NO_x formation and other nitrogen reactions in the hydrogen-air system [22].

The objectives of the present study are to extend the radiative heat transfer formulation used with the global two-step chemistry model [18, 19], to the more complete models namely the 9–species, 18–reaction model as well as the 15–species, 35–reaction model. The effect of radiative heat transfer in both transverse and streamwise directions is investigated. The finite-difference method using the explicit, unsplit MacCormack scheme [23] is used to solve the governing equations.

The flowfield in the combustor is represented by the Navier-Stokes equations and by the appropriate species continuity equations [2, 3]. Incorporation of the finite-rate chemistry models into the fluid dynamic equations can create a set of stiff differential equations. Stiffness is due to a disparity in the time scales of the governing equations. In the time accurate solution, after the fast transients have decayed and the solutions are changing slowly, taking a larger time step is more efficient. But explicit methods still require small time steps to maintain stability. One way around this problem is to use a fully implicit method. However, this requires the inversion of a block multi-diagonal system of algebraic equations, which is also computationally expensive. The use of a semi-implicit technique, suggested by several investigators [24–26], provides an alternative to the above problems. This method treats the source term (which is the cause of the stiffness) implicitly, and solves the remaining terms explicitly.

BASIC GOVERNING EQUATIONS

The physical model for analyzing the flowfield in a supersonic combustor is described by the Navier-Stokes and species continuity equations. For two-dimensional flows, these equations are expressed in physical coordinates as,

$$\frac{\partial U}{\partial t} + \frac{\partial F}{\partial x} + \frac{\partial G}{\partial y} + H = 0 \qquad (1)$$

2

where vectors U, F, G and H are written as,

$$U = \begin{bmatrix} \rho \\ \rho u \\ \rho v \\ \rho E \\ \rho f_j \end{bmatrix}$$

$$F = \begin{bmatrix} \rho u \\ \rho u^2 + p + \tau_{xx} \\ \rho u v + \tau_{xy} \\ (\rho E + p)u + \tau_{xx}u + \tau_{xy}v + q_{cx} + q_{Rx} \\ \rho u f_j - \rho D \frac{\partial f_j}{\partial x} \end{bmatrix}$$

$$G = \begin{bmatrix} \rho v \\ \rho u v + \tau_{yx} \\ \rho v^2 + p + \tau_{yy} \\ (\rho E + p)v + \tau_{xy}v + \tau_{yy}v + q_{cy} + q_{Ry} \\ \rho v f_j - \rho D \frac{\partial f_j}{\partial y} \end{bmatrix}$$

$$H = \begin{bmatrix} 0 \\ 0 \\ 0 \\ 0 \\ -w_j \end{bmatrix}$$

The viscous stress tensors in the F and G terms are given as,

$$\tau_{xx} = -\lambda \left(\frac{\partial u}{\partial x} + \frac{\partial v}{\partial y} \right) - 2\mu \frac{\partial u}{\partial x} \qquad (2a)$$

$$\tau_{xy} = -\mu \left(\frac{\partial u}{\partial x} + \frac{\partial v}{\partial y} \right) \qquad (2b)$$

$$\tau_{yy} = -\lambda \left(\frac{\partial u}{\partial x} + \frac{\partial v}{\partial y} \right) - 2\mu \frac{\partial v}{\partial y} \qquad (2c)$$

where $\lambda = -\frac{2}{3}\mu$. The quantities q_{cx} and q_{cy} in the F and G terms are the components of the conduction heat flux and are expressed as

$$q_{cx} = -k \frac{\partial T}{\partial x}$$
$$q_{cy} = -k \frac{\partial T}{\partial y} \qquad (3)$$

3

The molecular viscosity μ is evaluated from the Sutherland's formula. The total internal energy E in Eq. (2) is given by

$$E = -\frac{P}{\rho} + \frac{u^2 + v^2}{2} + \sum_{j=1}^{m} h_j f_j \tag{4}$$

Specific relations are needed for the chemistry and radiative flux terms. These are discussed in the following sections.

CHEMISTRY AND THERMODYNAMIC MODELS

Chemical reaction rate expressions are usually determined by summing the contributions from each relevant reaction path to obtain the total rate of change of each species. Each path is governed by a law of mass action expression in which the rate constants can be determined from a temperature dependent Arrhenius expression. The reaction mechanism is expressed in a general form as

$$\sum_{j=1}^{ns} \gamma'_{ij} C_j \underset{k_{b_i}}{\overset{k_{f_i}}{\rightleftharpoons}} \sum_{j=1}^{ns} \gamma''_{ij} C_j \quad , \quad i = 1, nr \tag{5}$$

where ns = number of species and nr = number of reactions. The chemistry source terms w_j in Eq. (1) are obtained, on a mass basis, by multiplying the molar changes and corresponding molecular weight as

$$w_j = M_j C_j = M_j \sum_{i=1}^{nr} \left(\gamma''_{ij} - \gamma'_{ij} \right) \left[k_{f_i} \prod_{m=1}^{ns} C_m^{\gamma'_{im}} \right]$$
$$\left[- k_{b_i} \prod_{m=1}^{ns} C_m^{\gamma''_{im}} \right] \quad , \quad j = 1, ns \tag{6}$$

The reaction rate constants $k_{f\,i}$ and $k_{b\,i}$ appearing in Eqs. (5) and (6) are determined from an Arrhenius rate expression as

$$k_{f_i} = A_i T^{N_i} exp\left(-\frac{E_i}{RT}\right) \tag{7}$$

where ,

$$k_{b_i} = \frac{k_{f_i}}{k_{eq_i}} \tag{8}$$

$$k_{eq_i} = \left(\frac{1}{RT}\right)^{\Delta n} exp\left(\frac{-\Delta G_{R_i}}{RT}\right) \tag{9}$$

The coefficients A , N and E appearing in Eq. (7) are given in Table 1. The term Δn in Eq. (9) denotes the difference in the number of moles of reactants and products.

The Gibbs energy term in Eq. (9) is calculated as

$$\Delta G_{R_i} = \sum_{j=1}^{ns} \gamma_{ij}'' g_i - \sum_{j=1}^{ns} \gamma_{ij}' g_i \ , \quad j = 1, nr \tag{10}$$

$$\begin{aligned} \frac{g_j}{R} = & A_j(T - lnT) + \frac{B_j}{2}T^2 + \frac{C_j}{6}T^3 \\ & + \frac{D_j}{12}T^4 + \frac{E_j}{20}T^5 + F_j + G_j T \end{aligned} \tag{11}$$

The gas constant for the mixture is evaluated by a mass-weighted summation over all species as

$$\overline{R} = \sum_{j=1} f_j R_j \tag{12}$$

$$P = \rho \overline{R} T \tag{13}$$

RADIATION TRANSFER MODEL

Evaluation of the energy equation presented in Eq. (1) requires an appropriate expression for the radiative flux term, q_R . Therefore, a suitable radiative transport model is needed.

Various models are available in the literature to represent the absorption-emission characteristics of the molecular species [10]. The equations of radiative transport are expressed generally in integro-differential forms. The integration involves both the frequency spectrum and physical coordinates. In many realistic three-dimensional physical problems, the complexity of the radiative transport equations can be reduced by introduction of the tangent-slab approximation. This approximation treats the gas layer as a one-dimensional slab in evaluation of the radiative flux (Fig. 1).

Detailed derivations of radiative flux equations for gray as well as nongray radiation have been carried out previously [15, 19]. For a multiband gaseous system, the nongray radiative flux in the normal direction is expressed as

$$
q_R(y) = e_1 - e_2 + \sum_{i=1}^{n} A_{oi} \{ \int_0^y \left[\frac{de_{\omega_i}(z)}{dz} \right] \times
$$

$$
\bar{A}_i \left[\frac{3}{2} \frac{u_{oi}}{L} (y - z) \right] dz +
$$

$$
+ \int_y^L \left[\frac{de_{\omega_i}(z)}{dz} \right] \bar{A}_i \left[\frac{3}{2} \frac{u_{0i}}{L} (z - y) \right] dz \}
$$

(14)

The information on the band absorptance $\bar{A}_i$ and other quantities is available in the cited references.

For a gray medium, the spectral absorption coefficient κ_ω is independent of the wave number, and an expression for the radiative flux is obtained as [5, 16, 19]

$$
q_R(y) = e_1 - e_2 + \frac{3}{2} \{ \int_0^y [e(z) - e_1] e^{-\frac{3\kappa(y-z)}{2}} \kappa dz
$$

$$
- \int_y^L [e(z) - e_2] e^{-\frac{3\kappa(y-z)}{2}} \kappa dz \}
$$

(15)

It is computationally more efficient to use Eq. (15) in the general energy equation than Eq. (14). This is because by differentiating Eq. (15) twice (using the Leibnitz formula) the integrals are eliminated and the following inhomogenous ordinary differential equation is obtained :

6

$$\frac{1}{\kappa^2}\frac{d^2 q_R(y)}{dy^2} - \frac{9}{4}q_R(y) = \frac{3}{\kappa}\frac{de(y)}{dy} \tag{16}$$

The solution of Eq. (16) requires two boundary conditions which are given for non-black diffuse surfaces as [5]

$$\left(\frac{1}{\epsilon_1} - \frac{1}{2}\right)[q_R(y)]_{y=0} - \frac{1}{3\kappa}\left[\frac{dq_R}{dy}\right]_{y=0} = 0 \tag{17a}$$

$$\left(\frac{1}{\epsilon_2} - \frac{1}{2}\right)[q_R(y)]_{y=L} + \frac{1}{3\kappa}\left[\frac{dq_R}{dy}\right]_{y=L} = 0 \tag{17b}$$

For black surfaces $\epsilon_1 = \epsilon_2 = 1$ and Eqs. (17) reduce to simpler forms.

An appropriate model for a gray gas absorption coefficient is required in Eqs. (15) — (17). This is represented by the Planck mean absorption coefficient, which is expressed for a multi-band system as [5, 19]

$$\kappa = \kappa_P = \frac{P_j}{\sigma T^4(y)}\sum_{i=1}^{n} e_{\omega_i}(T)S_i(T) \tag{18}$$

It should be noted that κ_P is a function of the temperature and the partial pressures P_j of the species.

METHOD OF SOLUTION

The governing equations are transformed from the physical domain (x , y) to a computational domain (ξ , η), using an algebraic grid generation technique similar to the one used by Smith and Weigel [27]. In the computational domain, Eq. (1) is expressed as

$$\frac{\partial \widehat{U}}{\partial t} + \frac{\partial \widehat{F}}{\partial \xi} + \frac{\partial \widehat{G}}{\partial \eta} + \widehat{H} = 0 \tag{19}$$

where

$$\widehat{U} = UJ , \quad \widehat{F} = Fy_\eta - Gx_\eta$$

$$\widehat{G} = Gx_\xi - Fy_\xi , \quad \widehat{H} = HJ \tag{20}$$

$$J = x_\xi y_\eta - y_\xi x_\eta$$

Once the temporal discretization has been performed, the resulting system is spatially differenced using the explicit, unsplit MacCormack predictor-corrector scheme [23]. This results in a spatially and temporally discrete, simultaneous system of equations at each grid point [25, 26]. Each simultaneous system is solved, subject to initial and boundary conditions, by using the Householder technique [28, 29]. At the supersonic inflow boundary, all flow quantities are specified as freestream conditions. At the supersonic outflow boundary, non-reflective boundary conditions are used, i.e. all flow quantities are extrapolated from interior grid points. The upper and lower boundaries are treated as solid walls. This implies a non-slip boundary condition (i.e. zero velocities). The wall temperature and pressure are extrapolated from interior grid points. Initial conditions are obtained by specifying freestream conditions throughout the flowfield. The resulting set of equations is marched in time, until convergence is achieved. The details of the radiative flux formulation and method of solution are available in [19].

RESULTS AND DISCUSSION

Based on the theory and computational procedures described previously, an algorithm has been developed to solve the two-dimensional Navier-Stokes equations for chemically reacting and radiating supersonic flows. The extent of radiative heat transfer in supersonic flows undergoing hydrogen-air chemical reactions, has been investigated using three chemical kinetics models, accounting for increasing number of reactions and participating species. For the temperature range considered in this study, the important radiating species are OH, NO and H_2O. The gray gas formulations are based on the Planck mean absorption coefficient which accounts for the detailed information on different molecular bands. The radiative fluxes have been computed using this 'pseudo-gray' formulation. The justification for using this model is provided in [19]. Important results for radiative effects of participating species and of chemical interactions were presented at the 29th Aerospace Sciences Meeting in Reno, Nevada, January 7–10, 1991 (AIAA Papers 91–0373 and 91–0572). These are provided in this report as Appendices A and B.

The specific problem considered is the supersonic flow of premixed hydrogen and air (stoichiometric equivalence ratio $\phi = 1.0$) in a channel with a compression corner on the lower boundary (Fig. 2). The physical dimensions considered for obtaining results are $L = 2$ cm., $X_1 = 1$cm., $X_2 = 2$cm., $L_X = X_1 + X_2 = 3$ cm. , and $\alpha = 10$ degrees . The flow is ignited by the shock from the compression corner. The inlet conditions which are representative of scramjet operating conditions, are $P_{oo} = 1.0$ atm., $T_{oo} = 900$ K and $M_{oo} = 4.0$. This same flow has been computed by several CFD research groups [4, 18, 19, 21] as a benchmark case.

Figures 3–7 show the computed results using a 31×31 grid , for temperature and pressure as well as H_2O and OH species mass fractions. Figure 3 shows the flowfield contours for temperature and pressure for the non-reacting (cold) case.The oblique shock is seen to arise from the compression corner at the lower wall. The hottest regions in the flowfield are in the upper and lower boundary layers. Figures 4 and 5 show the effect of the three chemistry models on the temperature and pressure profiles, varying along x at the location $y = 0.02$ cm from the lower wall (boundary layer region). The temperatures in the boundary layer show a gradual increase(Fig. 4). The pressure profiles are plotted at $y = 0.13$ cm. (inviscid region) and show a sharp increase due to the shock (Fig. 5). The ignition-phase inaccuracies of the three chemistry models can be seen in Figs. 6 and 7. The shock is occurring after $x / L_X = 0.3$. However, the 2–step model predicts ignition before the shock (shorter ignition delay) due to the high temperature in the boundary layer. On the other hand, the 18–step model predicts a longer ignition delay, at $x / L_X = 0.37$ (Fig. 6). The 35–step model's prediction of ignition delay appears to be an average of the other two models. Although the three models do not differ much in prediction of temperature and pressure profiles, they do differ significantly in predictions of species productions (Figs. 6, 7).

In order to resolve this discrepancy, a grid sensitivity study was carried out to examine whether the grid size affects the flow predictions. The results of three grid distributions 11×31 , 31×31 and 61×31 are shown in Fig. 8, and it appears that the 31×31 grid is

sufficient for the present study.

The reason for the varying predictions of species production by the three models was further examined and the results are shown in Figs. 9 and 10. Figure 9 shows that the Reaction No. 8 in Table 1 is critical in determining the extent of chemical heat release and H_2O production. Reaction No. 8 deals with production of HO_2 radical. This reaction is absent from the 2–step model, while it is common to both the 18–step and 35–step models. Figure 9 shows that the 35–step model experiences nearly a 30% drop in temperature at the channel exit, when the rate of Reaction No. 8 is reduced by a factor of 1000 (effectively cutting off the production of the HO_2 radical). In contrast, the 18–step model shows a 15% drop in temperature, when subjected to the same reduction in rate of Reaction No. 8. This shows that the Reaction No. 8 controls the overall H_2O production occurring in Reaction Nos. 9–18 (Table 1). Due to the high temperatures ($\tilde{} $ 3000 K) in the flowfield, there is a pool of highly reactive free radicals like H , O, etc. The HO_2 radical is converted to the very reactive OH radical, by the free radicals (Reaction Nos. 11 and 12). This establishes the HO_2 radical as a very important species in promoting flame propagation in hydrogen-air flames. A similar study has been carried out in [30]. Since the 2–step model does not have the HO_2 radical, it predicts lesser amounts of OH and H_2O.

It was necessary to determine the reason for the higher sensitivity of the 35–step model to the HO_2 radical, as compared to the 18–step model. Figure 10 shows that the Reaction Nos. 21 and 23 in Table 1 are critical in determining the extent of chemical heat release and H_2O production. Reaction Nos. 21 and 23 deal with production of the NO radical. These reactions are absent from the 2–step and 18–step models, whereas they play an important role in the 35–step model. Figure 10 shows that the 35–step model undergoes a 30% reduction in temperature, when the rates of Reaction Nos. 21 and 23 are reduced by a factor of 1000 (effectively cutting off the production of the NO radical). This is nearly the same reduction caused by reducing the rate of Reaction No. 8 by a factor of 1000. Due to the high temperatures in the flowfield, the usually inert nitrogen dissociates into the highly reactive N free radical. This free radical N is then

10

oxidized in Reaction Nos. 21 and 23, thereby producing the NO radical. This NO radical converts the HO_2 radical into the highly reactive OH radical, through Reaction No. 29. This confirms that the NO radical is a very important species for flame propagation in a hydrogen-fueled supersonic combustor. Since the 35–step model has the NO radical, it predicts higher amounts of OH and H_2O than the 18–step model.

Figures 11–13 describe flowfield contours affected by exothermic chemical reactions. Comparison of Figs. 3a and 11 shows that the boundary layer on the lower wall is considerably thickened due to the heat release from chemical reaction. Figures 3b and 12 show that the chemical reaction in the boundary layer causes the shock to get curved upwards, thereby increasing the shock strength. In the case of the 35–step model (Fig. 12b), two weak shocks arise from the channel entrance region. These could be responsible for some of the flow instabilities observed in the figures. Figure 13 shows the computed H_2O flame structure for the 2–step and 35–step models. The 35–step flame(Fig. 13b) appears to be stronger and undergoes a quenching effect (discontinuity in the flame sheet) which is not observed in the 2–step flame.

Based on the above understanding of the chemical kinetics of supersonic hydrogen-air flames, the radiative interactions were examined. Figure 14 shows the profiles of the normalized streamwise radiative flux q_{Rx} predicted by the three chemistry models, along the location y = 0.02 cm. from the lower wall. The q_{Rx} flux reduces towards the end of the channel due to cancellation of fluxes in positive and negative directions. It is seen from Fig. 14 that the 18–step and 35–step models predict significantly higher amounts (50% more and 100% more , respectively) of q_{Rx} than the 2-step model. This is because radiative heat tranfer is a strong function of temperature, pressure and species concentrations. So the larger values of radiative fluxes are caused by higher amounts of H_2O concentrations, which in turn, depend on reactions involving HO_2 and NO species. Figure 15 shows the variations of the normal radiative flux q_{Ry} along x , at the location y = 0.02 cm. These do not appear to vary significantly between the three chemistry models. However, in all three cases, the q_{Ry} value increases rapidly after

the shock.

Figures 16–19 show the computed results for reacting flows with and without radiation, for the three chemistry models. It is seen from that the 2–step model shows only slight effect of radiative interaction, as compared to the 18–step and 35–step models. The 18–step and 35–step models predict lower temperature and lower H_2O and OH concentrations after the shock. This is because of the q_{Rx} flux, which reduces the total energy. For reacting flows without radiation, it was seen from Figs. 6 and 7 that the 18–step model had a longer ignition delay (ignition at $x / L_X = 0.37$), while the 35–step model had a shorter ignition delay (ignition at $x / L_X = 0.27$). Another effect of radiative interactions, seen in Fig. 18, is to nullify this difference in predictions of ignition delay. For both 18–step and 35–step models, with radiation, the ignition is seen to occur at the same point, $x / L_X = 0.33$. No such effect is seen on the ignition characteristics of the 2–step model.

Comparison of results in Figs. 16–19 shows that the 35–step model exhibits stronger effect of radiative interactions, than the other two models. Accordingly, Figs. 20–22 show flowfield contours affected by the 35–step chemistry model, as well as by radiation. It can be seen from Figs. 11b and 20 that the effect of radiation is to lower the temperature after the shock (cooling effect). Figures 12b and 21 show another effect of radiation — elimination of the two weak shocks arising from the channel entrance. This is understood from Fig. 14, where the q_{Rx} radiative flux is higher in the upstream region of the flow. Figures 13b and 22 show that the radiative interactions enable the development of a continuous flame sheet, wherein the flame quenching effect observed in Fig. 13b is nullified.

CONCLUSIONS

The two-dimensional, spatially elliptic Navier-Stokes equations have been used to obtain solutions for supersonic flows undergoing finite-rate chemical reactions along with radiative interactions. The specific problem considered is of the premixed flow in a channel with a ten-

12

degree compression ramp. The inlet conditions used in the present study correspond to typical flow conditions of a scramjet engine. Three different chemistry models were used for parametric studies, accounting for increasing number of reactions and participating species. It is seen that the radiative interactions vary significantly, depending particularly on chemical reactions involving HO_2 and NO species. These reactions have a substantial effect on the flowfield, with regard to H_2O concentration , temperature and pressure. Also, it is observed that the difference in the ignition delays of two chemistry models invoving HO_2 reactions is nullified as a result of radiative interaction. The results also show that the streamwise radiative flux reduces the temperature and concentration of species. This effect is a strong function of the amount of H_2O species concentration.

REFERENCES

1. Kumar, A., "Numerical Simulation of Scramjet Inlet Flowfield," NASA TP-25117, May 1986.

2. Drummond, J. P., Hussaini, M. Y. and Zang, T. A., "Spectral Methods for Modelling Supersonic Chemically Reacting Flowfields,"AIAA Journal , Vol. 24, No. 9, September 1986, pp. 1461–1467 ; also Drummond, J. P., "Numerical Simulation of Supersonic Chemically Reacting Mixing Layers," Ph.D. Dissertation, George Washington University, May 1987.

3. Drummond, J. P., Rogers, R. C. and Hussaini, M. Y., "A Detailed Numerical Model of a Supersonic Reacting Mixing Layer," AIAA Paper No. 86–1427, June 1986.

4. Chitsomboon, T., Kumar, A., Drummond, J. P. and Tiwari, S. N., "Numerical Study of Supersonic Combustion Using a Finite-Rate Chemistry Model," AIAA Paper 86–0309, January 1986.

5. Sparrow, E. M. and Cess, R. D., "Radiation Heat Transfer," Brooks/Cole, Belmont, CA, 1966 and 1970. New Augmented Edition, Hemisphere Publ. Corp. Washington, D.C., 1978.

6. Tien, C. L., "Thermal Radiation Properties of Gases," Advances in Heat Transfer, Vol. 5,

Academic Press, New York, 1968.

7. Cess, R. D. and Tiwari, S. N., "Infrared Radiative Energy Transfer in Gases," Advances in Heat Transfer, Vol. 8, Academic Press, New York, 1972.

8. Edwards, D. K., "Molecular Gas Band Radiation," Advances in Heat Transfer, Vol. 12, Academic Press, New York, 1976.

9. Tiwari, S. N., "Band Models and Correlations for Infrared Radiation," Radiative Transfer and Thermal Control (Progress in Aeronautics and Astronautics, Vol. 49), American Institute of Aeronautics and Astronautics, New York, 1979.

10. Tiwari, S. N., "Models for Infrared Atmospheric Radiation," Advances in Geophysics, Vol. 20, Academic Press, New York, 1978, pp. 1–85.

11. Tsai, S.S. and Chan, S. H., "Multi-Dimensional Radiative Transfer in Non-Gray Gases-General Formulation and the Bulk Radiative Exchange Approximation," Journal of Heat Transfer, Vol. 100, August 1978.

12. Chung, T.J. and Kim, J. Y., "Two-Dimensional Combined Mode Heat Transfer by Conduction, Convection and Radiation in Emitting, Absorbing and Scattering Media-Solution By Finite Elements," Journal of Heat Transfer, Vol. 106, pp. 448–452, May 1984.

13. Im, K.H. Ahluwalia, R. K., "Combined Convection and Radiation in Rectangular Duct," International Journal of Heat and Mass Transfer, Vol. 27, pp. 221–231, 1984.

14. Soufiani, A. and Taine, J., "Application of Statistical Narrow-Band Models to Coupled Radiation and Convection at High Temperature," International Journal of Heat and Mass Transfer, Vol. 30, No. 3, pp. 437–447, 1987.

15. Tiwari, S. N., "Radiative Interaction in Transient Energy Transfer in Gaseous Systems," NASA CR-176644, December 1985.

16. Mani, M., Tiwari, S. N. and Drummond, J. P., "Numerical Solution of Chemically Reacting and Radiating Flows," AIAA Paper 87–0324, January, 1987.

17. Tiwari, S. N. and Singh, D. J., "Interaction of Transient Radiation in Fully Developed Lam-

inar Flow," AIAA Paper 86–1521, June 1987.

18. Mani, M., Tiwari, S. N. and Drummond, J. P., "Investigation of Two-Dimensional Chemically Reacting and Radiative Supersonic Channel Flows," AIAA Paper 88–0462, January 1988.

19. Mani, M. and Tiwari, S. N., "Investigation of Supersonic Chemically Reacting and Radiating Channel Flow," NASA CR-182726, January 1988 ; also Ph.D. Dissertation by M. Mani, Old Dominion University, May 1988.

20. Rogers, R. C. and Shnexnayder, C. J., Jr., "Chemical Kinetic Analysis of Hydrogen-Air Ignition and reaction Time," NASA TP-1856, 1981.

21. Shuen, S. J. and Yoon, S., "Numerical Study of Chemically Reacting Flows Using a Lower-Upper Symmetric Successive Overrelaxation Scheme," AIAA Journal , Vol. 27, No. 12, December 1989.

22. Carpenter, M. H., "A Generalized Chemistry Version of SPARK," NASA CR-4196, December 1988.

23. MacCormack, R. W., "The Effect of Viscosity in Hypervelocity Impact Cratering," AIAA Paper 69–354, May, 1969.

24. Smoot, L. D., Hecker, W. C. and Williams, G. A., "Prediction of Propagating Methane-Air Flames," Combustion and Flame , Vol. 26, 1976.

25. Stalnaker, J. F., Robinson, M. A., Spradley, L. W., Kurzius, S. C. and Theores, D., "Development of the General Interpolants Methods for the CYBER 200 series of Computers," Report TR-0867354, Lockheed-Huntsville Research Engg. Center, Huntsville, Alabama, October 1983.

26. Bussing, T. R. and Murman, E. M., "A Finite Volume Method for the Calculation of Compressible Chemically Reacting Flows," AIAA Paper 85–0331, January 1985.

27. Smith, R. E. and Weigel, B. L., "Analytical and Approximation Boundary Fitted Coordinates System for Fluid Flow Simulation," AIAA Paper 80–0192, January 1980.

28. Wilkins, J. H., The Algebraic Eigenvalue Problem , Oxford University Press, Oxford, England, 1965, pp. 233–236.

29. Householder, A. S., The Theory of Matrices in Numerical Solution Analysis , Dover Publication, New York, 1964, pp. 122–140.

30. Jachimowski, C. J., "An Analytical Study of the Hydrogen-Air Reaction Mechanism with Application to Scramjet Combustion," NASA TP-2791, February 1988.

Table 1. Hydrogen-Air Combustion Mechanism [22]

REACTION	A(moles)	N(cm³)	E(calories/gm-mole)

** following reactions constitute the 18-step model **

REACTION	A(moles)	N(cm³)	E(calories/gm-mole)
(1) $O_2 + H_2 \leftrightarrow OH + OH$	1.70×10^{13}	0	48150
(2) $O_2 + H \leftrightarrow OH + O$	1.42×10^{14}	0	16400
(3) $H_2 + OH \leftrightarrow H_2O + H$	3.16×10^{7}	1.8	3030
(4) $H_2 + O \leftrightarrow OH + H$	2.07×10^{14}	0	13750
(5) $OH + OH \leftrightarrow H_2O + O$	5.50×10^{13}	0	7000
(6) $H + OH + M \leftrightarrow H_2O + M$	2.21×10^{22}	—2.0	0
(7) $H + H + M \leftrightarrow H_2 + M$	6.53×10^{17}	—1.0	0
(8) $H + O_2 + M \leftrightarrow HO_2 + M$	3.20×10^{18}	—1.0	0
(9) $OH + HO_2 \leftrightarrow O_2 + H_2O$	5.00×10^{13}	0	1000
(10) $H + HO_2 \leftrightarrow H_2 + O_2$	2.53×10^{13}	0	700
(11) $H + HO_2 \leftrightarrow OH + OH$	1.99×10^{14}	0	1800
(12) $O + HO_2 \leftrightarrow O_2 + OH$	5.00×10^{13}	0	1000
(13) $HO_2 + HO_2 \leftrightarrow O_2 + H_2O_2$	1.99×10^{12}	0	0
(14) $H_2 + HO_2 \leftrightarrow H + H_2O_2$	3.01×10^{11}	0	18700
(15) $OH + H_2O_2 \leftrightarrow H_2O + HO_2$	1.02×10^{13}	0	1900
(16) $H + H_2O_2 \leftrightarrow H_2O + OH$	5.00×10^{14}	0	10000
(17) $O + H_2O_2 \leftrightarrow OH + HO_2$	1.99×10^{13}	0	5900
(18) $H_2O_2 + M \leftrightarrow OH + OH + M$	1.21×10^{17}	0	45500

** remaining reactions complete the 35-step model **

REACTION	A(moles)	N(cm³)	E(calories/gm-mole)
(19) $O_2 + M \leftrightarrow O + O + M$	2.75×10^{19}	—1.0	118700
(20) $N_2 + M \leftrightarrow N + N + M$	3.70×10^{21}	—1.6	225000
(21) $N + O_2 \leftrightarrow O + NO$	6.40×10^{9}	1.0	6300
(22) $N + NO \leftrightarrow O + N_2$	1.60×10^{13}	0	0
(23) $N + OH \leftrightarrow H + NO$	6.30×10^{11}	0.5	0
(24) $H + NO + M \leftrightarrow HNO + M$	5.40×10^{15}	0	—600
(25) $H + HNO \leftrightarrow H_2 + NO$	4.80×10^{12}	0	0
(26) $O + HNO \leftrightarrow OH + NO$	5.00×10^{11}	0.5	0
(27) $OH + HNO \leftrightarrow H_2O + NO$	3.60×10^{13}	0	0
(28) $HO_2 + HNO \leftrightarrow H_2O_2 + NO$	2.00×10^{12}	0	0
(29) $HO_2 + NO \leftrightarrow OH + NO_2$	3.43×10^{12}	0	—260
(30) $H + NO_2 \leftrightarrow OH + NO$	3.50×10^{14}	0	1500
(31) $O + NO_2 \leftrightarrow O_2 + NO$	1.00×10^{13}	0	600
(32) $NO_2 + M \leftrightarrow O + NO + M$	1.16×10^{16}	0	66000
(33) $M + OH + NO \leftrightarrow HNO_2 + M$	5.60×10^{15}	0	—1700
(34) $M + OH + NO_2 \leftrightarrow HNO_3 + M$	3.00×10^{15}	0	—3800
(35) $OH + HNO_2 \leftrightarrow H_2O + NO_2$	1.60×10^{12}	0	0

** following reactions constitute the global 2-step model [4, 16, 18, 19] **

REACTION	A(moles)	N(cm³)	E(calories/gm-mole)
(1") $H_2 + O_2 \leftrightarrow 2 OH$	11.4×10^{47}	—10.0	4865
(2") $2 OH + H_2 \leftrightarrow 2 H_2O$	2.50×10^{44}	—13.0	42500

Fig. 1   Plane radiating layer between parallel boundaries

Fig. 2 Geometry for the premixed H_2—Air reacting flow

$\alpha = 10°$
$L = 2$ cm
$L_x = 3$ cm
$X_1 = 1$cm
$X_2 = 2$cm

$M = 4$
$T = 900$ K
$P = 1$ atm

19

Level	T (K)
F	2344.
E	2244.
D	2144.
C	2043.
B	1943.
A	1842.
9	1742.
8	1642.
7	1541.
6	1441.
5	1341.
4	1240.
3	1140.
2	1040.
1	939.7

Fig. 3a   Temperature contours for non-reacting (cold) case

Level	P (Pa)
F	26565
E	25274
D	23983
C	22693
B	21402
A	20111
9	18820
8	17529
7	16238
6	14947
5	13656
4	12366
3	11075
2	97843
1	84935
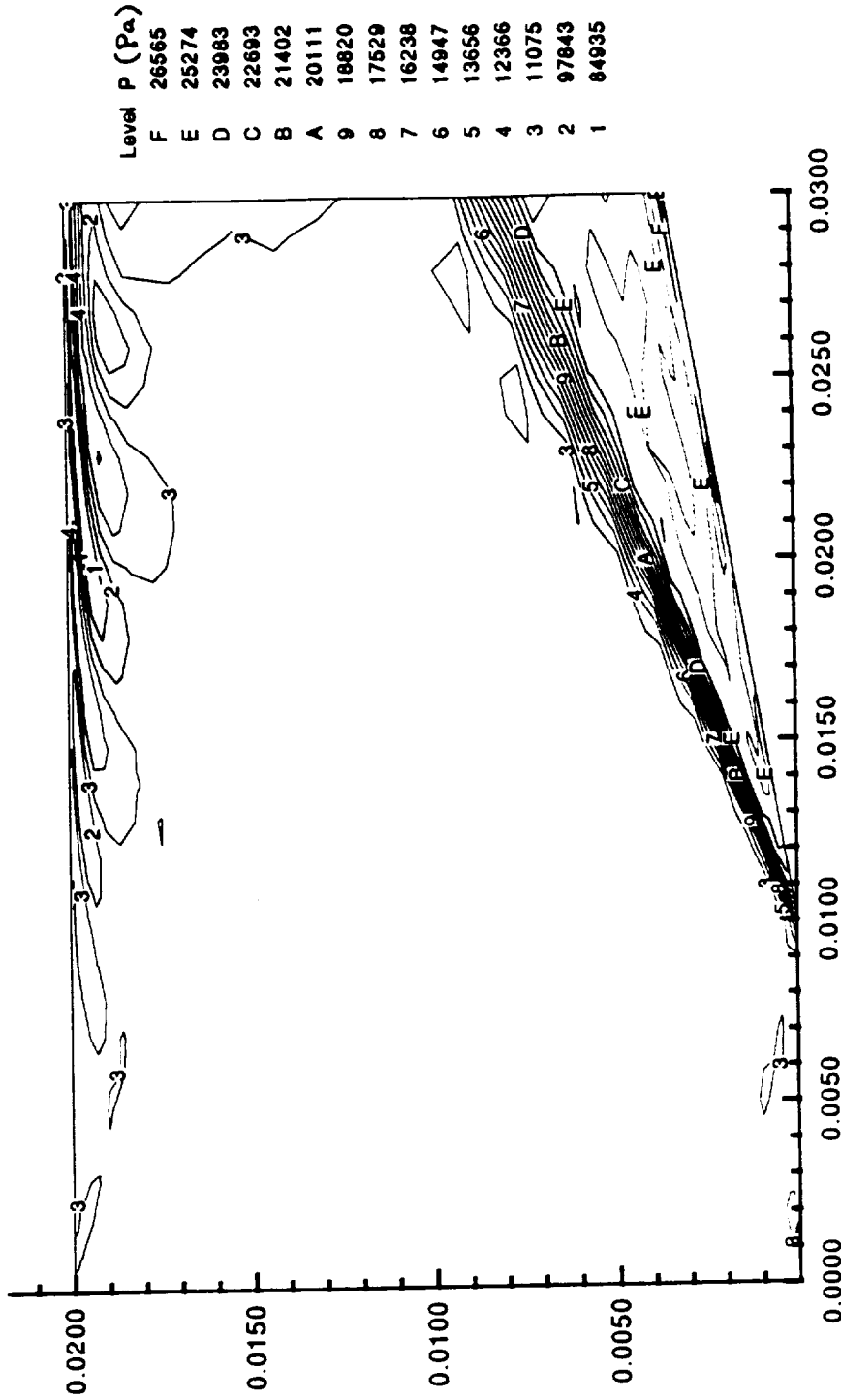
Fig. 3b   Pressure contours for non-reacting (cold) case

21
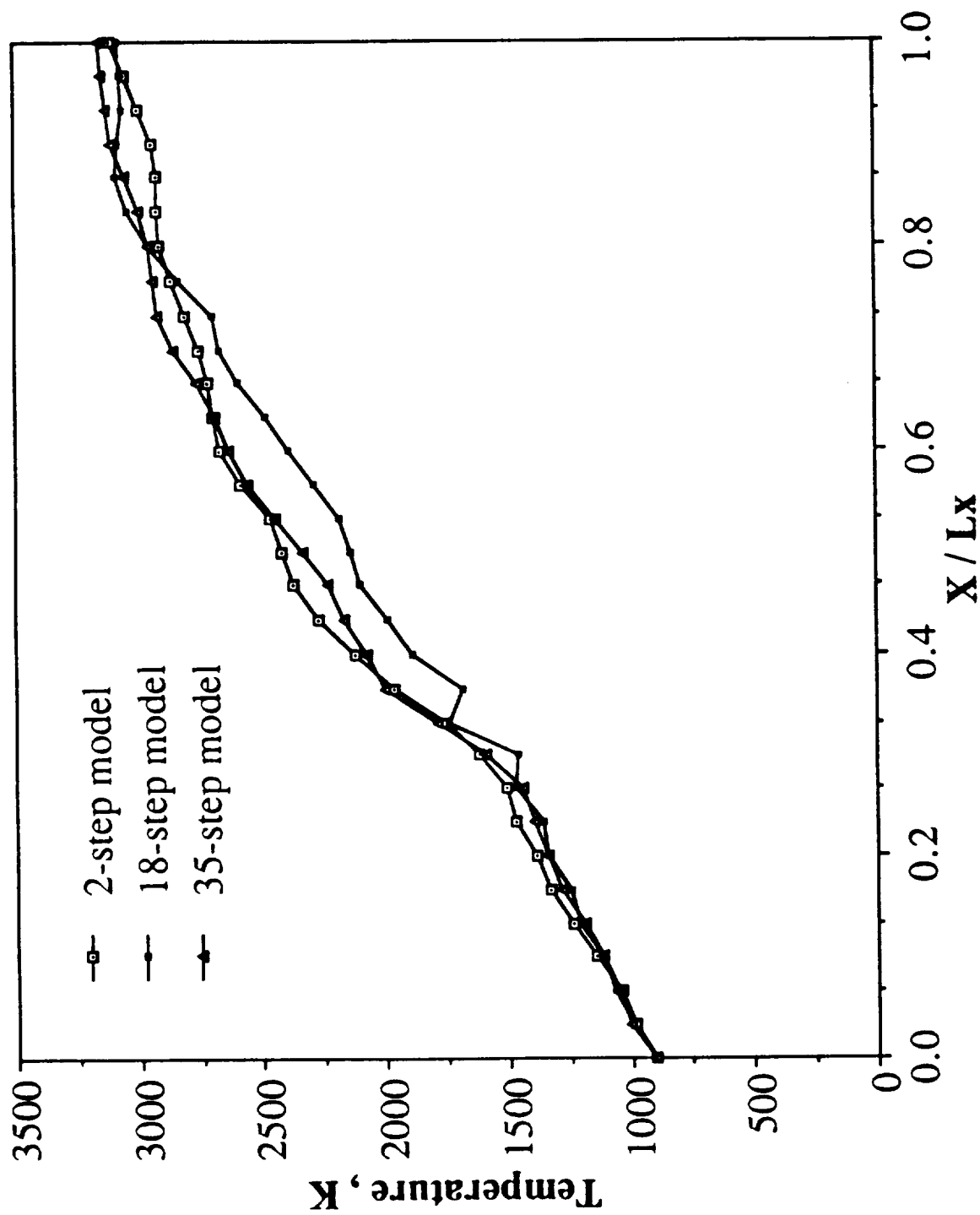
Fig. 4 Temperature profiles (y = 0.02 cm.)

22
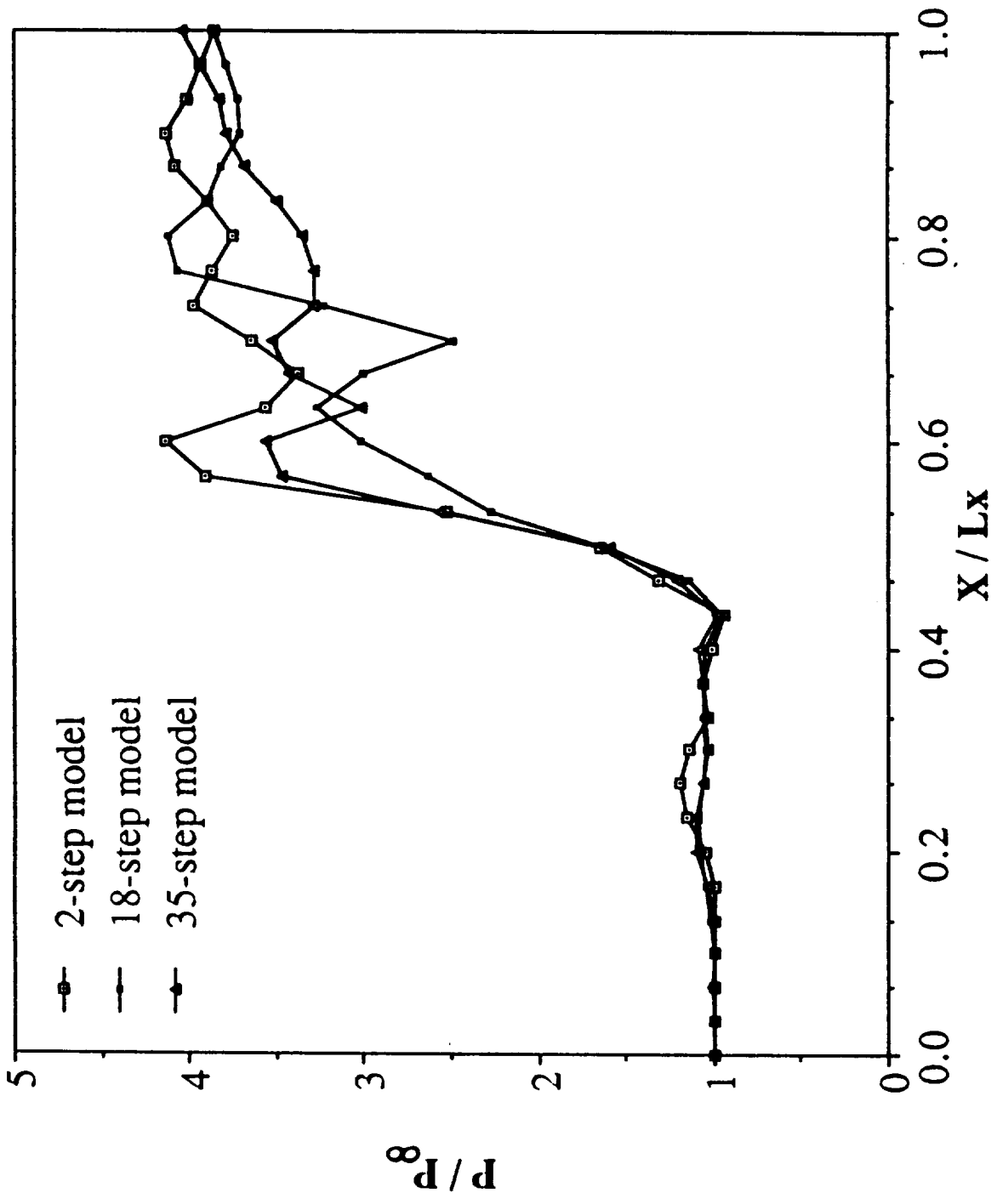
Fig. 5   Pressure profiles (y = 0.13 cm.)
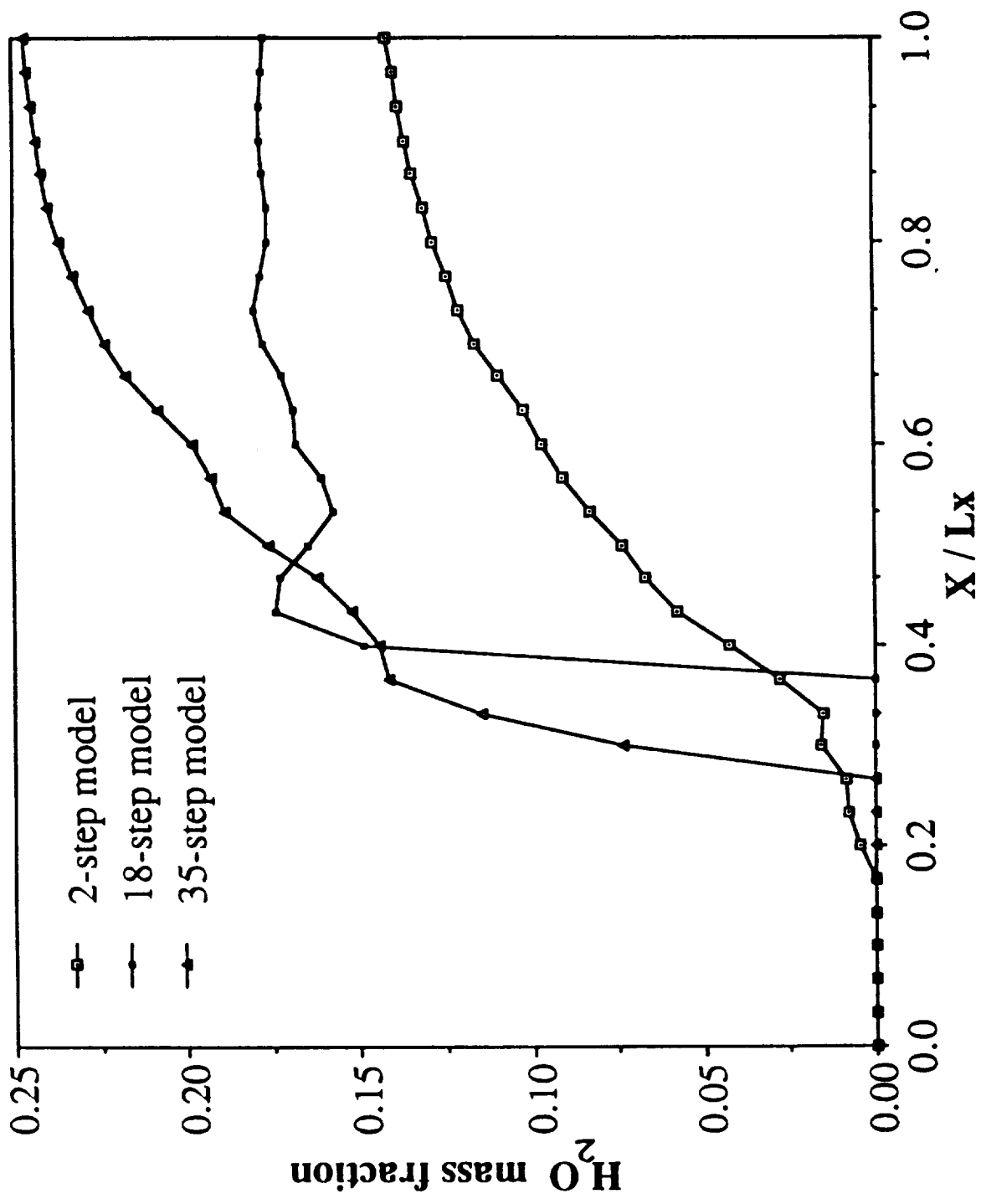
Fig. 6 H_2O mass fraction profiles (y = 0.02 cm.)

24
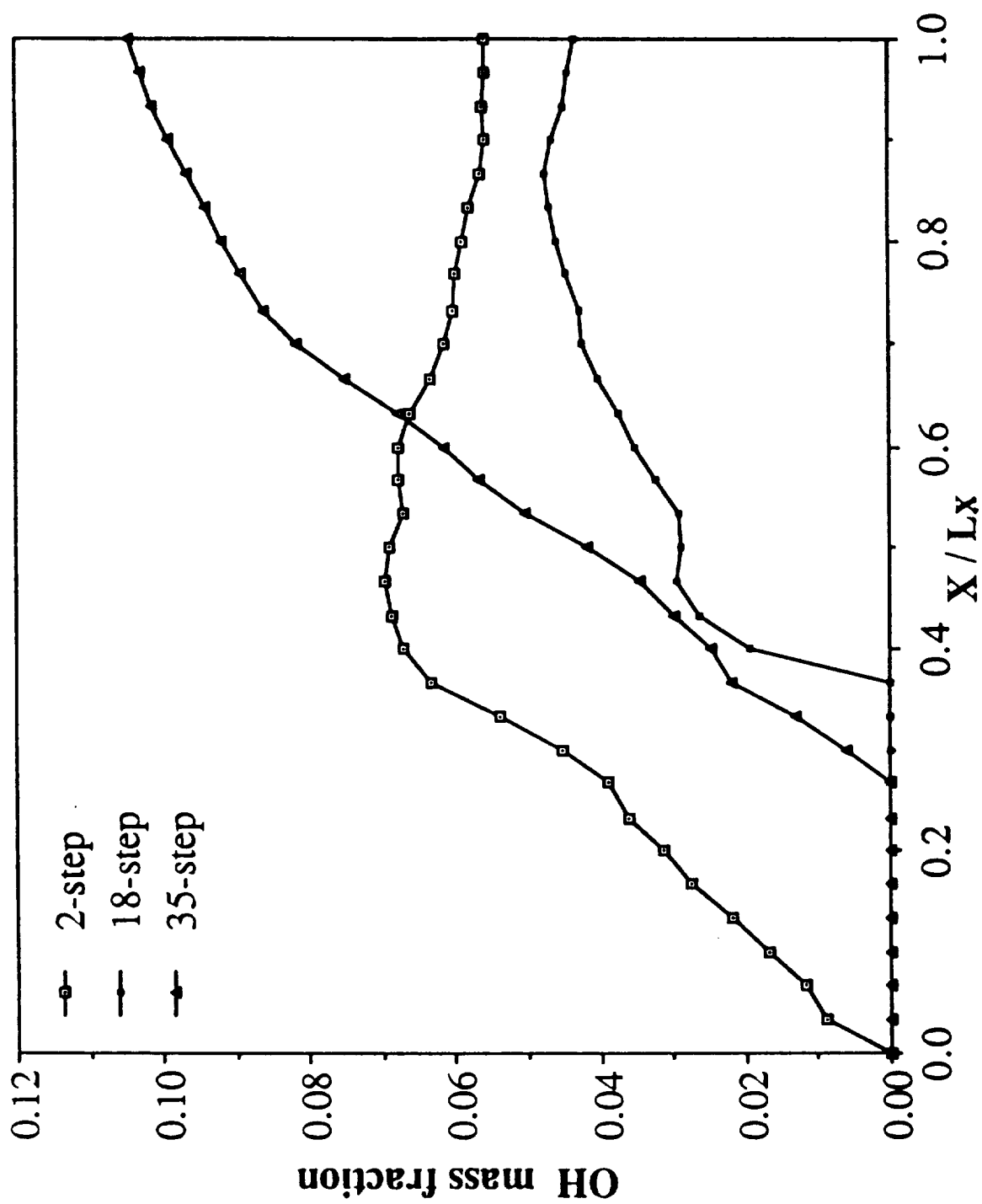
Fig. 7 OH mass fraction profiles (y = 0.02 cm.)

25
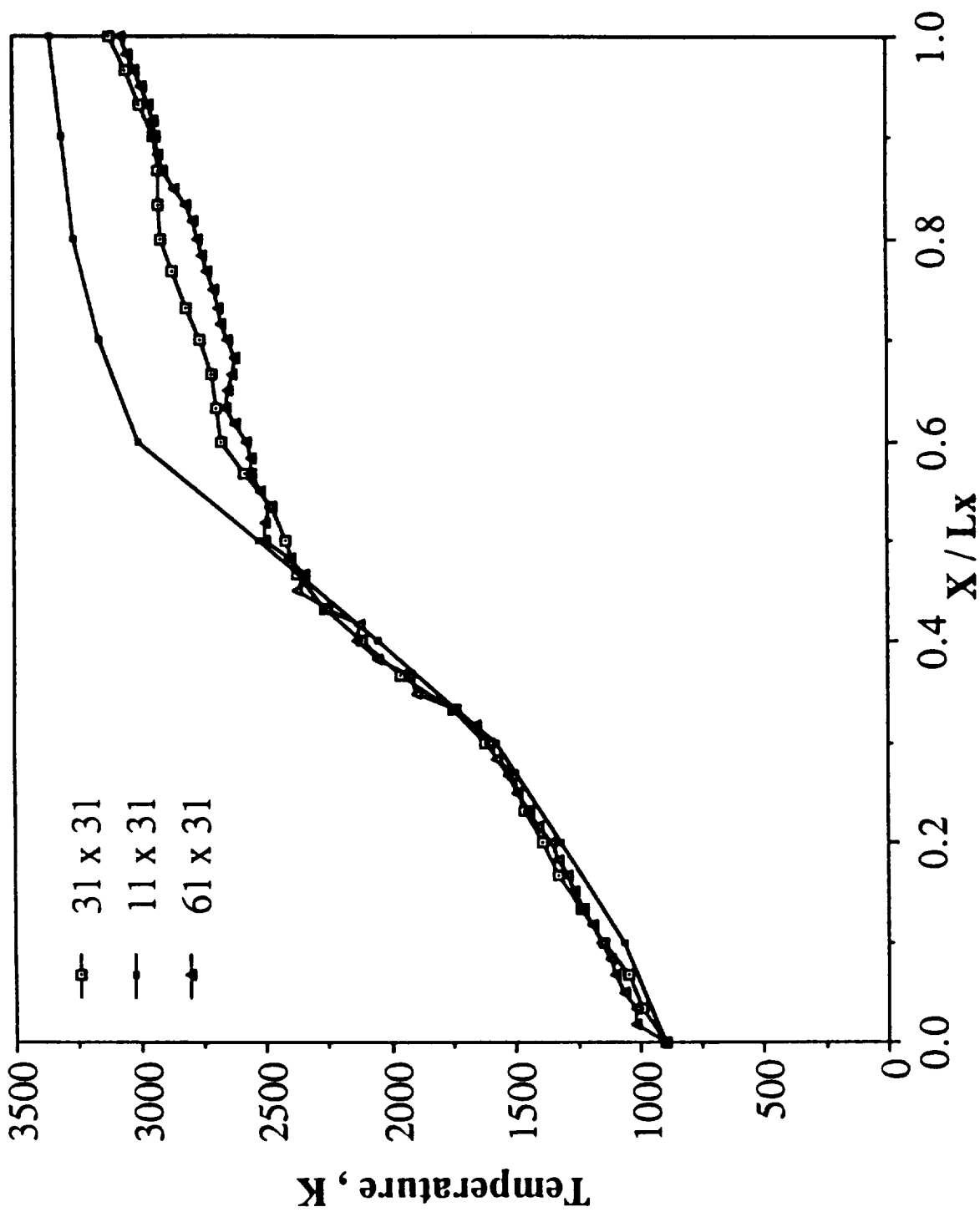
Fig. 8 Grid sensitivity results
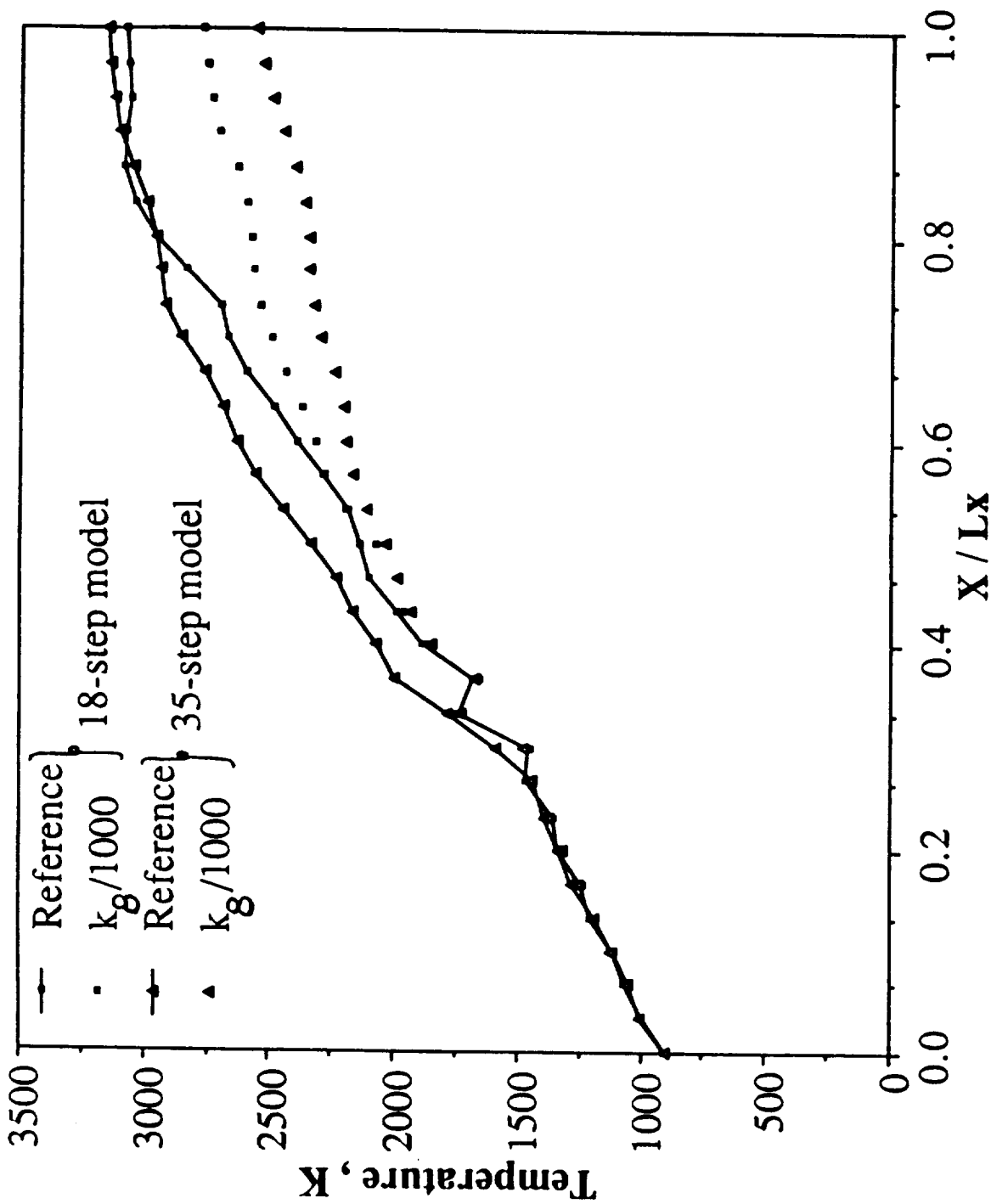
Fig. 9 Effect of reaction rates
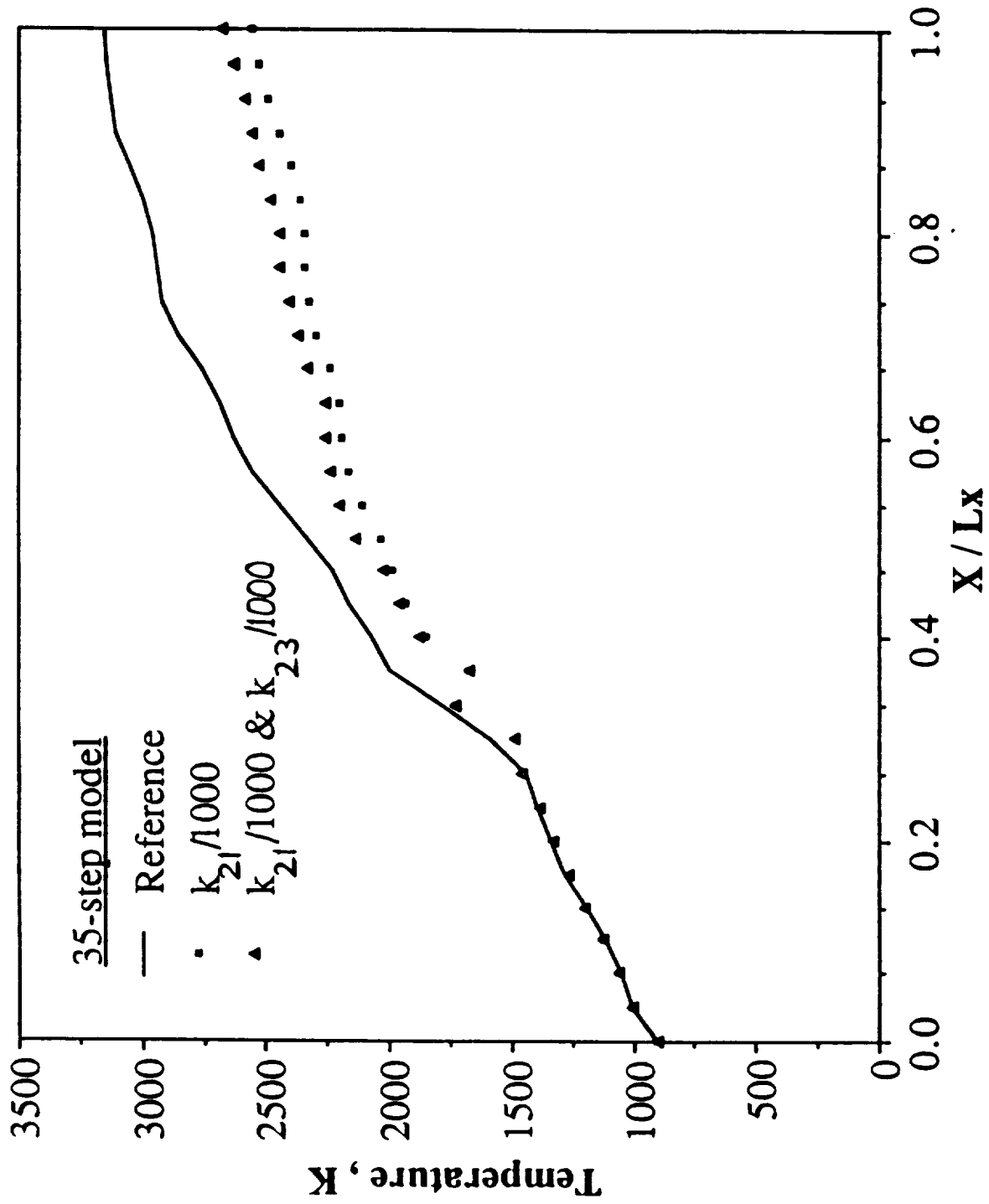
Fig. 10 Effect of NO and HO$_2$ reactions

Level	T (K)
F	3060.
E	2911.
D	2761.
C	2612.
B	2462.
A	2313.
9	2163.
8	2014.
7	1864.
6	1715.
5	1565.
4	1416.
3	1266.
2	1117.
1	967.8

Fig. 11a   Temperature contours for reacting (2-step model) case

29

Level	T (K)
F	3284.
E	3111.
D	2938.
C	2766.
B	2593.
A	2421.
9	2248.
8	2076.
7	1903.
6	1730.
5	1558.
4	1385.
3	1213.
2	1040.
1	868.0
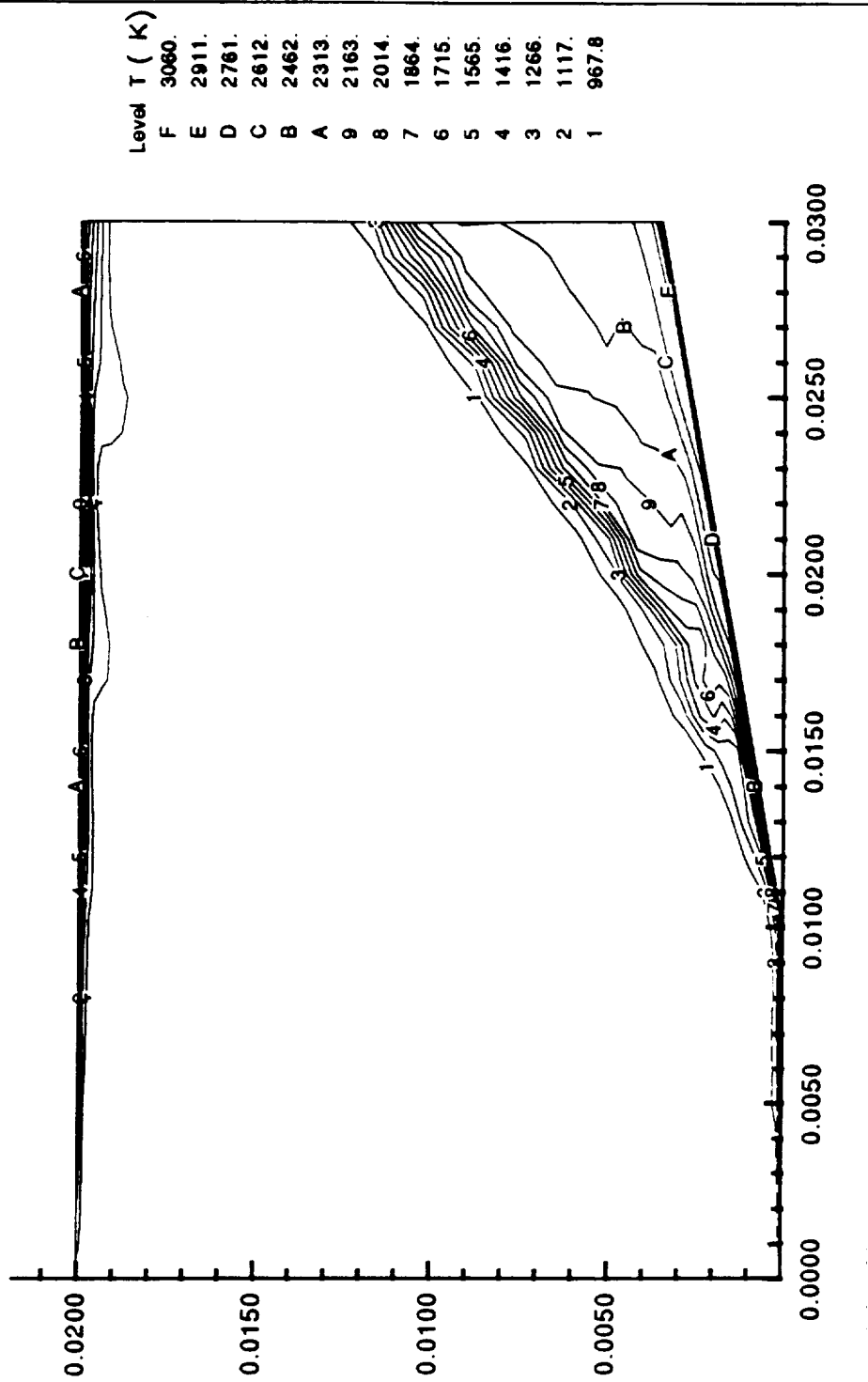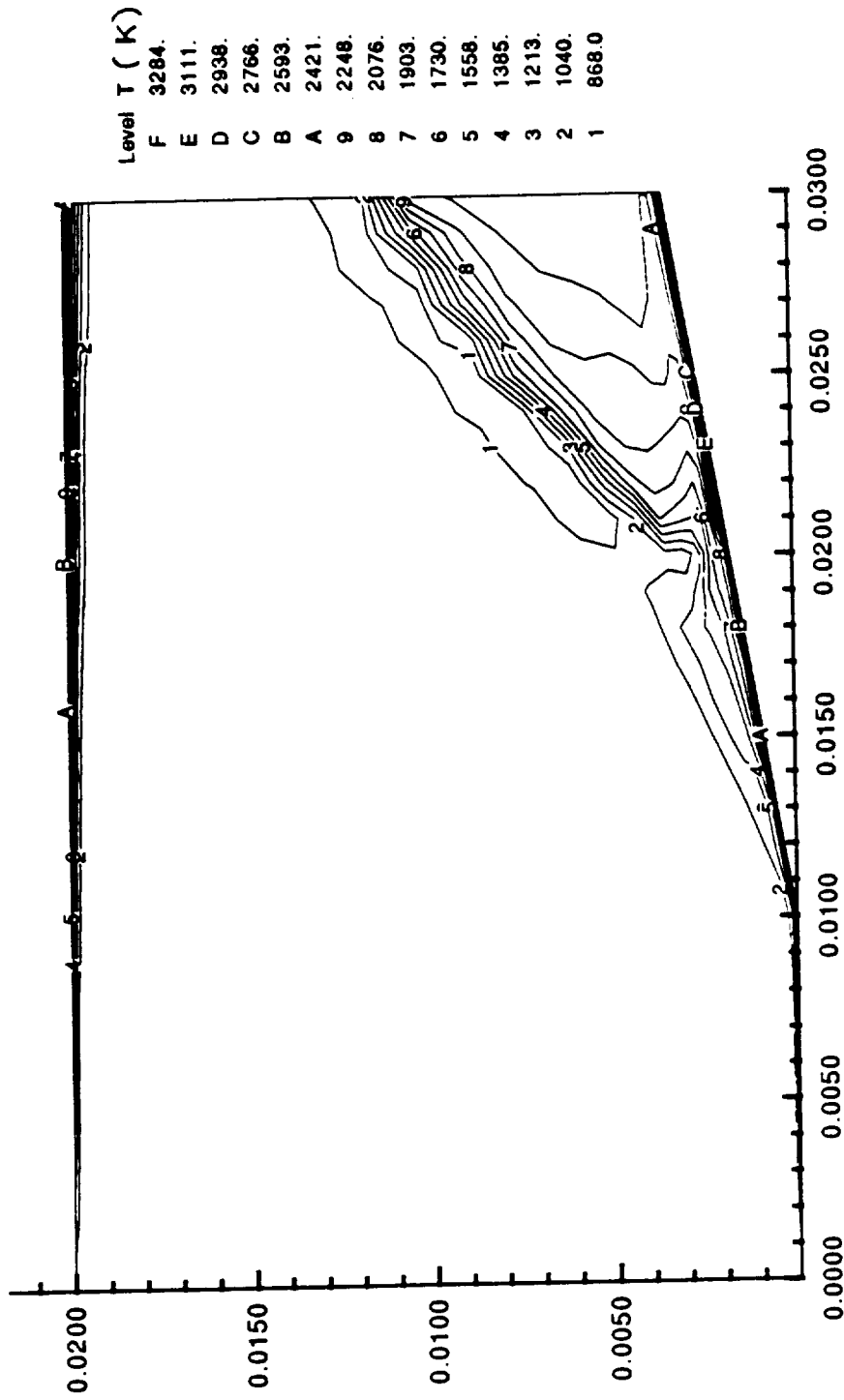
Fig. 11b Temperature contours for reacting (35-step model) case

Level	P (Pa)
F	47315
E	44620
D	41924
C	39228
B	36532
A	33836
9	31140
8	28445
7	25749
6	23053
5	20357
4	17661
3	14965
2	12270
1	95742
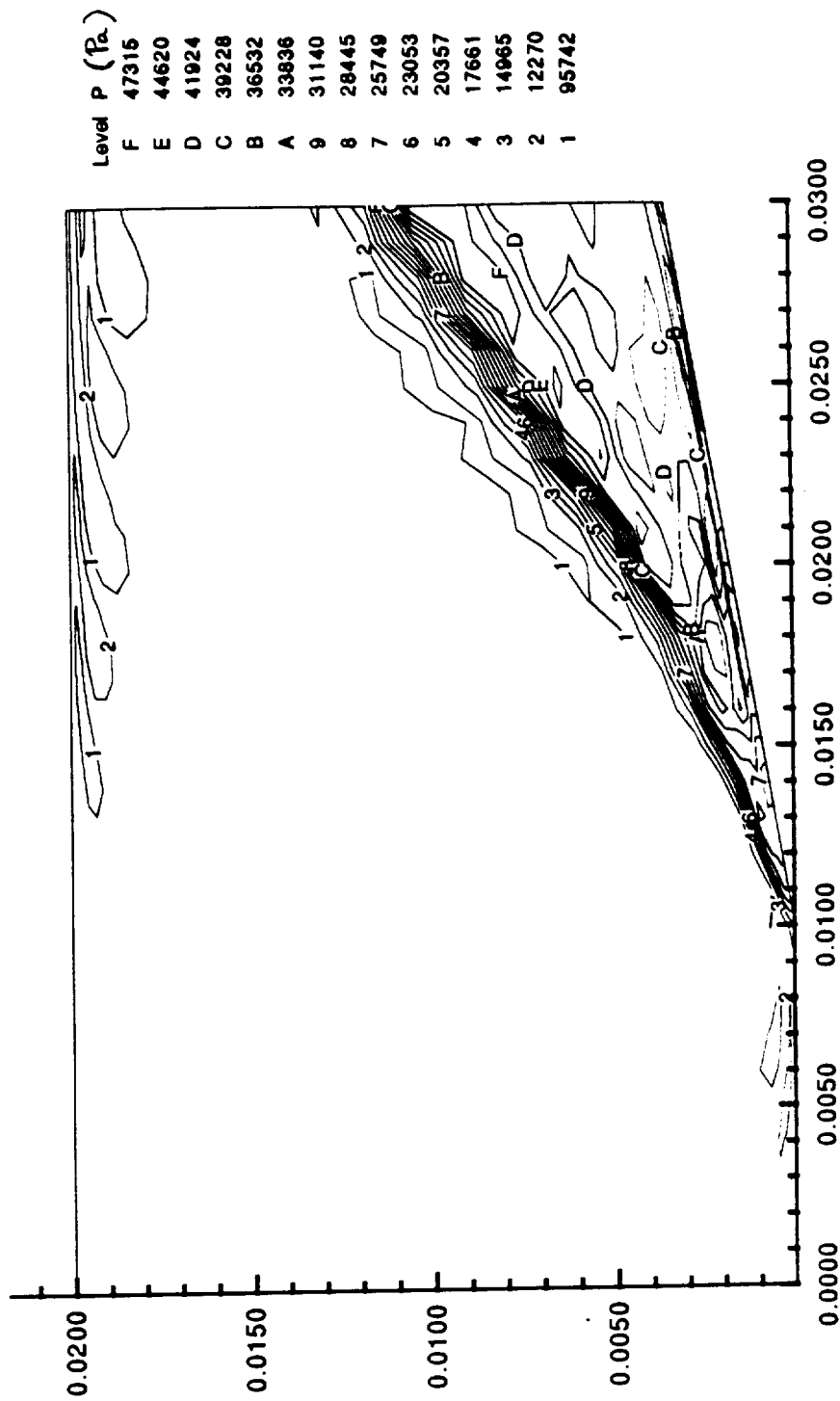
Fig. 12a   Pressure contours for reacting (2-step model) case
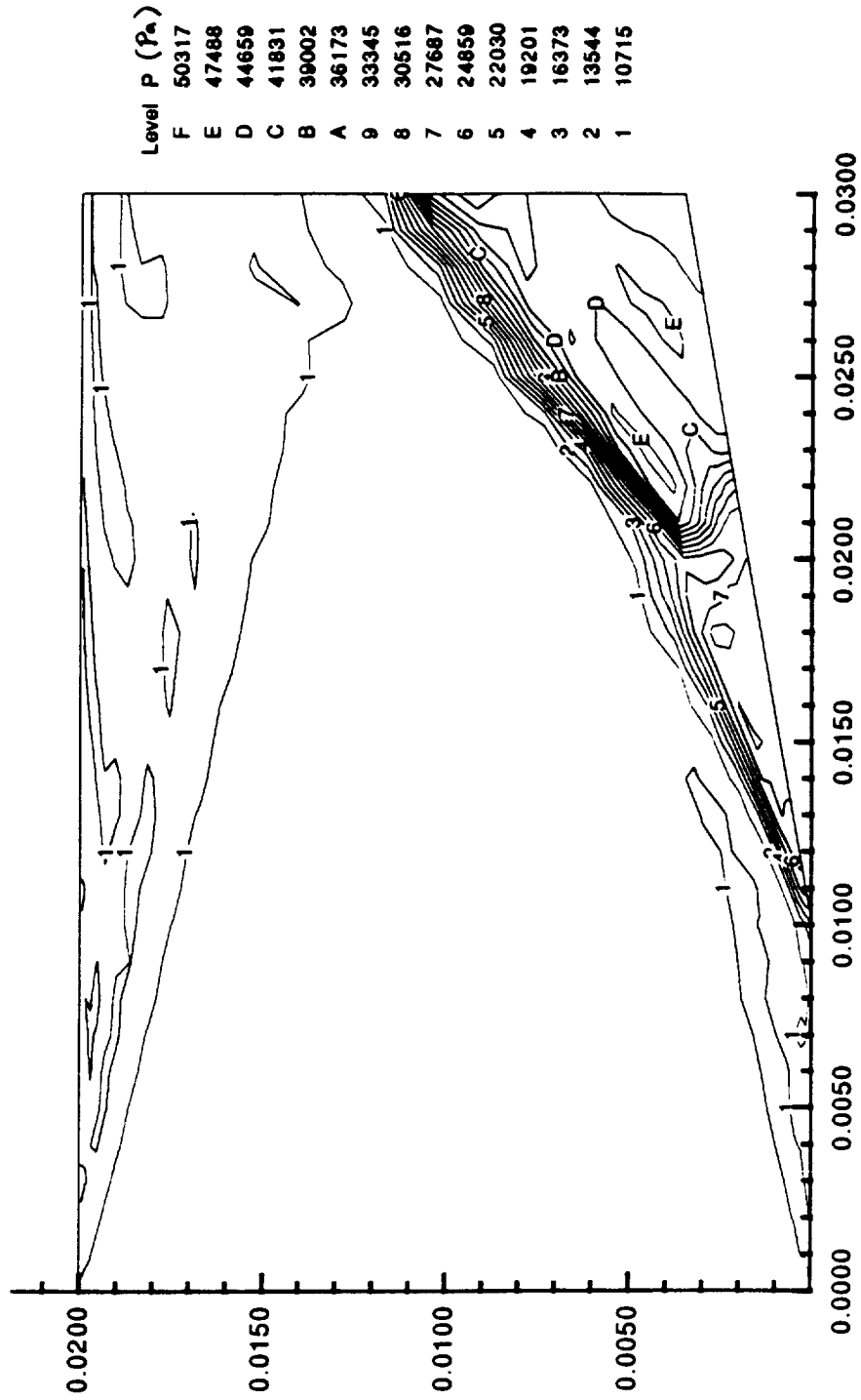
31

Level	P (Pa)
F	50317
E	47488
D	44659
C	41831
B	39002
A	36173
9	33345
8	30516
7	27687
6	24859
5	22030
4	19201
3	16373
2	13544
1	10715

Fig. 12b   Pressure contours for reacting (35-step model) case

Level	FH2O
F	0.15
E	0.14
D	0.13
C	0.12
B	0.11
A	0.10
9	0.09
8	0.08
7	0.07
6	0.06
5	0.05
4	0.04
3	0.03
2	0.02
1	0.01
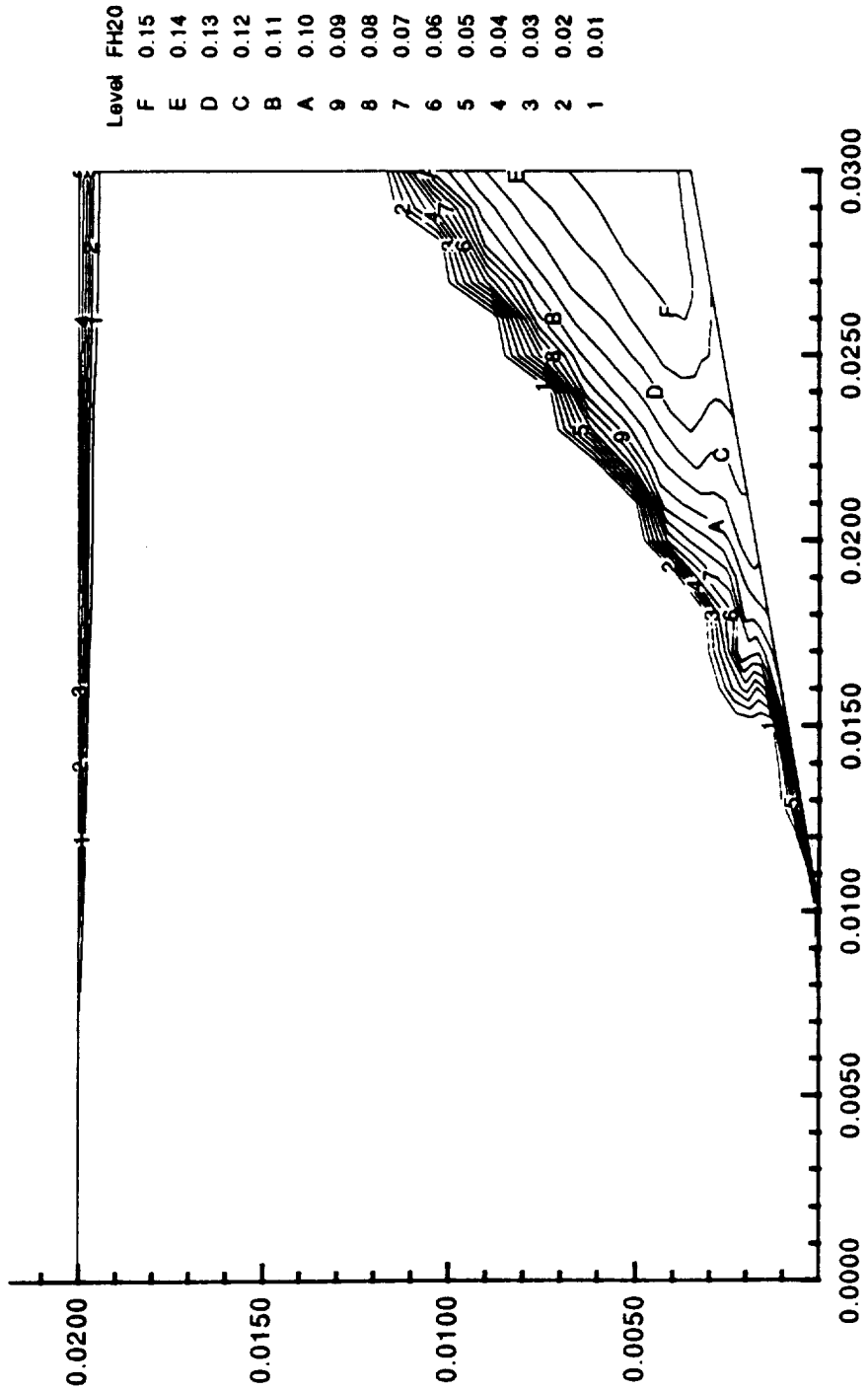
Fig. 13a H_2O mass fraction contours for reacting (2-step model) case

Level	FH20
F	0.26
E	0.24
D	0.23
C	0.21
B	0.19
A	0.17
9	0.16
8	0.14
7	0.12
6	0.10
5	0.09
4	0.07
3	0.05
2	0.03
1	0.02
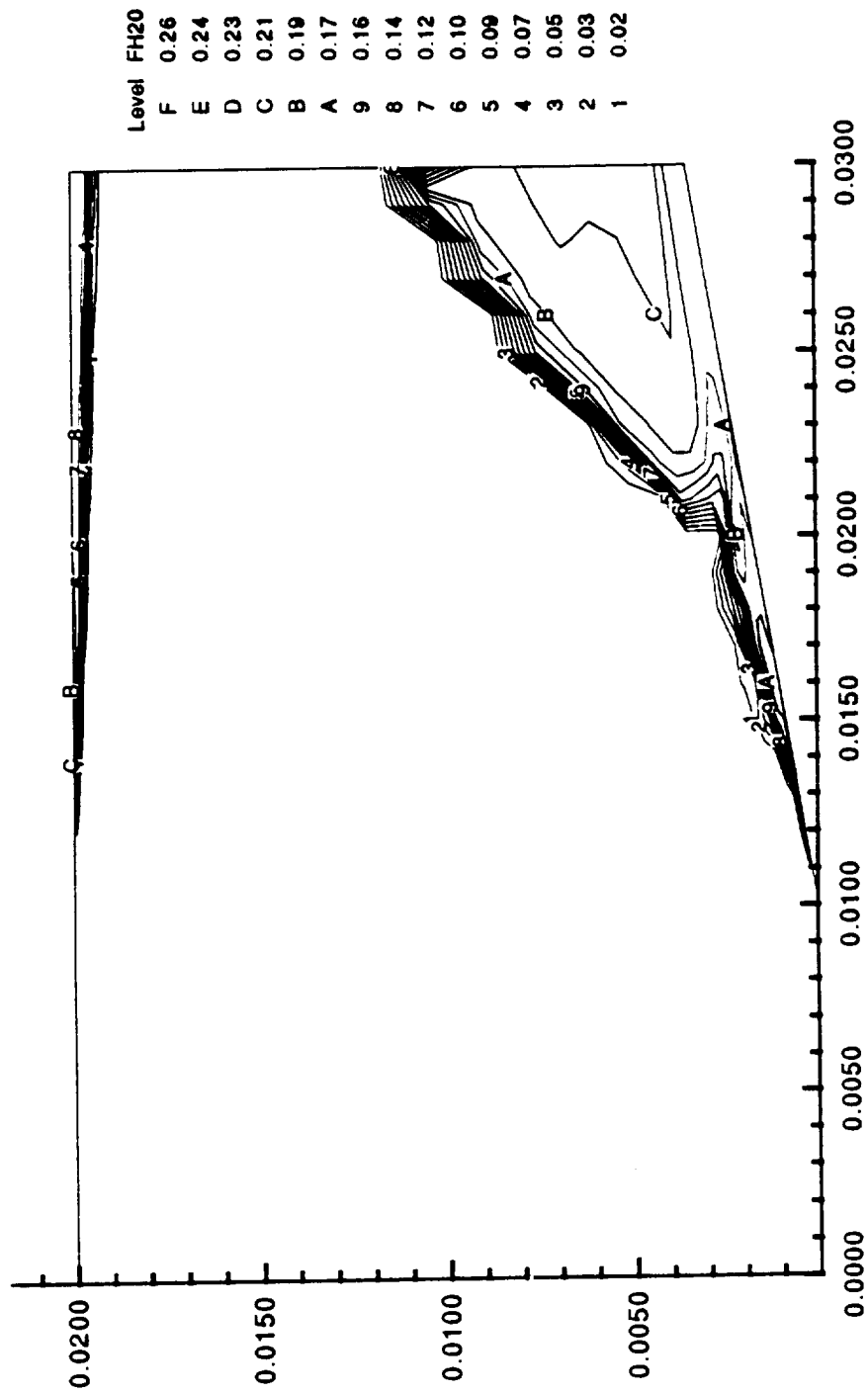
Fig. 13b H_2O mass fraction contours for reacting (35-step model) case

34
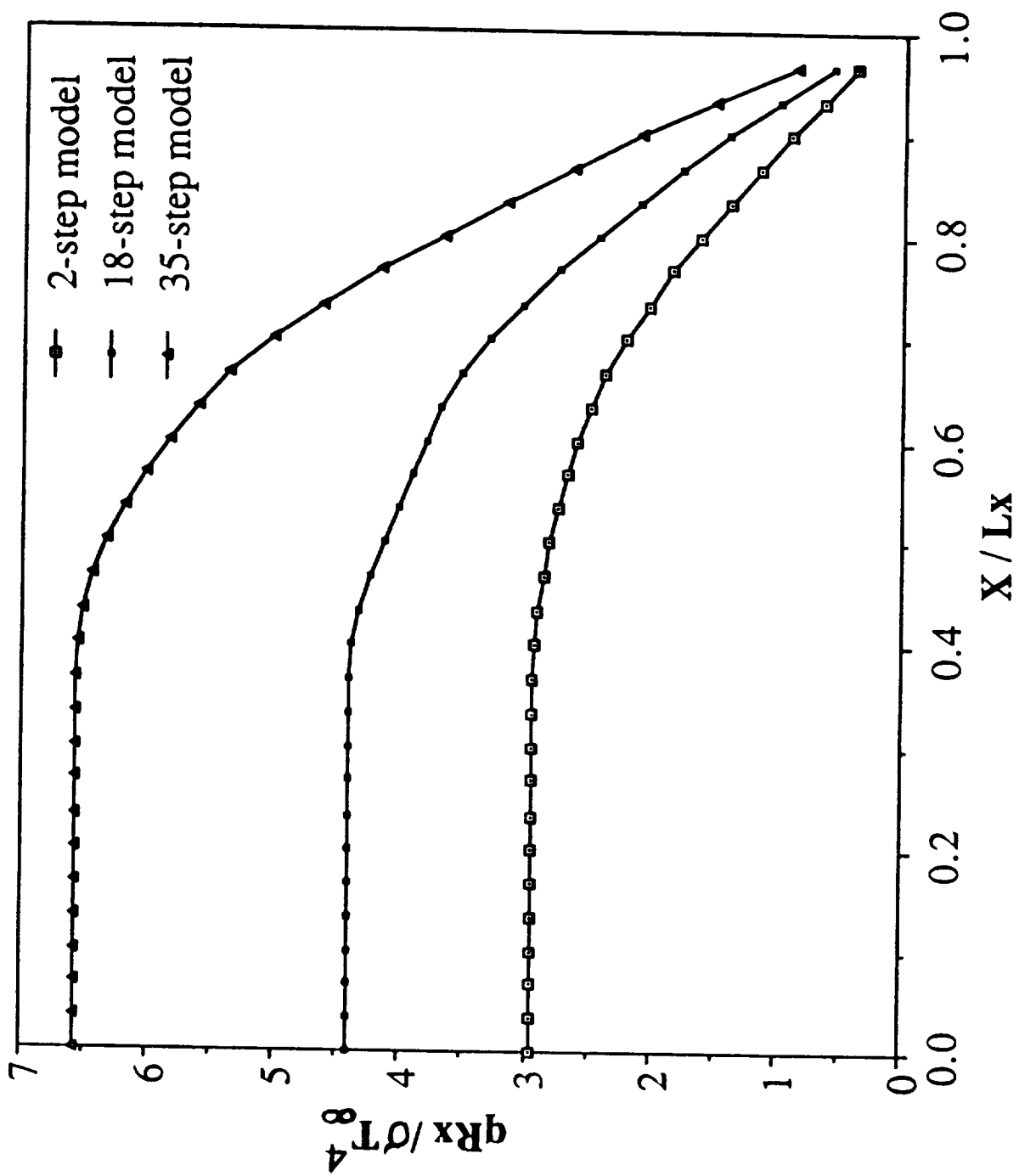
Fig. 14   Profiles of streamwise radiative flux (y = 0.02 cm.)
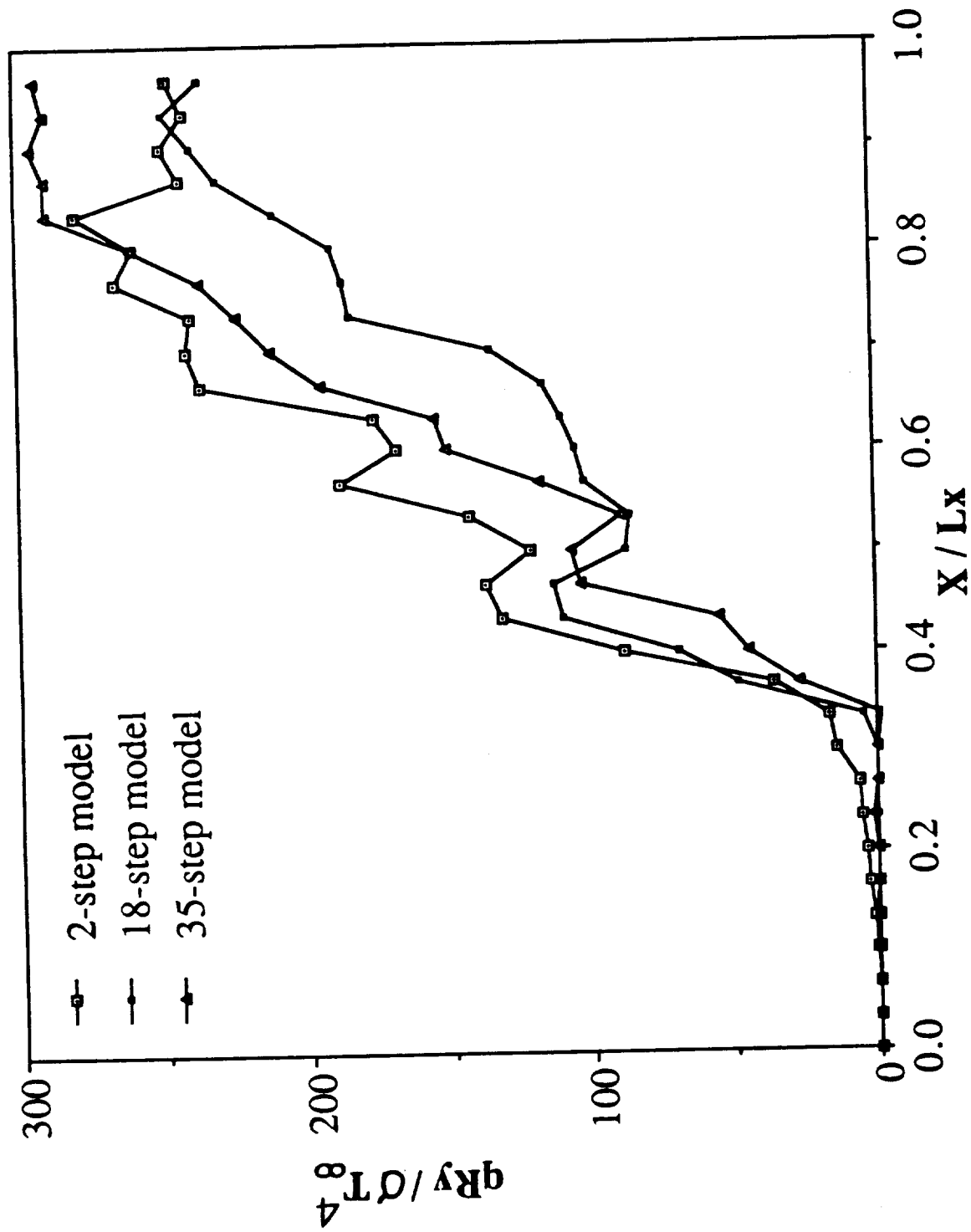
Fig. 15   Profiles of normal radiative flux (y = 0.02 cm.)
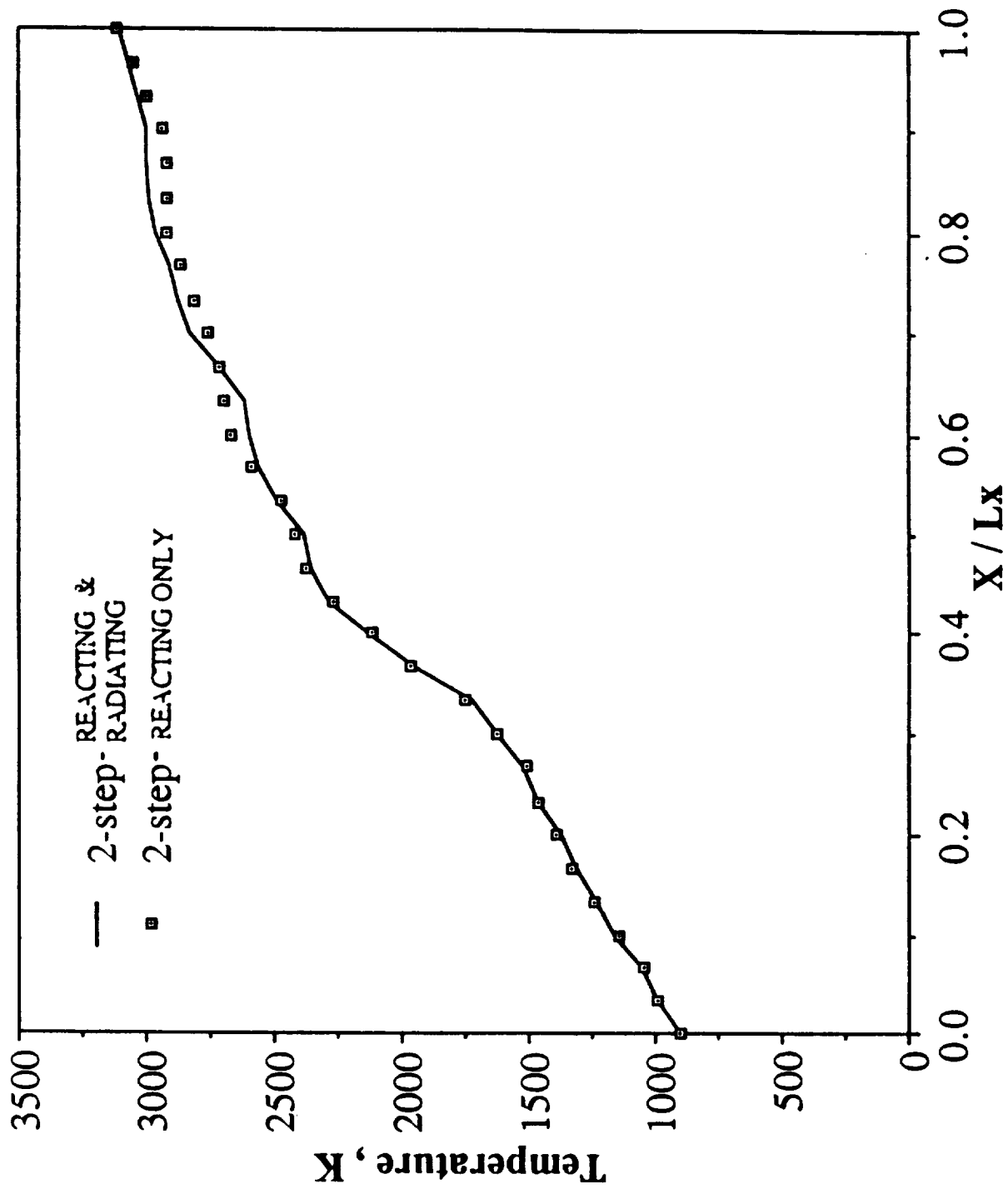
Fig. 16a   Radiation effects on temperature profiles using 2-step model (y = 0.02 cm.)
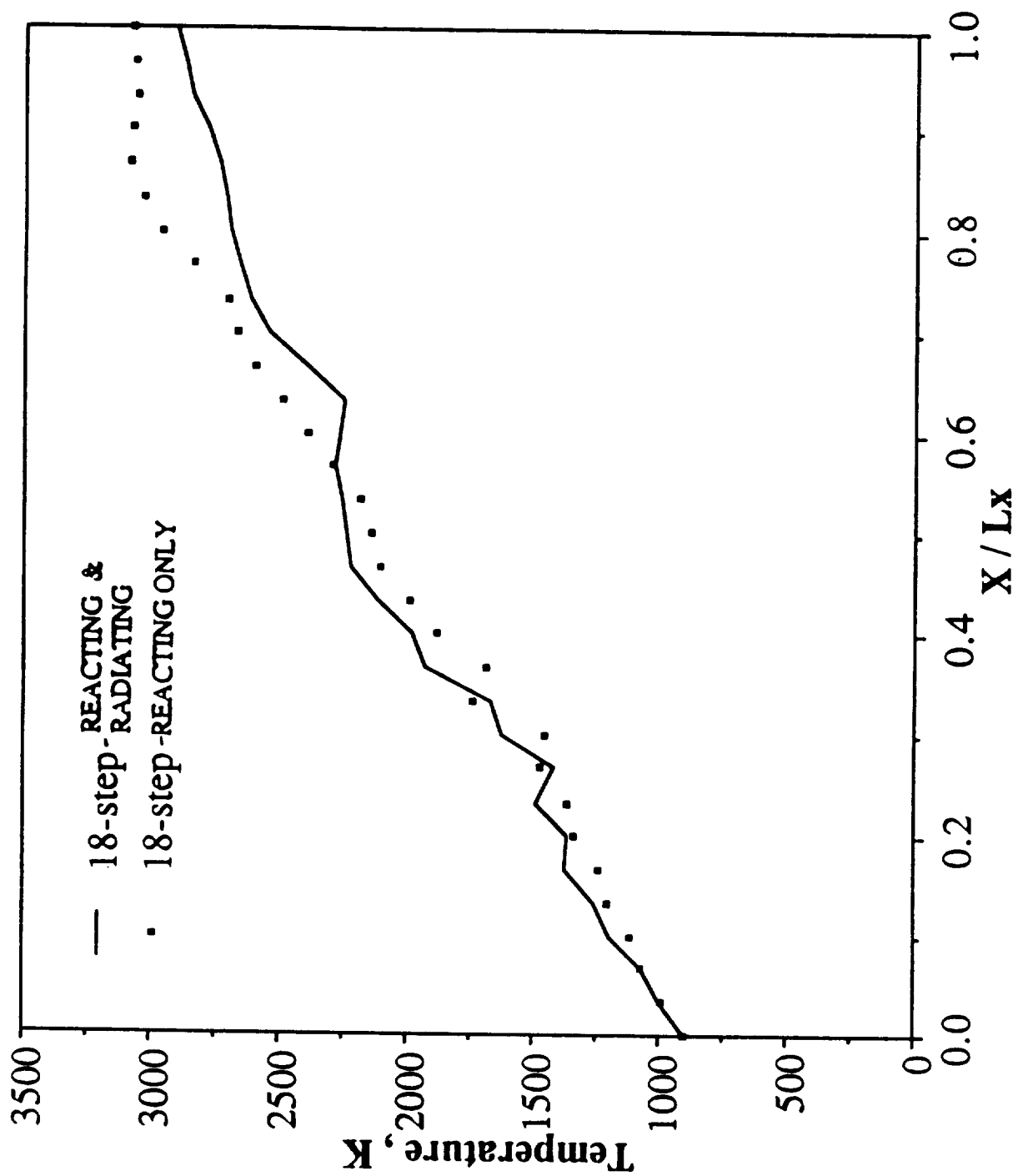
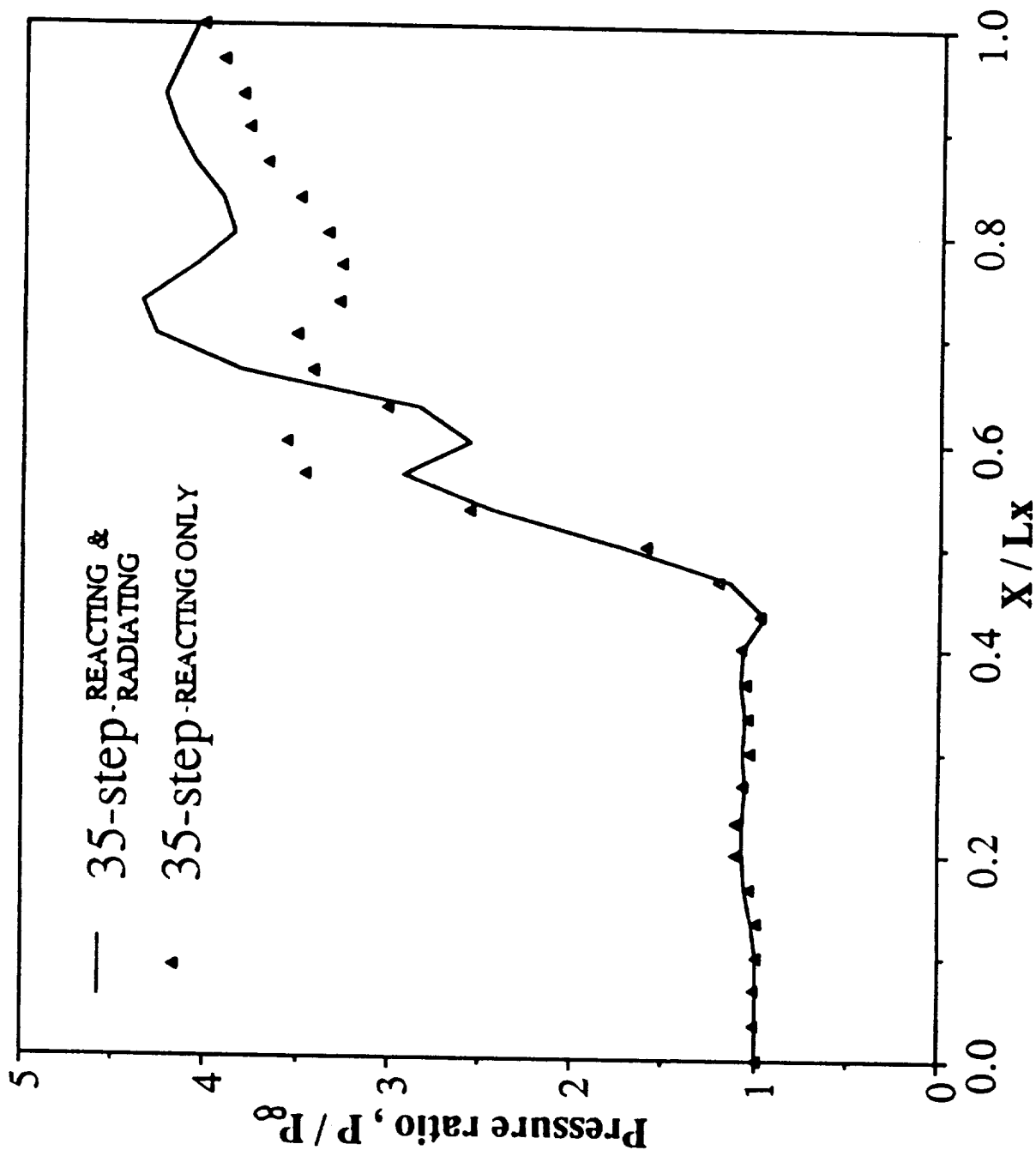Fig. 16b   Radiation effects on temperature profiles using 18-step model (y = 0.02 cm.)
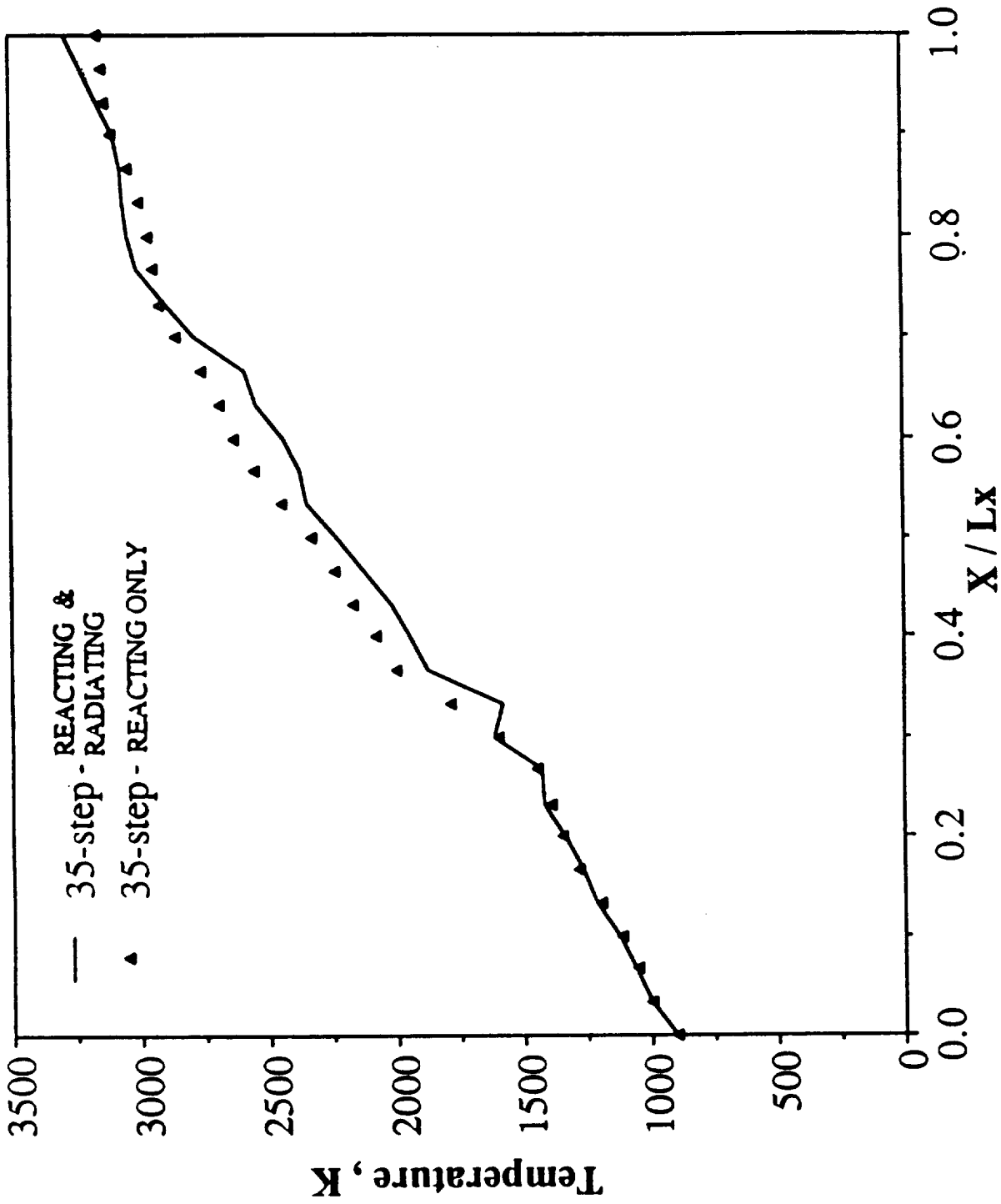
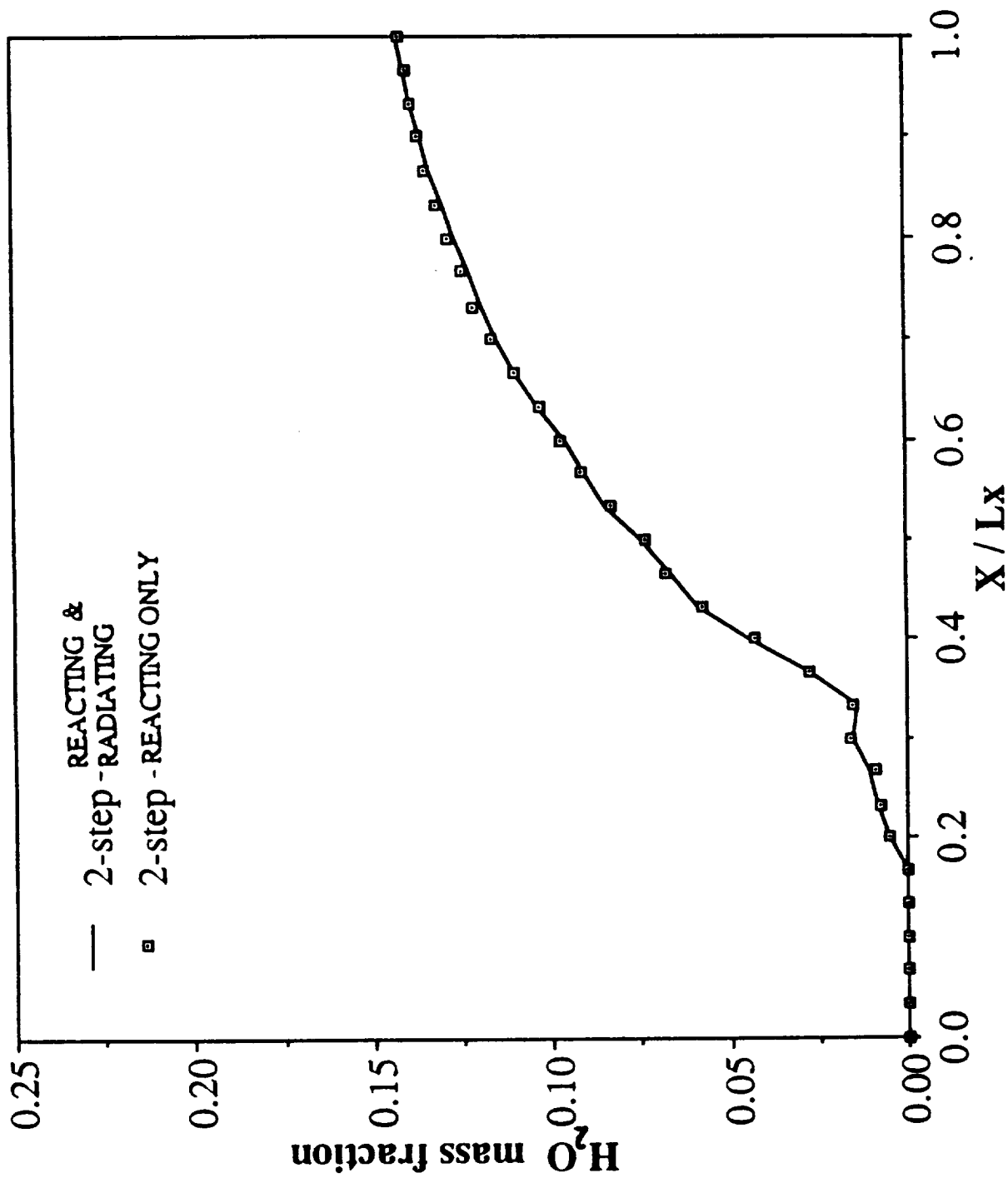Fig. 16c   Radiation effects on temperature profiles using 35–step model (y = 0.02 cm.)
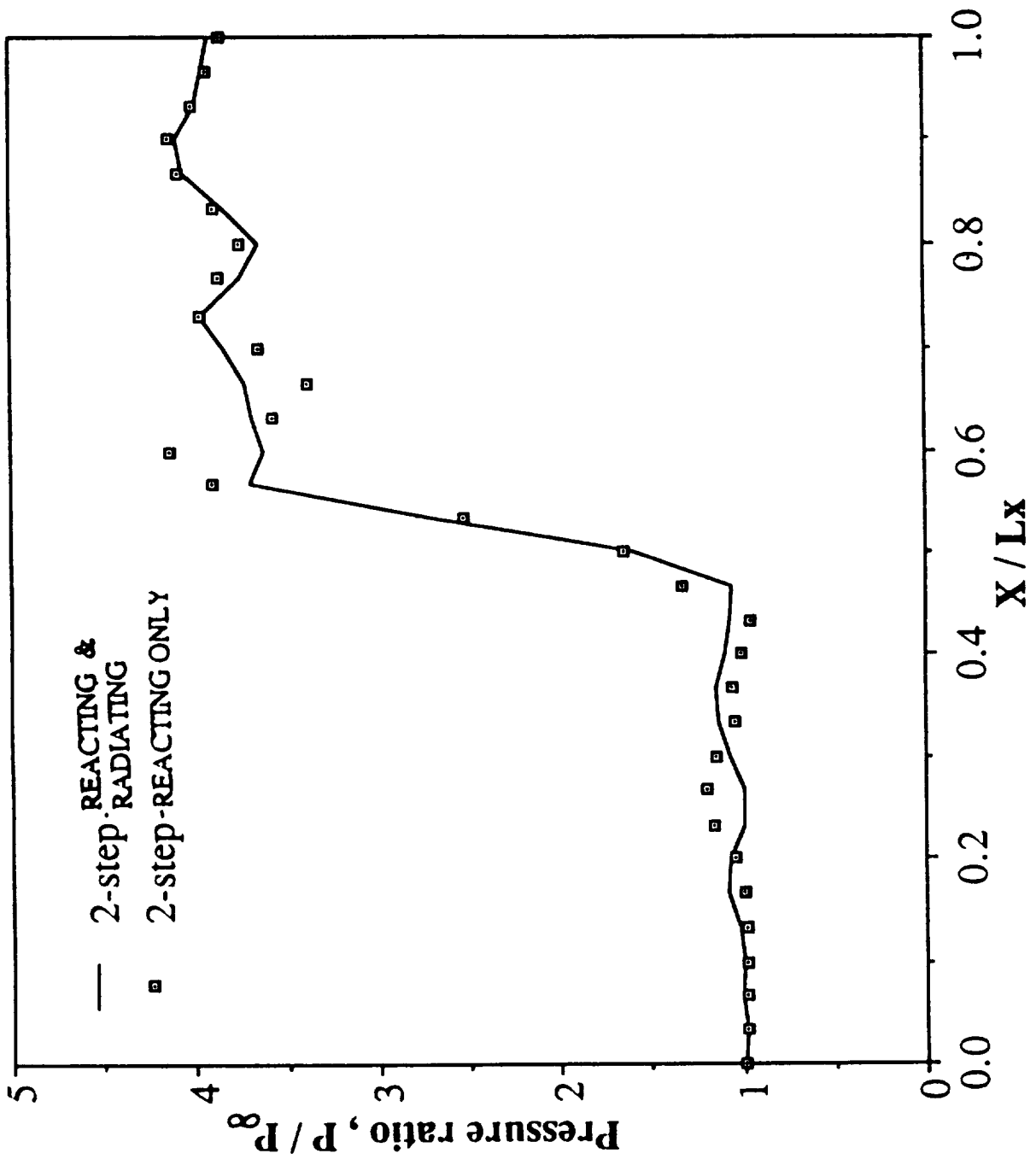
Fig. 17a   Radiation effects on pressure profiles using 2-step model (y = 0.13 cm.)
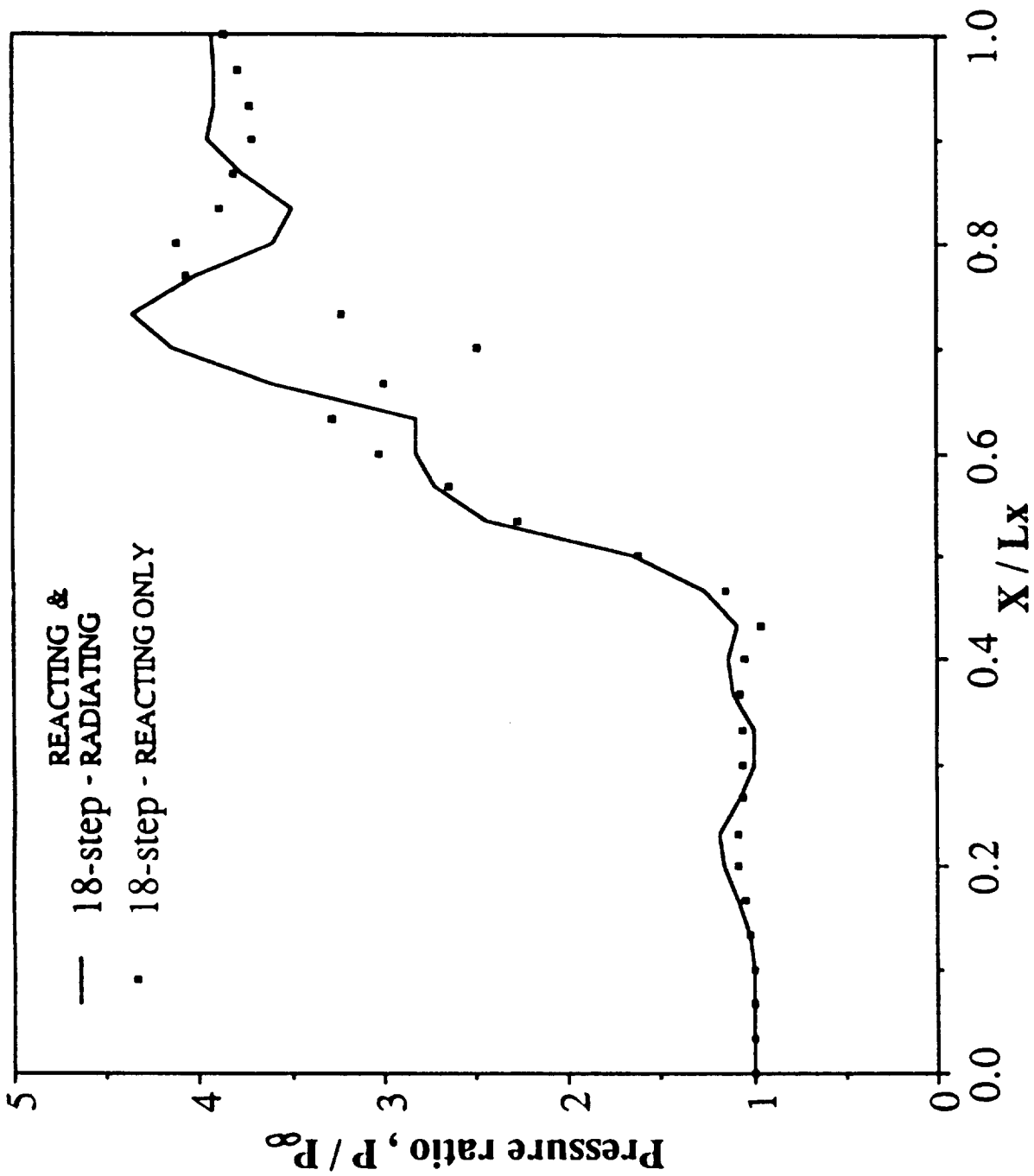
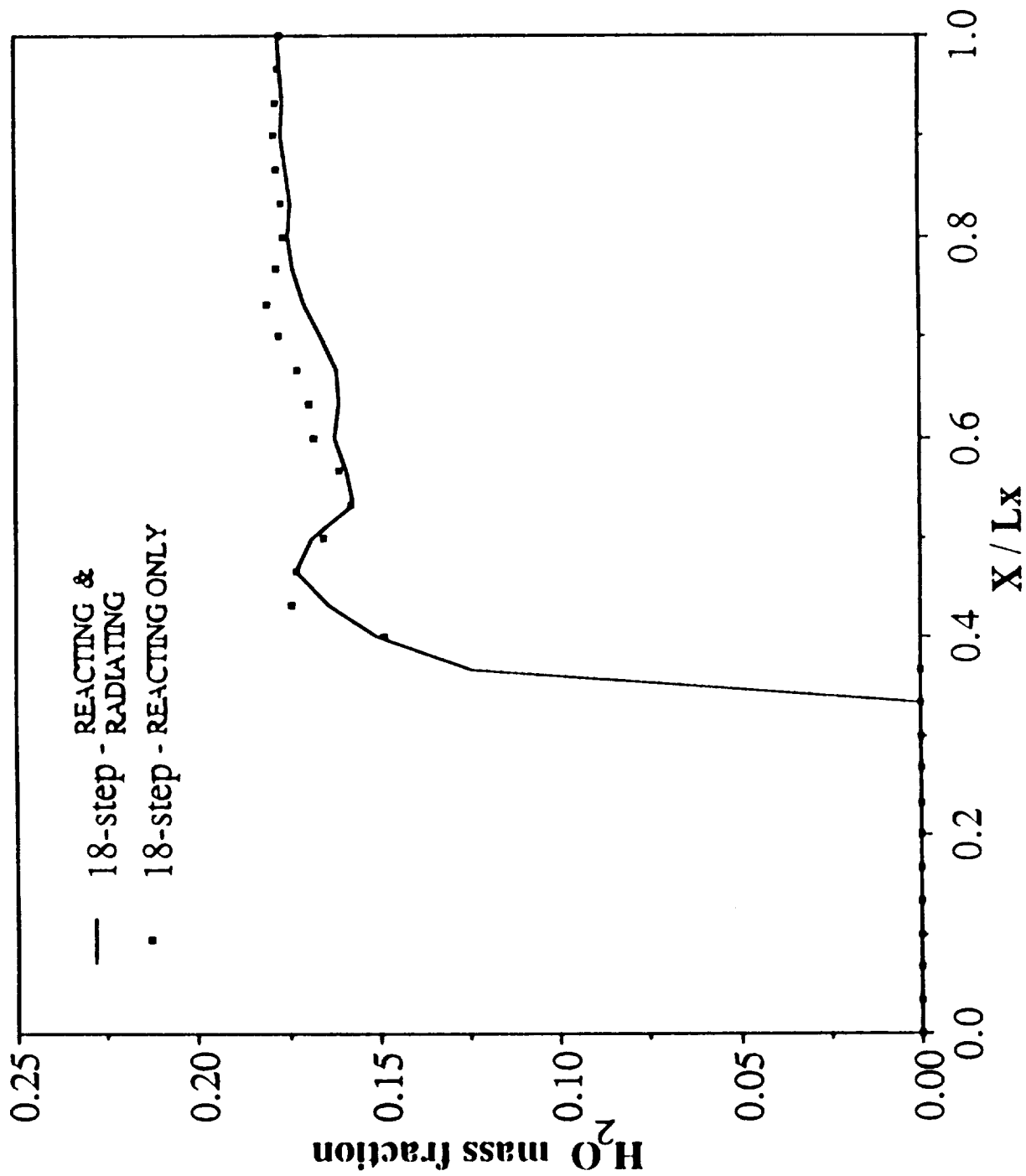Fig. 17b   Radiation effects on pressure profiles using 18-step model (y = 0.13 cm.)

41

Fig. 17c   Radiation effects on pressure profiles using 35-step model (y = 0.13 cm.)

42

Fig. 18a   Radiation effects on H_2O mass fraction profiles using 2-step model (y = 0.02 cm.)

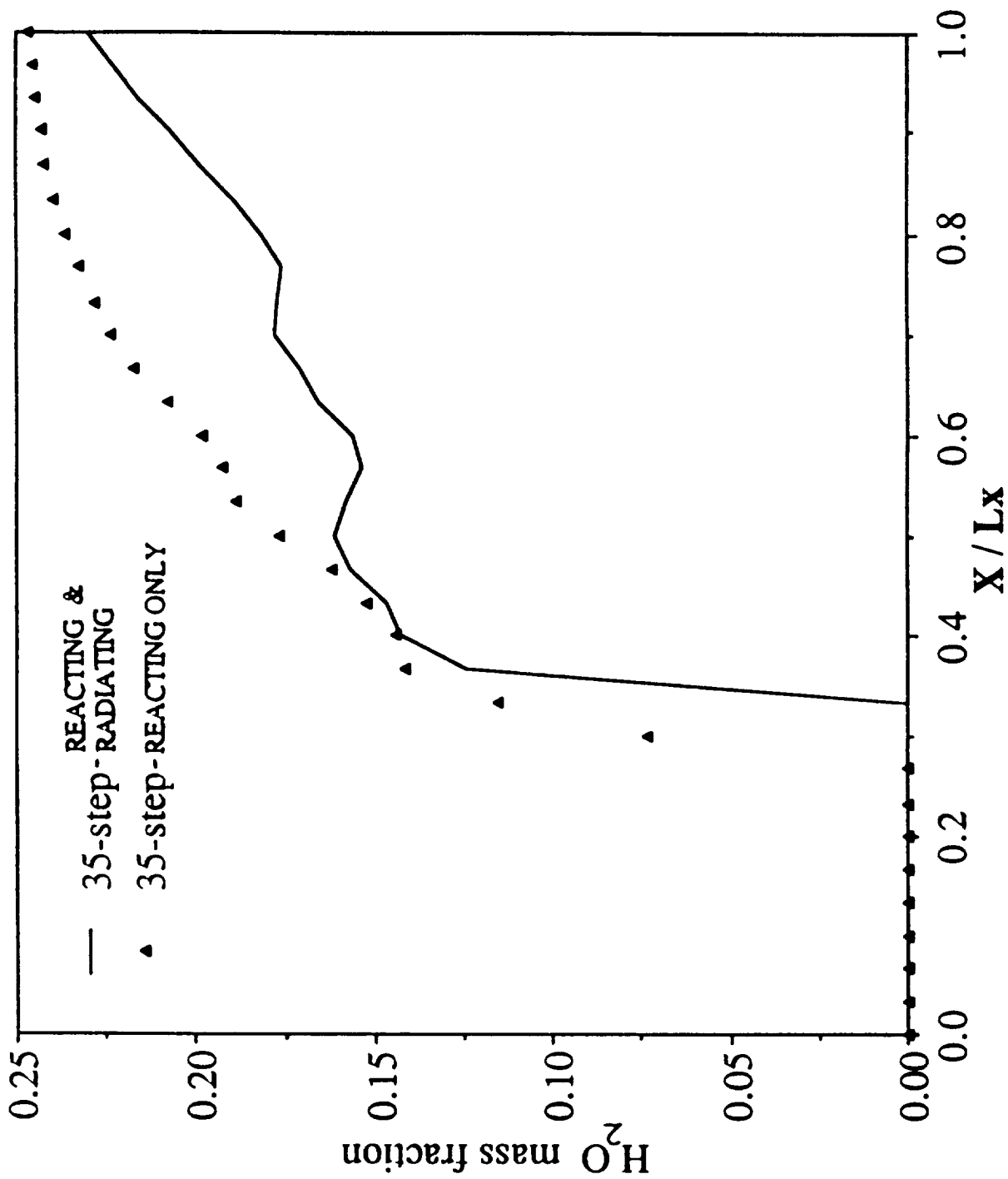Fig. 18b   Radiation effects on H_2O mass fraction profiles using 18-step model (y = 0.02 cm.)

44

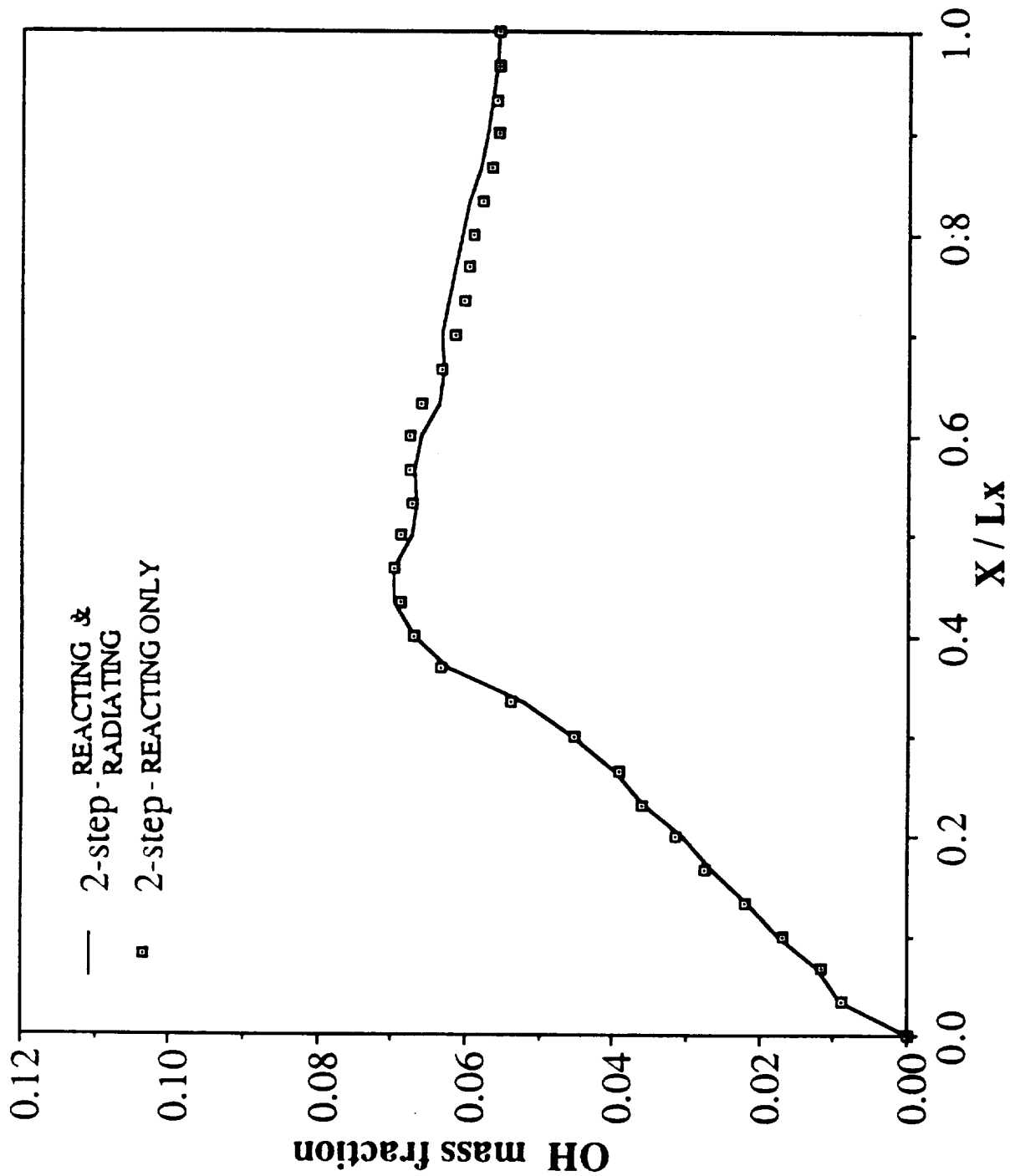Fig. 18c Radiation effects on H_2O mass fraction profiles using 35-step model (y = 0.02 cm.)

45

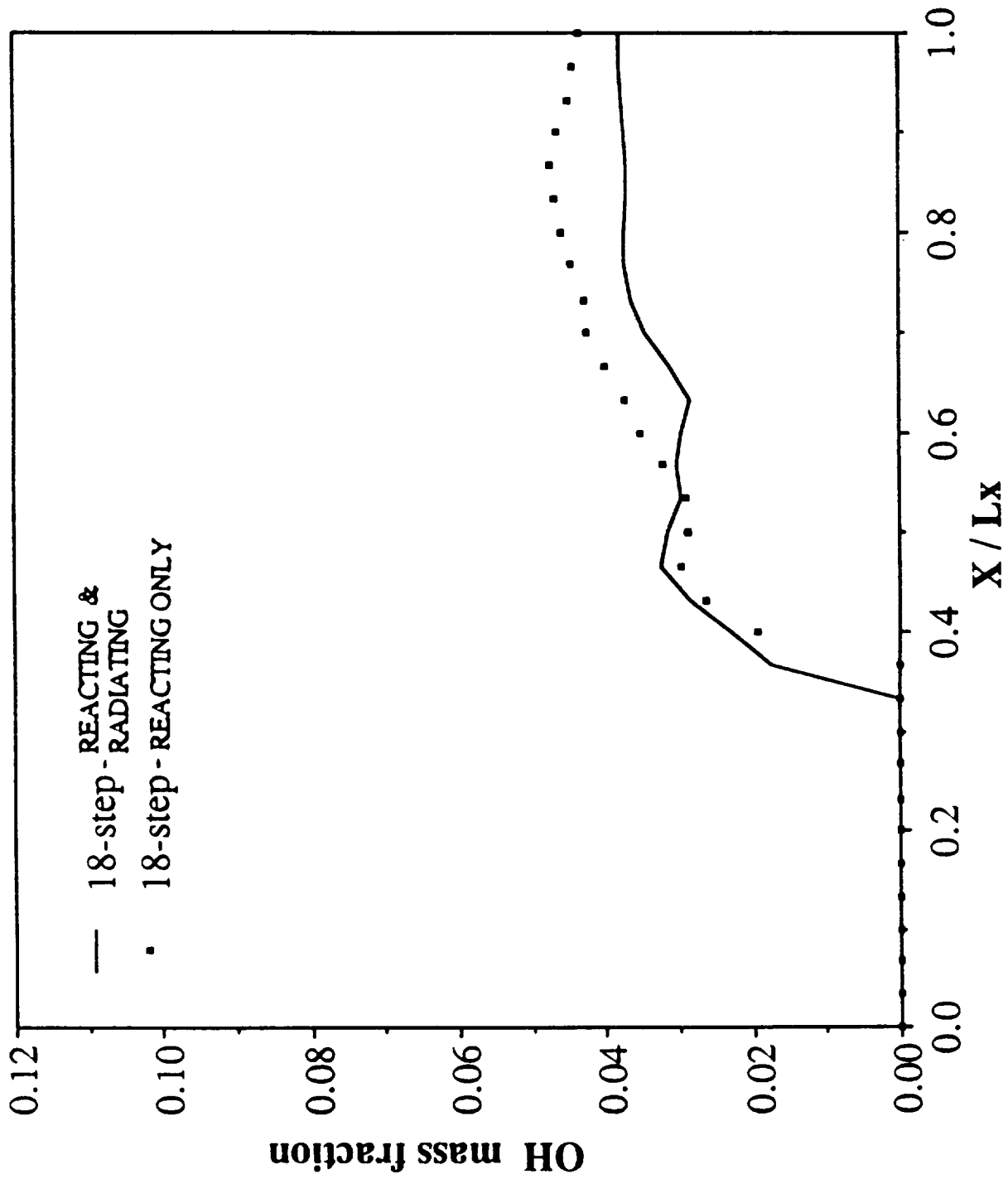Fig. 19a   Radiation effects on OH mass fraction profiles using 2-step model (y = 0.02 cm.)

46

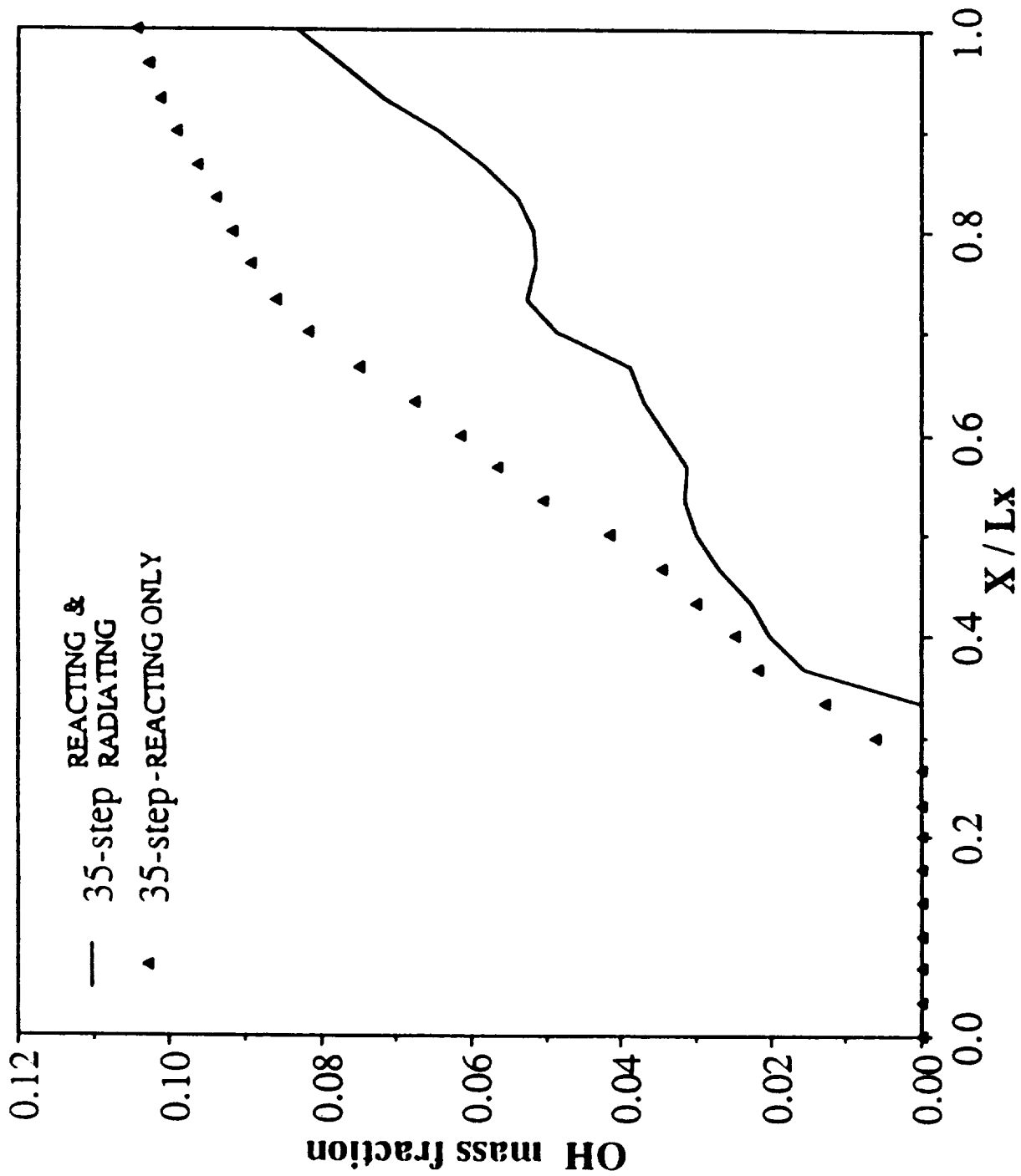Fig. 19b Radiation effects on OH mass fraction profiles using 18-step model (y = 0.02 cm.)

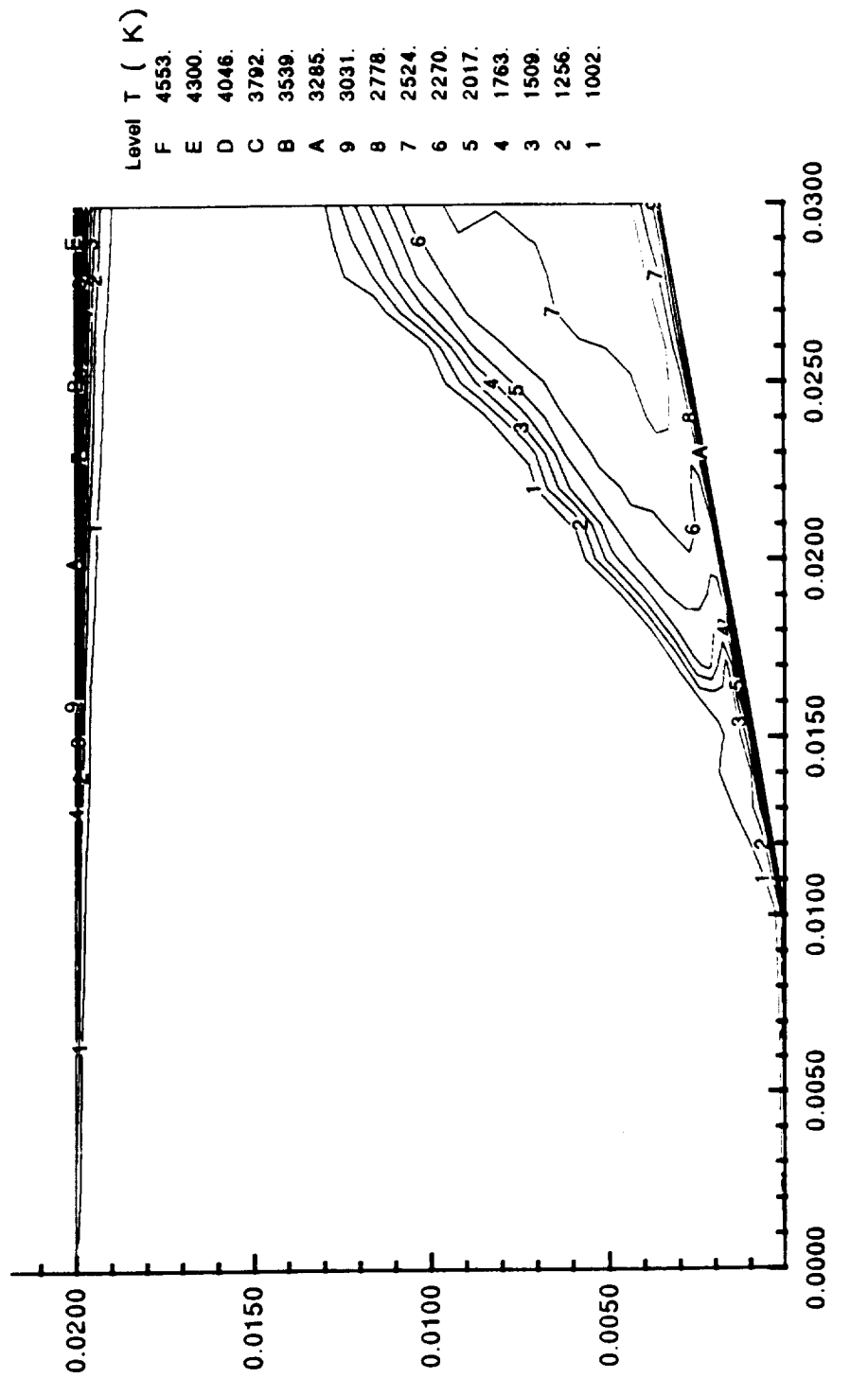Fig. 19c Radiation effects on OH mass fraction profiles using 35-step model (y = 0.02 cm.)

Level	T (K)
F	4553.
E	4300.
D	4046.
C	3792.
B	3539.
A	3285.
9	3031.
8	2778.
7	2524.
6	2270.
5	2017.
4	1763.
3	1509.
2	1256.
1	1002.

Fig. 20   Radiation effects on temperature contours

49

Level	P (Pa)
F	50444
E	47648
D	44853
C	42057
B	39262
A	36466
9	33670
8	30875
7	28079
6	25283
5	22488
4	19692
3	16897
2	14101
1	11305
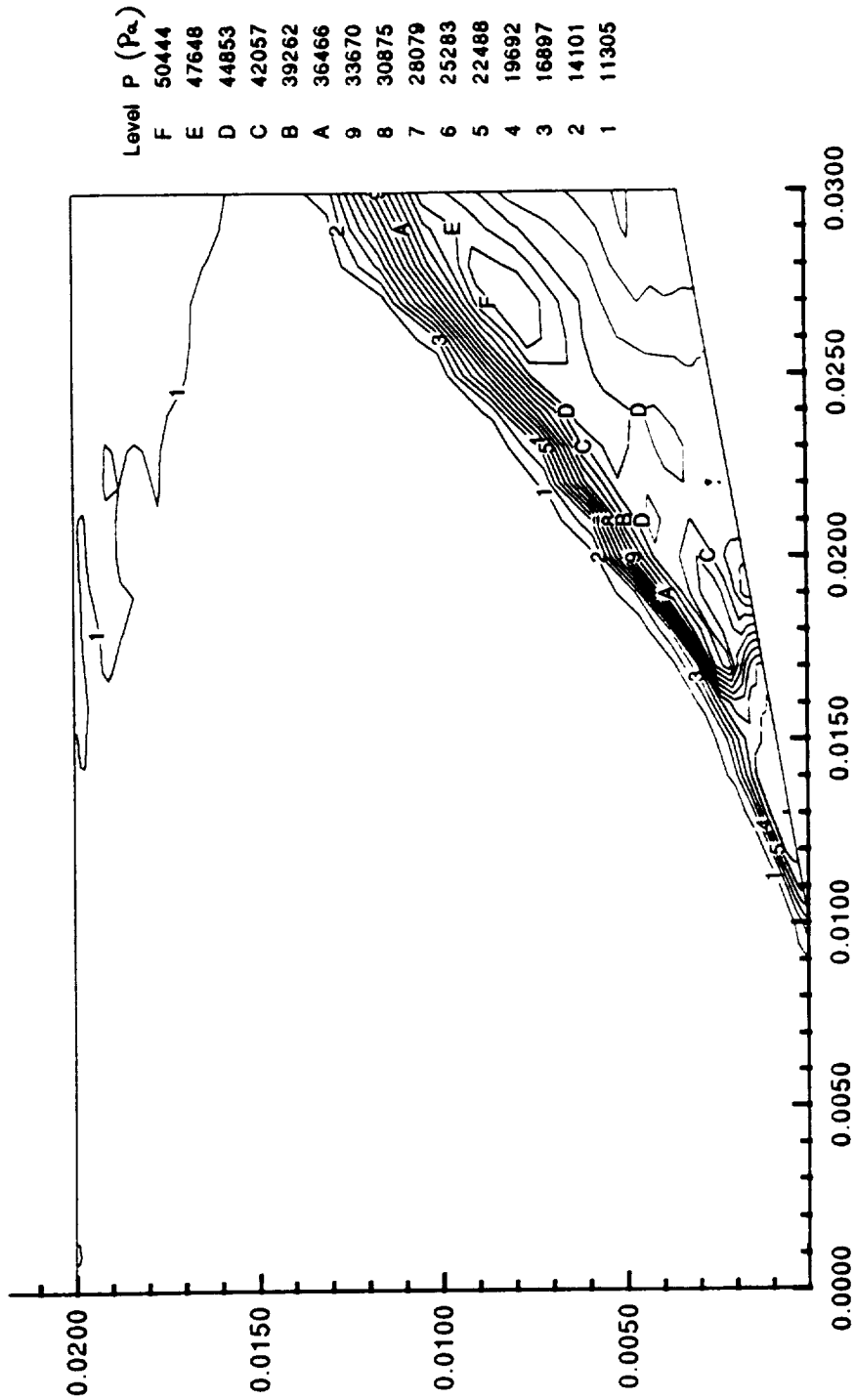
Fig. 21   Radiation effects on pressure contours

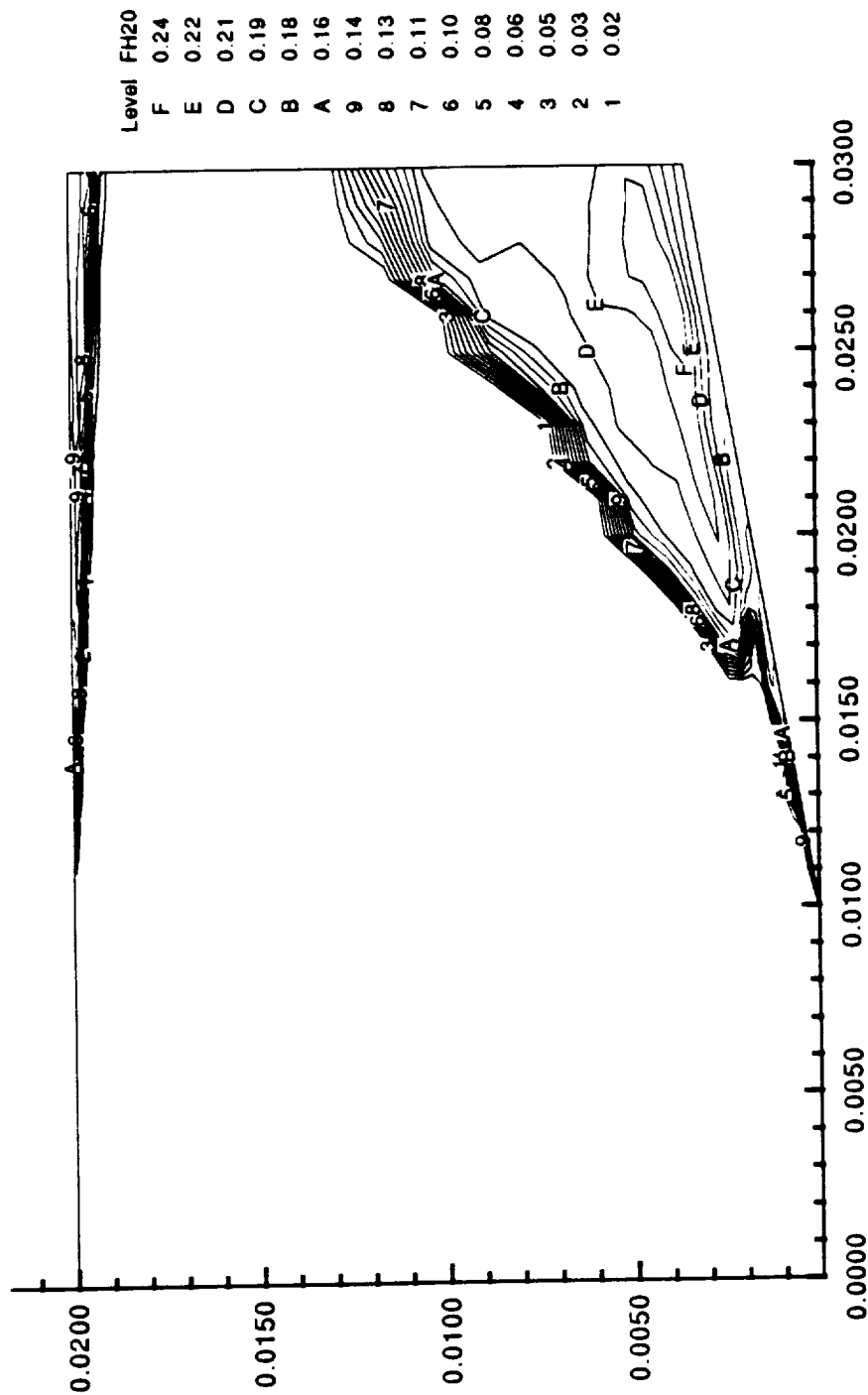| Level	FH20
F	0.24
E	0.22
D	0.21
C	0.19
B	0.18
A	0.16
9	0.14
8	0.13
7	0.11
6	0.10
5	0.08
4	0.06
3	0.05
2	0.03
1	0.02

Fig. 22   Radiation effects on H_2O mass fraction contours

APPENDICES

AIAA-91-0373

Radiative Interactions in a Hydrogen-Fueled Supersonic Combustor

R. Chandrasekhar and S. N. Tiwari,
Old Dominion University,
Norfolk, VA

J. P. Drummond,
NASA Langley Research Center,
Hampton, VA

29th Aerospace Sciences Meeting
January 7-10, 1991/Reno, Nevada

RADIATIVE INTERACTIONS IN A HYDROGEN-FUELED SUPERSONIC COMBUSTOR

R. Chandrasekhar[*] and S. N. Tiwari[†]
Old Dominion University, Norfolk, VA 23529-0247
and
J. P. Drummond[‡]
NASA-Langley Research Center, Hampton, VA 23665

Abstract

The two-dimensional, elliptic Navier-Stokes equations are used to investigate supersonic flows with finite-rate chemistry and radiation, for hydrogen-air systems. The chemistry source term in the species equation is treated implicitly to alleviate the stiffness associated with fast reactions. The explicit, unsplit MacCormack finite-difference scheme is used to advance the governing equations in time, until convergence is achieved. The specific problem considered is the premixed flow in a channel with a ten-degree compression ramp. Three different chemistry models are used, accounting for increasing number of reactions and participating species. Two chemistry models assume nitrogen as inert, while the third model accounts for nitrogen reactions and NO_x formation. The tangent slab approximation is used in the radiative flux formulation. A pseudo-gray model is used to represent the absorption-emission characteristics of the participating species. Results obtained for specific conditions indicate that the radiative interactions vary substantially, depending on reactions involving HO_2 and NO species, and that this can have a significant influence on the flowfield.

Nomenclature

A band absorptance, m^{-1}
A_v band width parameter, m^{-1}
C_j concentration of the jth species, $kg-mole/m^3$
C_p constant pressure specific heat, $J/kg - K$
C_o correlation parameter, $(N/m^2)^{-1} m^{-1}$
E total internal energy
e_ω Planck's function
f_j mass fraction of jth species
H total enthalpy, J/kg
h static enthalpy, J/kg
k thermal conductivity

k_b backward rate constant
k_f forward rate constant
P pressure, N/m^2
P_j partial pressure of jth species
q_R total radiative flux
R gas constant
S integrated band intensity, $(N/m^2)^{-1} m^{-2}$
T temperature, K
u, v velocity in $x-$ and $y-$directions, m/s
$\dot{w}_j$ production rate of jth species, $kg/m^3 - s$
x, y physical coordinates
γ ratio of specific heats
κ_p Planck mean absorption coefficient
λ second coefficient of viscosity, wavelength
μ dynamic viscosity, $kg/m - s$
ξ, η computational coordinates
ρ density
σ Stefan $-$ Boltzmann constant
τ shear stress
ϕ equivalence ratio
ω wave number, m^{-1}

---

[*] Graduate Research Assistant, Department of Mechanical Engineering and Mechanics. Student Member AIAA.

[†] Eminent Professor, Department of Mechanical Engineering and Mechanics. Associate Fellow AIAA.

[‡] Senior Research Scientist, Theoretical Flow Physics Branch, Fluid Mechanics Division. Associate Fellow AIAA.

Introduction

In recent years there has been a renewed interest in the development of a hypersonic transatmospheric aerospace vehicle capable of flying at suborbital speeds. A hydrogen-fueled supersonic combustion ramjet (scramjet) engine is a strong candidate for propelling such a vehicle. For a better understanding of the complex flowfield in different regions of the engine, both experimental and computational techniques are employed. Several computer programs have been developed [1-4] and applied to gain more insight into the problem involving the flow in the various sections of the scramjet module.

The combustion of hydrogen and air in the scramjet combustor results in absorbing-emitting gases such as water vapor and hydroxyl radicals. Existence of such gases makes the study of radiation heat transfer an important issue. There are several models available in the literature to represent the absorption-emission characteristics of molecular gases [5-10]. One- and two-dimensional radiative heat transfer equations for various flow and combustion related problems are available [11-19]. In earlier studies [16,18,19], both pseudo-gray and nongray gas models were employed to evaluate radiative heat transfer for chemically reacting supersonic

flow. Results of both models were compared and the pseudo-gray model was found to be computationally more efficient.

Considerable work has been carried out in the past decade to model the chemical kinetic mechanism of the hydrogen-air system. A most complete model would involve some 60 reaction paths [20], rendering numerical solution very difficult, if not impossible. A two-step chemistry model, has been used for computing supersonic combustion [4, 16, 18, 19]. This model has only four species and two reaction paths, and is useful for preliminary studies. However, there are several limitations to this model, such as ignition-phase inaccuracy (i.e. a much shorter ignition delay) and also, overprediction of flame temperature and longer reaction times. Recent improvements in this area include a 8-species, 14-reaction model [21] and a 9-species, 18-reaction model [2, 22]. While none of these aforementioned models account for nitrogen reactions (assuming nitrogen as inert), recent developments in this area include a 15-species, 35-reaction model which accounts for NO_x formation and other nitrogen reactions in the hydrogen-air system [22].

The objectives of the present study are to extend the radiative heat transfer formulation used with the global two-step chemistry model [18, 19], to the more complete models namely the 9-species, 18-reaction model as well as the 15-species, 35-reaction model. The effect of radiative heat transfer in both transverse and streamwise directions is investigated. The finite-difference method using the explicit, unsplit MacCormack scheme [23] is used to solve the governing equations.

The flowfield in the combustor is represented by the Navier-Stokes equations and by the appropriate species continuity equations [2, 3]. Incorporation of the finite-rate chemistry models into the fluid dynamic equations can create a set of stiff differential equations. Stiffness is due to a disparity in the time scales of the governing equations. In the time accurate solution, after the fast transients have decayed and the solutions are changing slowly, taking a larger time step is more efficient. But explicit methods still require small time steps to maintain stability. One way around this problem is to use a fully implicit method. However, this requires the inversion of a block multi-diagonal system of algebraic equations, which is also computationally expensive. The use of a semi-implicit technique, suggested by several investigators [24–26], provides an alternative to the above problems. This method treats the source term (which is the cause of the stiffness) implicitly, and solves the remaining terms explicitly.

Basic Governing Equations

The physical model for analyzing the flowfield in a supersonic combustor is described by the Navier-

Stokes and species continuity equations. For two-dimensional flows, these equations are expressed in physical coordinates as,

$$\frac{\partial U}{\partial t} + \frac{\partial F}{\partial x} + \frac{\partial G}{\partial y} + H = 0 \qquad (1)$$

where vectors U, F, G and H are written as,

$$U = \begin{bmatrix} \rho \\ \rho u \\ \rho v \\ \rho E \\ \rho f_j \end{bmatrix}$$

$$F = \begin{bmatrix} \rho u \\ \rho u^2 + p + \tau_{xx} \\ \rho uv + \tau_{xy} \\ (\rho E + p)u + \tau_{xx}u + \tau_{xy}v + q_{cx} + q_{Rx} \\ \rho u f_j - \rho D\frac{\partial f_j}{\partial x} \end{bmatrix}$$

$$G = \begin{bmatrix} \rho v \\ \rho uv + \tau_{yx} \\ \rho v^2 + p + \tau_{yy} \\ (\rho E + p)v + \tau_{xy}v + \tau_{yy}v + q_{cy} + q_{Ry} \\ \rho v f_j - \rho D\frac{\partial f_j}{\partial y} \end{bmatrix}$$

$$H = \begin{bmatrix} 0 \\ 0 \\ 0 \\ 0 \\ -\dot{w}_j \end{bmatrix}$$

The viscous stress tensors in the F and G terms are given as,

$$\tau_{xx} = -\lambda\left(\frac{\partial u}{\partial x} + \frac{\partial v}{\partial y}\right) - 2\mu\frac{\partial u}{\partial x} \qquad (2a)$$

$$\tau_{xy} = -\mu\left(\frac{\partial u}{\partial x} + \frac{\partial v}{\partial y}\right) \qquad (2b)$$

$$\tau_{yy} = -\lambda\left(\frac{\partial u}{\partial x} + \frac{\partial v}{\partial y}\right) - 2\mu\frac{\partial v}{\partial y} \qquad (2c)$$

where $\lambda = -\frac{2}{3}\mu$. The quantities q_{cx} and q_{cy} in the F and G terms are the components of the conduction heat flux and are expressed as

$$q_{cx} = -k\frac{\partial T}{\partial x}$$
$$q_{cy} = -k\frac{\partial T}{\partial y} \qquad (3)$$

The molecular viscosity μ is evaluated from the Sutherland's formula. The total internal energy E in Eq. (2) is given by

$$E = -\frac{p}{\rho} + \frac{u^2 + v^2}{2} + \sum_{j=1}^{m} h_j f_j \qquad (4)$$

2

Specific relations are needed for the chemistry and radiative flux terms. These are discussed in the following sections.

Chemistry and Thermodynamic Model

Chemical reaction rate expressions are usually determined by summing the contributions from each relevant reaction path to obtain the total rate of change of each species. Each path is governed by a law of mass action expression in which the rate constants can be determined from a temperature dependent Arrhenius expression. The reaction mechanism is expressed in a general form as

$$\sum_{j=1}^{ns} \gamma'_{ij} C_j \underset{k_{b_i}}{\overset{k_{f_i}}{\rightleftharpoons}} \sum_{j=1}^{ns} \gamma''_{ij} C_j \quad , \quad i = 1, nr \qquad (5)$$

where ns = number of species and nr = number of reactions. The chemistry source terms $\dot{w}_j$ in Eq. (1) are obtained, on a mass basis, by multiplying the molar changes and corresponding molecular weight as

$$\dot{w}_j = M_j \dot{C}_j = M_j \sum_{i=1}^{nr} \left(\gamma''_{ij} - \gamma'_{ij} \right) \left[k_{f_i} \prod_{m=1}^{ns} C_m^{\gamma'_{im}} \right]$$
$$\left[- k_{b_i} \prod_{m=1}^{ns} C_m^{\gamma''_{im}} \right] \quad , \quad j = 1, ns \qquad (6)$$

The reaction rate constants k_{f_i} and k_{b_i} appearing in Eqs. (5) and (6) are determined from an Arrhenius rate expression as

$$k_{f_i} = A_i T^{N_i} exp\left(-\frac{E_i}{RT} \right) \qquad (7)$$

where ,

$$k_{b_i} = \frac{k_{f_i}}{k_{eq_i}} \qquad (8)$$

$$k_{eq_i} = \left(\frac{1}{RT} \right)^{\Delta n} exp\left(\frac{-\Delta G_{R_i}}{RT} \right) \qquad (9)$$

The coefficients A , N and E appearing in Eq. (7) are given in Table 1. The term Δn in Eq. (9) denotes the difference in the number of moles of reactants and products.

The Gibbs energy term in Eq. (9) is calculated as

$$\Delta G_{R_i} = \sum_{j=1}^{ns} \gamma''_{ij} g_j - \sum_{j=1}^{ns} \gamma'_{ij} g_i \quad , \quad j = 1, nr \quad (10)$$

$$\frac{g_j}{R} = A_j(T - lnT) + \frac{B_j}{2}T^2 + \frac{C_j}{6}T^3$$
$$+ \frac{D_j}{12}T^4 + \frac{E_j}{20}T^5 + F_j + G_j T \qquad (11)$$

The gas constant for the mixture is evaluated by a mass-weighted summation over all species as

$$\overline{R} = \sum_{j=1}^{n} f_j R_j \qquad (12)$$

$$P = \rho \overline{R} T \qquad (13)$$

Radiation Transfer Model

Evaluation of the energy equation presented in Eq. (1) requires an appropriate expression for the radiative flux term, q_R . Therefore, a suitable radiative transport model is needed. Various models are available in the literature to represent the absorption-emission characteristics of the molecular species [10]. The equations of radiative transport are expressed generally in integro-differential forms. The integration involves both the frequency spectrum and physical coordinates. In many realistic three-dimensional physical problems, the complexity of the radiative transport equations can be reduced by introduction of the tangent-slab approximation. This approximation treats the gas layer as a one-dimensional slab in evaluation of the radiative flux (Fig. 1).

Detailed derivations of radiative flux equations for gray as well as nongray radiation have been carried out previously [15, 19]. For a multiband gaseous system, the nongray radiative flux in the normal direction is expressed as

$$q_R(y) = e_1 - e_2 + \sum_{i=1}^{n} A_{oi} \{ \int_0^y \left[\frac{de_{\omega_i}(z)}{dz} \right] \times$$
$$\bar{A}_i \left[\frac{3}{2} \frac{u_{o_i}}{L}(y - z) \right] dz + \qquad (14)$$
$$+ \int_y^L \left[\frac{de_{\omega_i}(z)}{dz} \right] \bar{A}_i \left[\frac{3}{2} \frac{u_{0i}}{L}(z - y) \right] dz \}$$

The information on the band absorptance $\bar{A}_i$ and other quantities is available in the cited references.

For a gray medium, the spectral absorption coefficient κ_ω is independent of the wave number, and an expression for the radiative flux is obtained as [5, 16, 19]

$$q_R(y) = e_1 - e_2 + \frac{3}{2} \{ \int_0^y [e(z) - e_1] e^{-\frac{3\kappa(y-z)}{2}} \kappa dz$$
$$- \int_y^L [e(z) - e_2] e^{-\frac{3\kappa(y-z)}{2}} \kappa dz \} \qquad (15)$$

3

It is computationally more efficient to use Eq. (15) in the general energy equation than Eq. (14). This is because by differentiating Eq. (15) twice (using the Leibnitz formula) the integrals are eliminated and the following inhomogenous ordinary differential equation is obtained :

$$\frac{1}{\kappa^2}\frac{d^2 q_R(y)}{dy^2} - \frac{9}{4}q_R(y) = \frac{3}{\kappa}\frac{de(y)}{dy} \qquad (16)$$

The solution of Eq. (16) requires two boundary conditions which are given for non-black diffuse surfaces as [5]

$$\left(\frac{1}{\epsilon_1} - \frac{1}{2}\right)[q_R(y)]_{y=0} - \frac{1}{3\kappa}\left[\frac{dq_R}{dy}\right]_{y=0} = 0 \qquad (17a)$$

$$\left(\frac{1}{\epsilon_2} - \frac{1}{2}\right)[q_R(y)]_{y=L} + \frac{1}{3\kappa}\left[\frac{dq_R}{dy}\right]_{y=L} = 0 \qquad (17b)$$

For black surfaces $\epsilon_1 = \epsilon_2 = 1$ and Eqs. (17) reduce to simpler forms.

An appropriate model for a gray gas absorption coefficient is required in Eqs. (15) — (17). This is represented by the Planck mean absorption coefficient, which is expressed for a multi-band system as [5, 19]

$$\kappa = \kappa_P = \frac{P_j}{\sigma T^4(y)}\sum_{i=1}^{n}e_{\omega_i}(T)S_i(T) \qquad (18)$$

It should be noted that κ_P is a function of the temperature and the partial pressures P_j of the species.

Method of Solution

The governing equations are transformed from the physical domain (x , y) to a computational domain (ξ , η), using an algebraic grid generation technique similar to the one used by Smith and Weigel [27]. In the computational domain, Eq. (1) is expressed as

$$\frac{\partial \widehat{U}}{\partial t} + \frac{\partial \widehat{F}}{\partial \xi} + \frac{\partial \widehat{G}}{\partial \eta} + \widehat{H} = 0 \qquad (19)$$

where

$$\widehat{U} = UJ, \quad \widehat{F} = Fy_\eta - Gx_\eta$$
$$\widehat{G} = Gx_\xi - Fy_\xi, \quad \widehat{H} = HJ \qquad (20)$$
$$J = x_\xi y_\eta - y_\xi x_\eta$$

Once the temporal discretization has been performed, the resulting system is spatially differenced using the explicit, unsplit MacCormack predictor-corrector scheme [23]. This results in a spatially and temporally discrete, simultaneous system of equations at each grid point [25, 26]. Each simultaneous system is solved, subject to initial and boundary conditions, by using

the Householder technique [28, 29]. At the supersonic inflow boundary, all flow quantities are specified as freestream conditions. At the supersonic outflow boundary, non-reflective boundary conditions are used, i.e. all flow quantities are extrapolated from interior grid points. The upper and lower boundaries are treated as solid walls. This implies a non-slip boundary condition (i.e. zero velocities). The wall temperature and pressure are extrapolated from interior grid points. Initial conditions are obtained by specifying freestream conditions throughout the flowfield. The resulting set of equations is marched in time, until convergence is achieved. The details of the radiative flux formulation and method of solution are available in [19].

Results and Discussion

Based on the theory and computational procedures described previously, an algorithm has been developed to solve the two-dimensional Navier-Stokes equations for chemically reacting and radiating supersonic flows. The extent of radiative heat transfer in supersonic flows undergoing hydrogen-air chemical reactions, has been investigated using three chemical kinetics models, accounting for increasing number of reactions and participating species. For the temperature range considered in this study, the important radiating species are OH and H_2O. The gray gas formulations are based on the Planck mean absorption coefficient which accounts for the detailed information on different molecular bands. The radiative fluxes have been computed using this 'pseudo-gray' formulation. The justification for using this model is provided in [19].

The specific problem considered is the supersonic flow of premixed hydrogen and air (stoichiometric equivalence ratio $\phi = 1.0$) in a channel with a compression corner on the lower boundary (Fig. 2). The physical dimensions considered for obtaining results are L = 2 cm., X_1 = 1cm., X_2 = 2cm., L_X = X_1 + X_2 = 3 cm. , and α = 10 degrees . The flow is ignited by the shock from the compression corner. The inlet conditions which are representative of scramjet operating conditions, are P_{∞} = 1.0 atm., T_{∞} = 900 K and M_{∞} = 4.0. This same flow has been computed by several CFD research groups [4, 18, 19, 21] as a benchmark case.

Figures 3–6 show the computed results using a 31 x 31 grid , for temperature and pressure as well as H_2O and OH species mass fractions, varying along x at the location y = 0.02 cm from the lower wall (boundary layer region). Figures 3 and 4 show the temperature and pressure profiles predicted by the three chemistry models. The temperatures in the boundary layer show a gradual increase(Fig. 3). The pressure profiles are plotted at y = 0.13 cm. (inviscid region) and show a sharp increase due to the shock (Fig. 4). The ignition-phase inaccuracies of the three chemistry models can

4

be seen in Figs. 5 and 6. The shock is occurring after $x / L_X = 0.3$. However, the 2-step model predicts ignition before the shock (shorter ignition delay) due to the high temperature in the boundary layer. On the other hand, the 18-step model predicts a longer ignition delay, at $x / L_X = 0.37$ (Fig. 5). The 35-step model's prediction of ignition delay appears to be an average of the other two models. Although the three models do not differ much in prediction of temperature and pressure profiles, they do differ significantly in predictions of species productions (Figs. 5, 6).

In order to resolve this discrepancy, a grid sensitivity study was carried out to examine whether the grid size affects the flow predictions. The results of three grid distributions 11 x 31, 31 x 31 and 61 x 31 are shown in Fig. 7, and it appears that the 31 x 31 grid is sufficient for the present study.

The reason for the varying predictions of species production by the three models was further examined and the results are shown in Figs. 8 and 9. Figure 8 shows that the Reaction No. 8 in Table 1 is critical in determining the extent of chemical heat release and H_2O production. Reaction No. 8 deals with production of HO_2 radical. This reaction is absent from the 2-step model, while it is common to both the 18-step and 35-step models. Figure 8 shows that the 35-step model experiences nearly a 30% drop in temperature at the channel exit, when the rate of Reaction No. 8 is reduced by a factor of 1000 (effectively cutting off the production of the HO_2 radical). In contrast, the 18-step model shows a 15% drop in temperature, when subjected to the same reduction in rate of Reaction No. 8. This shows that the Reaction No. 8 controls the overall H_2O production occurring in Reaction Nos. 9-18 (Table 1). Due to the high temperatures (~ 3000 K) in the flowfield, there is a pool of highly reactive free radicals like H, O, etc. The HO_2 radical is converted to the very reactive OH radical, by the free radicals (Reaction Nos. 11 and 12). This establishes the HO_2 radical as a very important species in promoting flame propagation in hydrogen-air flames. A similar study has been carried out in [30]. Since the 2-step model does not have the HO_2 radical, it predicts lesser amounts of OH and H_2O.

It was necessary to determine the reason for the higher sensitivity of the 35-step model to the HO_2 radical, as compared to the 18-step model. Figure 9 shows that the Reaction Nos. 21 and 23 in Table 1 are critical in determining the extent of chemical heat release and H_2O production. Reaction Nos. 21 and 23 deal with production of the NO radical. These reactions are absent from the 2-step and 18-step models, whereas they play an important role in the 35-step model. Figure 9 shows that the 35-step model undergoes a 30% reduction in temperature, when the rates of Reaction Nos. 21 and 23 are reduced by a factor of 1000 (ef-

fectively cutting off the production of the NO radical). This is nearly the same reduction caused by reducing the rate of Reaction No. 8 by a factor of 1000. Due to the high temperatures in the flowfield, the usually inert nitrogen dissociates into the highly reactive N free radical. This free radical N is then oxidized in Reaction Nos. 21 and 23, thereby producing the NO radical. This NO radical converts the HO_2 radical into the highly reactive OH radical, through Reaction No. 29. This confirms that the NO radical is a very important species for flame propagation in a hydrogen-fueled supersonic combustor. Since the 35-step model has the NO radical, it predicts higher amounts of OH and H_2O than the 18-step model.

Based on the above understanding of the chemical kinetics of supersonic hydrogen-air flames, the radiative interactions were examined. Figure 10 shows the profiles of the normalized streamwise radiative flux q_{Rx} predicted by the three chemistry models, along the location $y = 0.02$ cm. from the lower wall. The q_{Rx} flux reduces towards the end of the channel due to cancellation of fluxes in positive and negative directions. It is seen from Fig. 10 that the 18-step and 35-step models predict significantly higher amounts (50% more and 100% more, respectively) of q_{Rx} than the 2-step model. This is because radiative heat tranfer is a strong function of temperature, pressure and species concentrations. So the larger values of radiative fluxes are caused by higher amounts of H_2O concentrations, which in turn, depend on reactions involving HO_2 and NO species.

Figure 11 shows the variations of the normal radiative flux q_{Ry} along x, at the location $y = 0.02$ cm. These do not appear to vary significantly between the three chemistry models. However, in all three cases, the q_{Ry} value increases rapidly after the shock.

Figures 12-15 show the computed results for reacting flows with and without radiation, for the three chemistry models. It is seen that the 2-step model shows only slight effect of radiative interaction, as compared to the 18-step and 35-step models. The 18-step and 35-step models predict lower temperature and lower H_2O and OH concentrations after the shock. This is because of the q_{Rx} flux, which reduces the total energy. Comparison of results in Figs. 12-15 shows that the 35-step model exhibits stronger effect of radiative interactions, than the other two models.

For reacting flows without radiation, it was seen from Figs. 5 and 6 that the 18-step model had a longer ignition delay (ignition at $x / L_X = 0.37$), while the 35-step model had a shorter ignition delay (ignition at $x / L_X = 0.27$). Another effect of radiative interactions, seen in Fig. 14, is to nullify this difference in predictions of ignition delay. For both 18-step and 35-step models, with radiation, the ignition is seen to occur at

the same point, $x / L_x = 0.33$. No such effect is seen on the ignition characteristics of the 2-step model.

Conclusions

The two-dimensional, spatially elliptic Navier-Stokes equations have been used to obtain solutions for supersonic flows undergoing finite-rate chemical reactions along with radiative interactions. The specific problem considered is of the premixed flow in a channel with a ten-degree compression ramp. The inlet conditions used in the present study correspond to typical flow conditions of a scramjet engine. Three different chemistry models were used for parametric studies, accounting for increasing number of reactions and participating species. It is seen that the radiative interactions vary significantly, depending particularly on chemical reactions involving HO_2 and NO species. These reactions have a substantial effect on the flow-field, with regard to H_2O concentration, temperature and pressure. Also, it is observed that the difference in the ignition delays of two chemistry models invoving HO_2 reactions is nullified as a result of radiative interaction. The results also show that the streamwise radiative flux reduces the temperature and concentration of species. This effect is a strong function of the amount of H_2O species concentration.

Acknowledgements

References

1. Kumar, A., "Numerical Simulation of Scramjet Inlet Flowfield," NASA TP-25117, May 1986.

2. Drummond, J. P., Hussaini, M. Y. and Zang, T. A., "Spectral Methods for Modelling Supersonic Chemically Reacting Flowfields,"AIAA Journal, Vol. 24, No. 9, September 1986, pp. 1461-1467 ; also Drummond, J. P., "Numerical Simulation of Supersonic Chemically Reacting Mixing Layers," Ph.D. Dissertation, George Washington University, May 1987.

3. Drummond, J. P., Rogers, R. C. and Hussaini, M. Y., "A Detailed Numerical Model of a Supersonic Reacting Mixing Layer," AIAA Paper No. 86-1427, June 1986.

4. Chitsomboon, T., Kumar, A., Drummond, J. P. and Tiwari, S. N., "Numerical Study of Supersonic Combustion Using a Finite-Rate Chemistry Model," AIAA Paper 86-0309, January 1986.

5. Sparrow, E. M. and Cess, R. D., "Radiation Heat Transfer," Brooks/Cole, Belmont, CA, 1966 and 1970. New Augmented Edition, Hemisphere Publ. Corp. Washington, D.C., 1978.

6. Tien, C. L., "Thermal Radiation Properties of Gases," Advances in Heat Transfer, Vol. 5, Academic Press, New York, 1968.

7. Cess, R. D. and Tiwari, S. N., "Infrared Radiative Energy Transfer in Gases," Advances in Heat Transfer, Vol. 8, Academic Press, New York, 1972.

8. Edwards, D. K., "Molecular Gas Band Radiation," Advances in Heat Transfer, Vol. 12, Academic Press, New York, 1976.

9. Tiwari, S. N., "Band Models and Correlations for Infrared Radiation," Radiative Transfer and Thermal Control (Progress in Aeronautics and Astronautics, Vol. 49), American Institute of Aeronautics and Astronautics, New York, 1979.

10. Tiwari, S. N., "Models for Infrared Atmospheric Radiation," Advances in Geophysics, Vol. 20, Academic Press, New York, 1978, pp. 1-85.

11. Tsai, S.S. and Chan, S. H., "Multi-Dimensional Radiative Transfer in Non-Gray Gases-General Formulation and the Bulk Radiative Exchange Approximation," Journal of Heat Transfer, Vol. 100, August 1978.

12. Chung, T.J. and Kim, J. Y., "Two-Dimensional Combined Mode Heat Transfer by Conduction, Convection and Radiation in Emitting, Absorbing and Scattering Media-Solution By Finite Elements," Journal of Heat Transfer, Vol. 106, pp. 448-452, May 1984.

13. Im, K.H. Ahluwalia, R. K., "Combined Convection and Radiation in Rectangular Duct," International Journal of Heat and Mass Transfer, Vol. 27, pp. 221-231, 1984.

14. Soufiani, A. and Taine, J., "Application of Statistical Narrow-Band Models to Coupled Radiation and Convection at High Temperature," International Journal of Heat and Mass Transfer, Vol. 30, No. 3, pp. 437-447, 1987.

15. Tiwari, S. N., "Radiative Interaction in Transient Energy Transfer in Gaseous Systems," NASA CR-176644, December 1985.

16. Mani, M., Tiwari, S. N. and Drummond, J. P., "Numerical Solution of Chemically Reacting and Radiating Flows," AIAA Paper 87-0324, January, 1987.

17. Tiwari, S. N. and Singh, D. J., "Interaction of Transient Radiation in Fully Developed Laminar Flow," AIAA Paper 86-1521, June 1987.

18. Mani, M., Tiwari, S. N. and Drummond, J. P., "Investigation of Two-Dimensional Chemically Reacting and Radiative Supersonic Channel Flows," AIAA Paper 88-0462, January 1988.

19. Mani, M. and Tiwari, S. N., "Investigation of Supersonic Chemically Reacting and Radiating Channel Flow," NASA CR-182726, January 1988 ; also Ph.D. Dissertation by M. Mani, Old Dominion University, May 1988.

20. Rogers, R. C. and Shnexnayder, C. J., Jr., "Chemical Kinetic Analysis of Hydrogen-Air Ignition and reaction Time," NASA TP-1856, 1981.

21. Shuen, S. J. and Yoon, S., "Numerical Study of Chemically Reacting Flows Using a Lower-Upper Symmetric Successive Overrelaxation Scheme," AIAA Journal , Vol. 27, No. 12, December 1989.

22. Carpenter, M. H., "A Generalized Chemistry Version of SPARK," NASA CR-4196, December 1988.

23. MacCormack, R. W., "The Effect of Viscosity in Hypervelocity Impact Cratering," AIAA Paper 69-354, May, 1969.

24. Smoot, L. D., Hecker, W. C. and Williams, G. A., "Prediction of Propagating Methane-Air Flames," Combustion and Flame , Vol. 26, 1976.

25. Stalnaker, J. F., Robinson, M. A., Spradley, L. W., Kurzius, S. C. and Theores, D., "Development of the General Interpolants Methods for the CYBER 200 series of Computers," Report TR-0867354, Lockheed-Huntsville Research Engg. Center, Huntsville, Alabama, October 1983.

26. Bussing, T. R. and Murman, E. M., "A Finite Volume Method for the Calculation of Compressible Chemically Reacting Flows," AIAA Paper 85-0331, January 1985.

27. Smith, R. E. and Weigel, B. L., "Analytical and Approximation Boundary Fitted Coordinates System for Fluid Flow Simulation," AIAA Paper 80-0192, January 1980.

28. Wilkins, J. H., The Algebraic Eigenvalue Problem , Oxford University Press, Oxford, England, 1965, pp. 233-236.

29. Householder, A. S., The Theory of Matrices in Numerical Solution Analysis , Dover Publication, New York, 1964, pp. 122-140.

30. Jachimowski, C. J., "An Analytical Study of the Hydrogen-Air Reaction Mechanism with Application to Scramjet Combustion," NASA TP-2791, February 1988.

Table 1. Hydrogen-Air Combustion Mechanism [22]

| REACTION	A(moles)	N(cm^3)	E(calories/gm-mole)
** following reactions constitute the 18-step model **			
(1) $O_2 + H_2 \leftrightarrow OH + OH$	1.70×10^{13}	0	48150
(2) $O_2 + H \leftrightarrow OH + O$	1.42×10^{14}	0	16400
(3) $H_2 + OH \leftrightarrow H_2O + H$	3.16×10^{7}	1.8	3030
(4) $H_2 + O \leftrightarrow OH + H$	2.07×10^{14}	0	13750
(5) $OH + OH \leftrightarrow H_2O + O$	5.50×10^{13}	0	7000
(6) $H + OH + M \leftrightarrow H_2O + M$	2.21×10^{22}	—2.0	0
(7) $H + H + M \leftrightarrow H_2 + M$	6.53×10^{17}	—1.0	0
(8) $H + O_2 + M \leftrightarrow HO_2 + M$	3.20×10^{18}	—1.0	0
(9) $OH + HO_2 \leftrightarrow O_2 + H_2O$	5.00×10^{13}	0	1000
(10) $H + HO_2 \leftrightarrow H_2 + O_2$	2.53×10^{13}	0	700
(11) $H + HO_2 \leftrightarrow OH + OH$	1.99×10^{14}	0	1800
(12) $O + HO_2 \leftrightarrow O_2 + OH$	5.00×10^{13}	0	1000
(13) $HO_2 + HO_2 \leftrightarrow O_2 + H_2O_2$	1.99×10^{12}	0	0
(14) $H_2 + HO_2 \leftrightarrow H + H_2O_2$	3.01×10^{11}	0	18700
(15) $OH + H_2O_2 \leftrightarrow H_2O + HO_2$	1.02×10^{13}	0	1900
(16) $H + H_2O_2 \leftrightarrow H_2O + OH$	5.00×10^{14}	0	10000
(17) $O + H_2O_2 \leftrightarrow OH + HO_2$	1.99×10^{13}	0	5900
(18) $H_2O_2 + M \leftrightarrow OH + OH + M$	1.21×10^{17}	0	45500
** remaining reactions complete the 35-step model **			
(19) $O_2 + M \leftrightarrow O + O + M$	2.75×10^{19}	—1.0	118700
(20) $N_2 + M \leftrightarrow N + N + M$	3.70×10^{21}	—1.6	225000
(21) $N + O_2 \leftrightarrow O + NO$	6.40×10^{9}	1.0	6300
(22) $N + NO \leftrightarrow O + N_2$	1.60×10^{13}	0	0
(23) $N + OH \leftrightarrow H + NO$	6.30×10^{11}	0.5	0
(24) $H + NO + M \leftrightarrow HNO + M$	5.40×10^{15}	0	—600
(25) $H + HNO \leftrightarrow H_2 + NO$	4.80×10^{12}	0	0
(26) $O + HNO \leftrightarrow OH + NO$	5.00×10^{11}	0.5	0
(27) $OH + HNO \leftrightarrow H_2O + NO$	3.60×10^{13}	0	0
(28) $HO_2 + HNO \leftrightarrow H_2O_2 + NO$	2.00×10^{12}	0	0
(29) $HO_2 + NO \leftrightarrow OH + NO_2$	3.43×10^{12}	0	—260
(30) $H + NO_2 \leftrightarrow OH + NO$	3.50×10^{14}	0	1500
(31) $O + NO_2 \leftrightarrow O_2 + NO$	1.00×10^{13}	0	600
(32) $NO_2 + M \leftrightarrow O + NO + M$	1.16×10^{16}	0	66000
(33) $M + OH + NO \leftrightarrow HNO_2 + M$	5.60×10^{15}	0	—1700
(34) $M + OH + NO_2 \leftrightarrow HNO_3 + M$	3.00×10^{15}	0	—3800
(35) $OH + HNO_2 \leftrightarrow H_2O + NO_2$	1.60×10^{12}	0	0
** following reactions constitute the global 2-step model [4, 16, 18, 19] **			
(1") $H_2 + O_2 \leftrightarrow 2 OH$	11.4×10^{47}	—10.0	4865
(2") $2 OH + H_2 \leftrightarrow 2 H_2O$	2.50×10^{44}	—13.0	42500
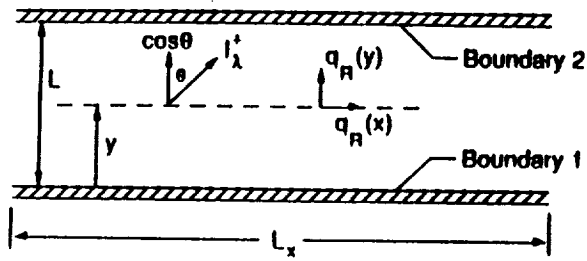
7

Fig. 1 Plane radiating layer between parallel boundaries
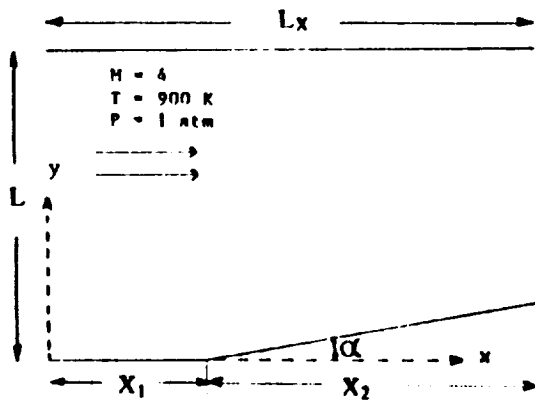
Fig. 2 Geometry for the premixed H_2—Air reacting flow

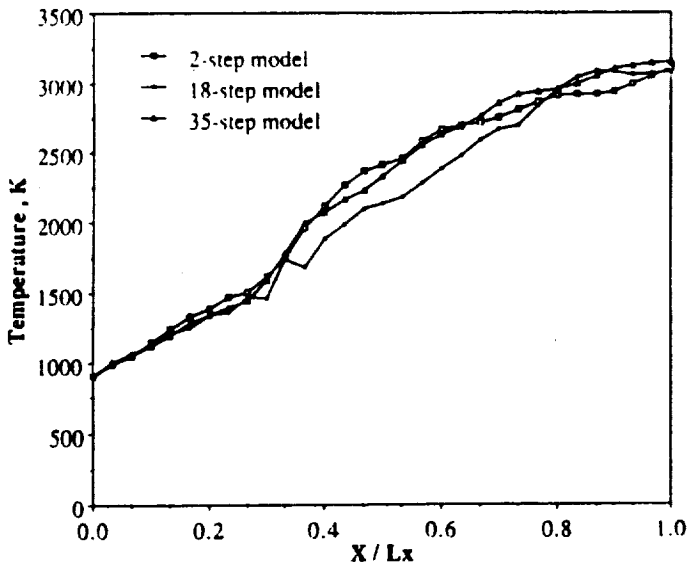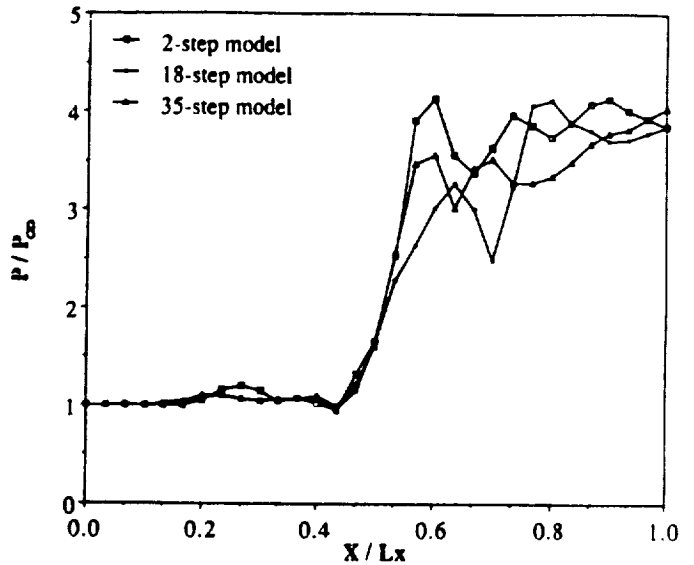Fig. 4 Pressure profiles (y = 0.13 cm.)

Fig. 5 H_2O mass fraction profiles
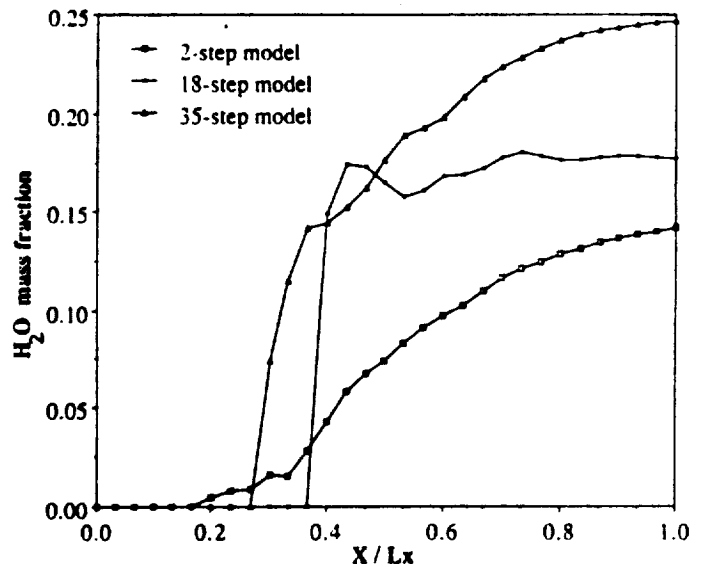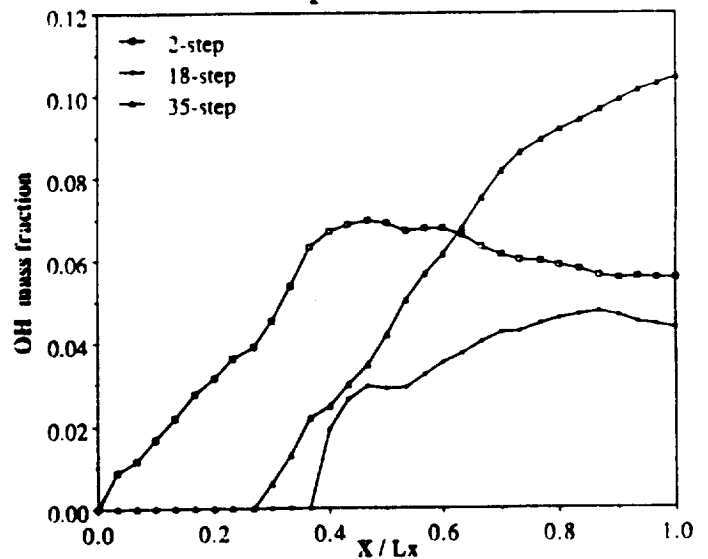

Fig. 3 Temperature profiles
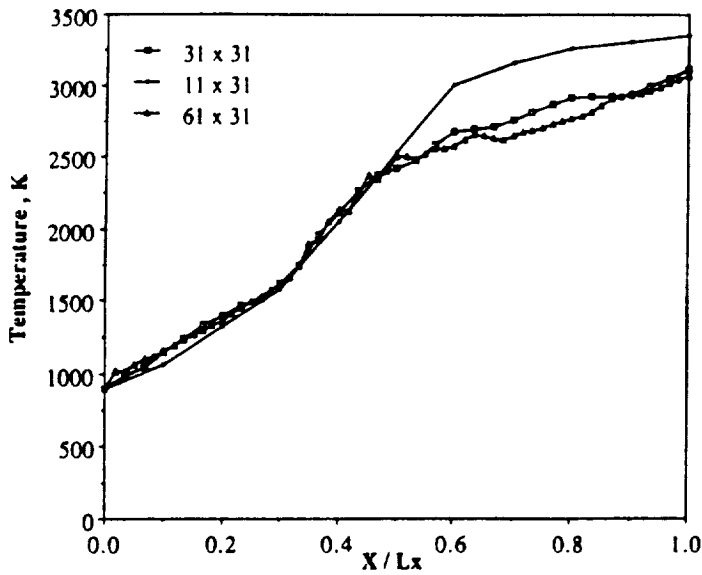

Fig. 6 OH mass fraction profiles
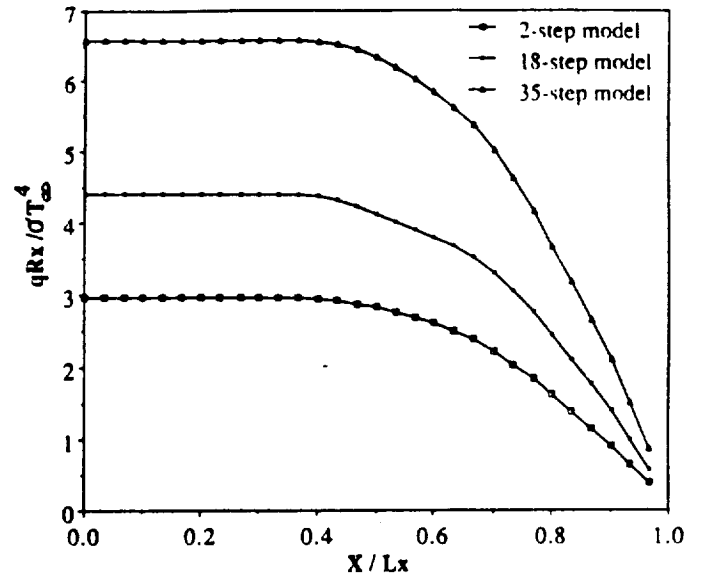
8

Fig. 7   Grid sensitivity results
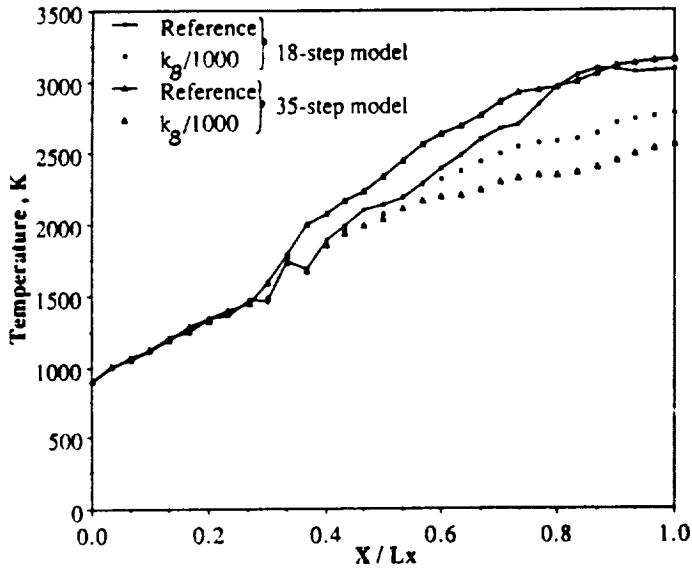

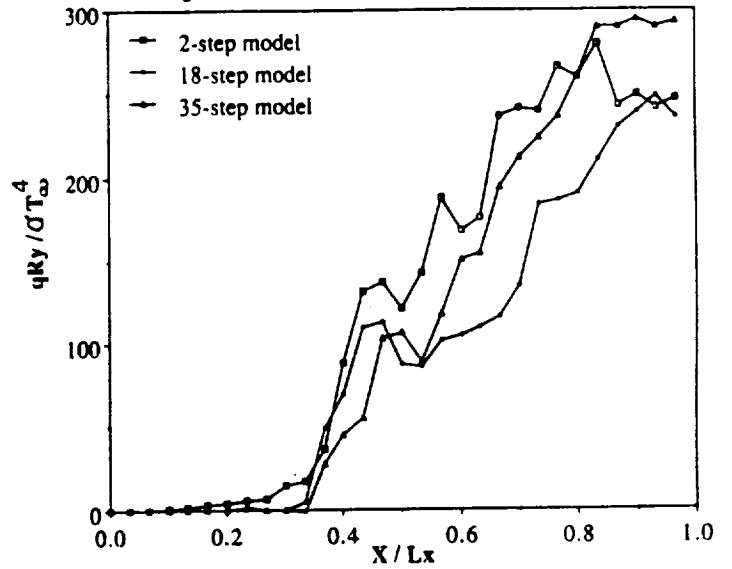Fig. 10   Profiles of streamwise radiative flux

Fig. 8   Effect of reaction rates
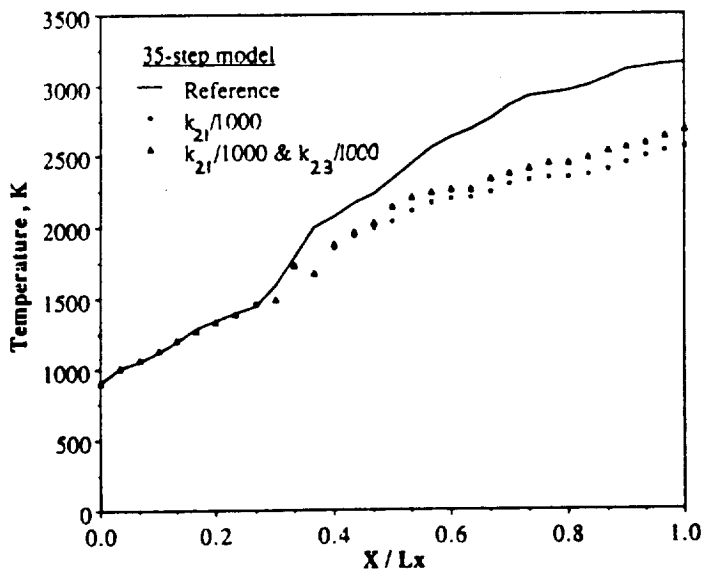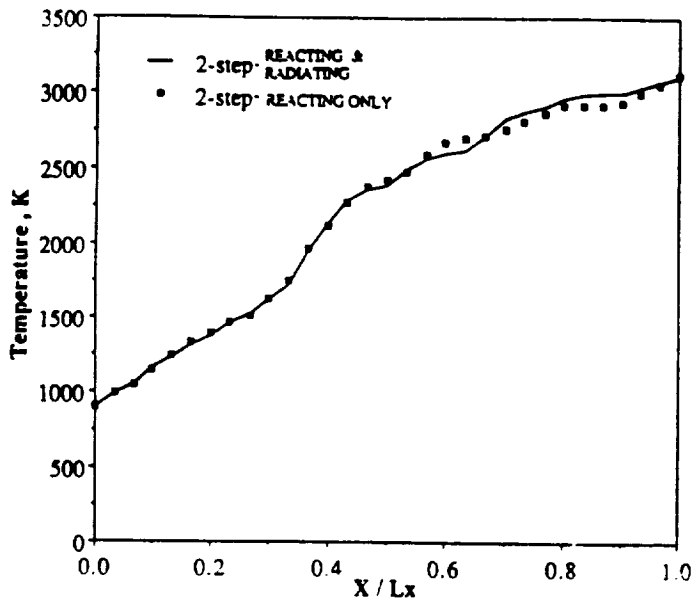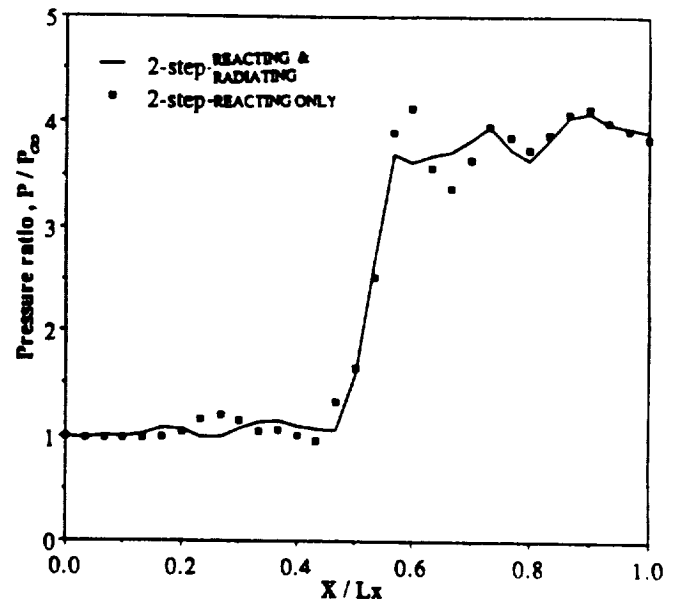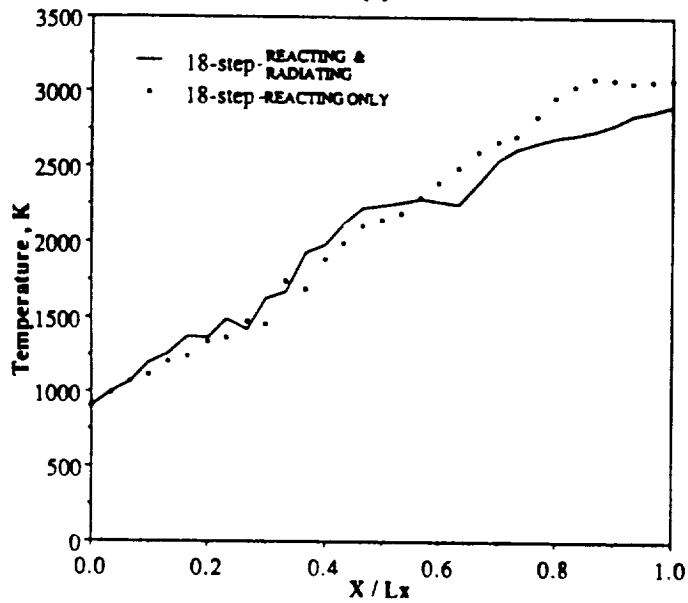

Fig. 11   Profiles of normal radiative flux

Fig. 9   Effect of NO and HO_2 reactions
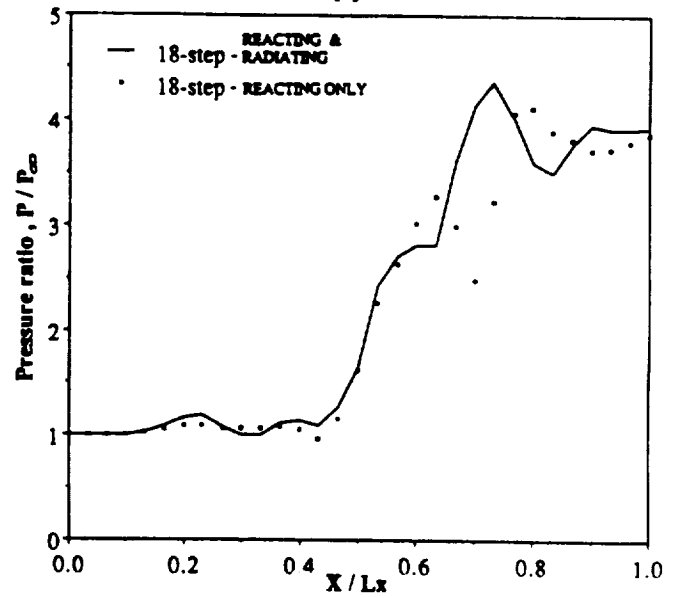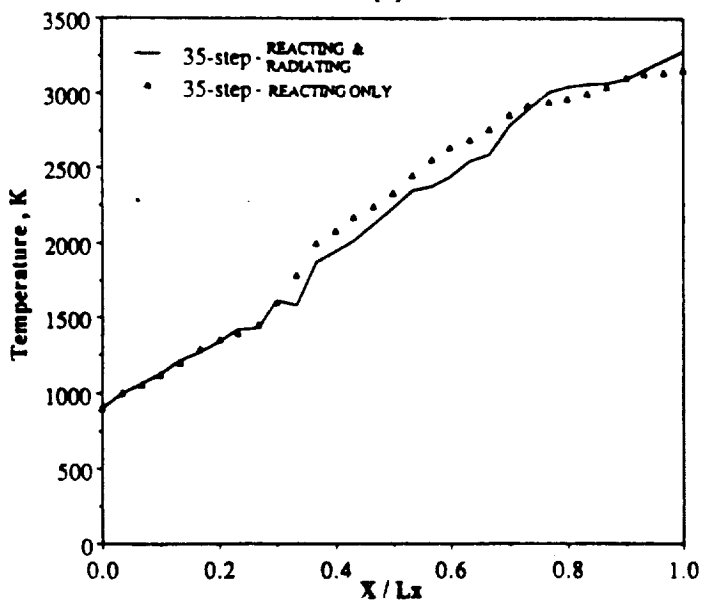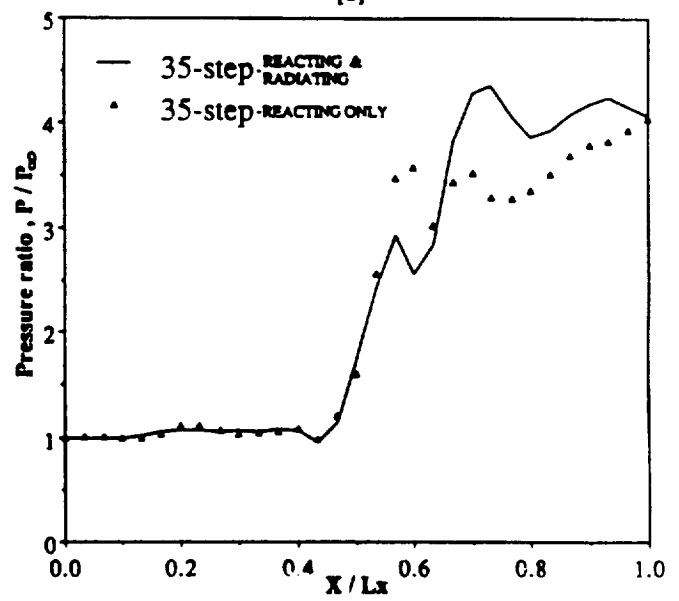
Fig. 12   Radiation effects on temperature profiles

Fig. 13   Radiation effects on pressure profiles (y = 0.13 cm)
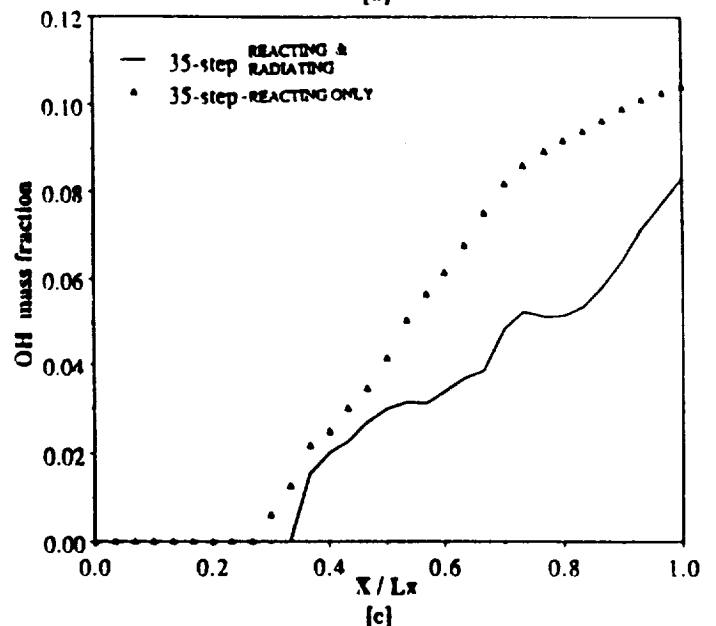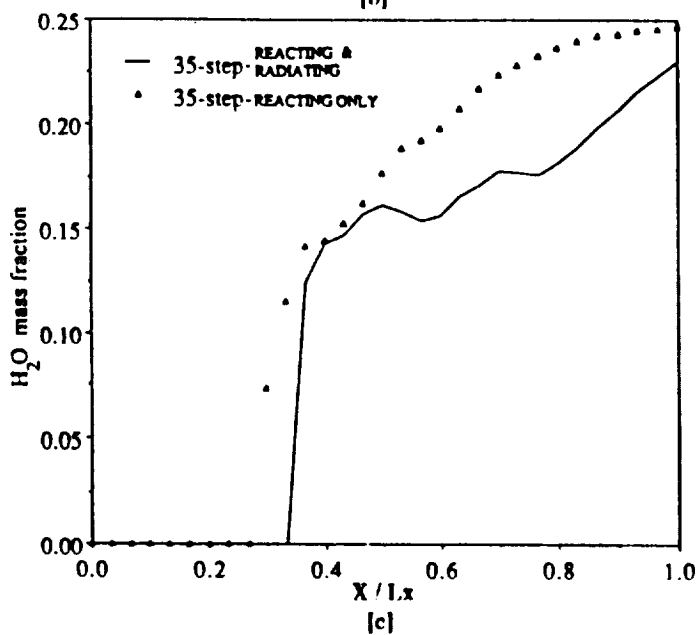
Fig. 14 Radiation effects on H_2O profiles
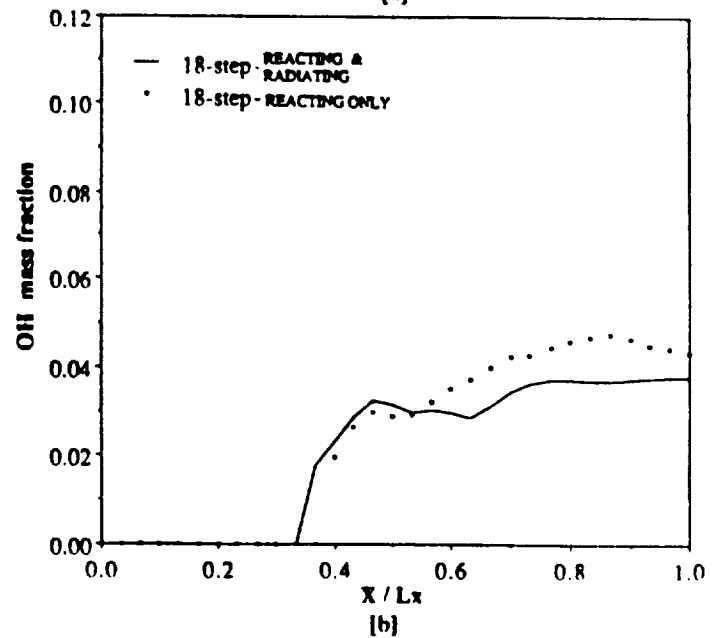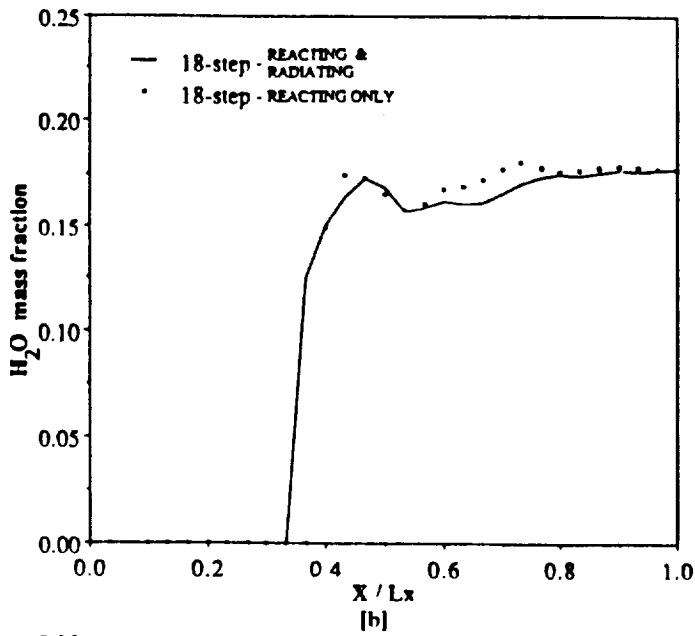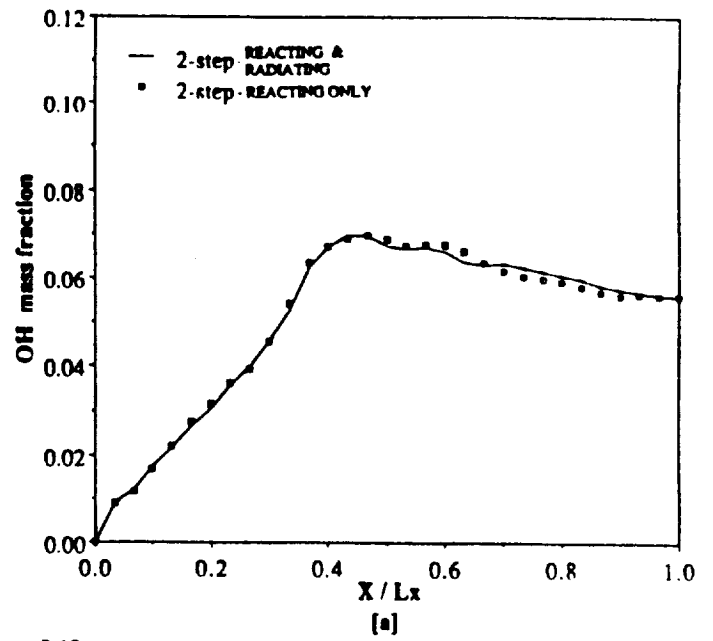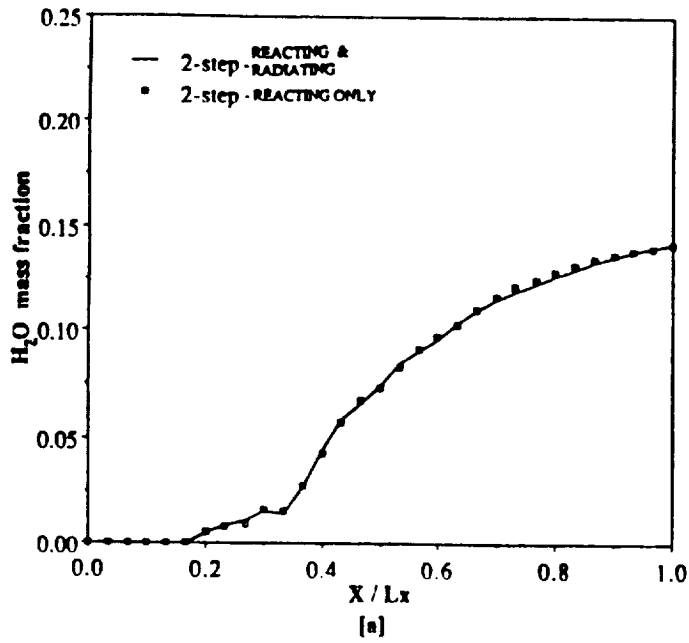
Fig. 15 Radiation effects on OH profiles

11

AIAA-91-0572

INVESTIGATION OF RADIATIVE INTERACTIONS IN CHEMICALLY REACTING SUPERSONIC INTERNAL FLOWS

S. N. Tiwari, R. Chandrasekhar, and A. M. Thomas
Old Dominion University
Norfolk, VA

J. P. Drummond
NASA Langley Research Center
Hampton, VA

29th Aerospace Sciences Meeting
January 7-10, 1991/Reno, Nevada

INVESTIGATION OF RADIATIVE INTERACTIONS IN CHEMICALLY REACTING SUPERSONIC INTERNAL FLOWS

S. N. Tiwari[1], R. Chandrasekhar[2], and A.M. Thomas[3]
Old Dominion University, Norfolk, Virginia 23529–0247
and
J.P. Drummond[4]
NASA Langley Research Center, Hampton, Virginia 23665–5225

Abstract

Analyses and numerical procedures are presented to investigate the radiative interactions of absorbing-emitting species in chemically reacting supersonic flow in various ducts. Specific attention is directed in investigating the radiative contributions of H_2O, OH, and NO under realistic physical and flow conditions. The radiative interactions in reacting flows are investigated by considering the supersonic flow of premixed hydrogen and air in a channel with a compression corner at the lower boundary. The results indicate that radiation can have significant influence on the flowfield and species production depending on the chemistry model employed.

Nomenclature

A	band absorptance, m^{-1}
A_o	band width parameter, m^{-1}
C_j	concentration of the jth species, kg-mole/m^3
e_ω	Planck's function
E	total internal energy
f_j	mass fraction of jth species
h	static enthalpy, J/kg
k	thermal conductivity, J/m-s-k

---

[1]   Eminent Professor, Dept. of Mechanical Engineering and Mechanics. AIAA Associate Fellow
[2]   Graduate Research Assistant, Dept. of Mechanical Engineering and Mechanics. AIAA Student Member
[3]   Graduate Research Assistant, Dept. of Mechanical Engineering and Mechanics.
[4]   Research Scientists, Theoretical Flow Physics Branch, Fluid Mechanics Division. AIAA Associate Fellow.

k_b	backward rate constant
k_f	forward rate constant
P	pressure, N/m^2
P_j	partial pressure of jth species
q_R	total radiative heat flux, J/m^2-s
$q_{R\omega}$	spectral radiative heat flux, J/m^3-s
R	gas constant, J/kg-K
S	integrated band intensity, $(N/m^2)^{-1}m^{-2}$
T	temperature, K
u,v	velocity in x- and y-direction, m/s
$\dot{w}_j$	production rate of jth species, kg/m^3-s
x,y	physical coordinates
κ_ω	spectral absorption coefficient, m^{-1}
κ_p	Planck mean absorption coefficient
λ	second coefficient of viscosity, wave length, m
μ	dynamic viscosity (laminar flow), kg/m-s
ξ, η	computational coordinates
ρ	density
σ	Stefan-Boltzmann constant, erg/S-cm^2-K^4
τ	shear stress
ϕ	equivalence ratio
ω	wave number, m^{-1}

Introduction

There is a renewed interest in investigating various aspects of radiative energy transfer in participating mediums. Radiative interactions become important in many engineering problems involving high temperature gases. Recent interest lies in the areas of design of high pressure combustion chambers and high enthalpy nozzles, entry and reentry phenomena, hypersonic propulsion, and defence oriented research.

Basic formulations on radiative energy transfer in participating mediums are available in standard references [1–5]. The review articles presented in [6–15] are useful in understanding the radiative properties of participating species and the nature of nongray radiation. The validity of radiative transfer analyses depends upon the accuracy with which absorption-emission and scattering characteristics of participating species are modeled. There are several models available to represent the absorption-emission characteristics of molecular species and these are reviewed in [12, 13]. These models have been used to investigate radiative interactions in several duct flows [16–29].

The purpose of this study is to investigate the effect of radiative heat transfer in chemically reacting supersonic flow in various ducts under different physical and flow conditions. This provides essential information for investigating the effect of radiative interactions in the combustor of a supersonic combustion ramjet (scramjet) engine. This hydrogen-fueled engine is proposed for propelling transatmospheric hypersonic vehicles. Several basic codes have been developed to compute the flowfield in a scramjet engine [21–24]. The combustion of hydrogen and air results in absorbing-emitting gases such as H_2O, OH, and NO. Specific attention, therefore, is directed in investigating the radiative contributions of these gases under realistic conditions. In essence, the present effort is a continuating of the earlier work conducted in this area of research [25–27]. Extensive literature survey is provided in the cited references. A comparison of different chemistry models used in investigating radiative interactions is presented in [28].

Basic Governing Equations

The physical problem considered to investigate the effect of radiative interactions in supersonic flow are two-dimensional laminar flow between two parallel plates (Fig. 1a) and within a circular tube (Fig. 1b). Another geometry is considered to study the effect of shocks and chemical reactions on the radiative heat transfer and this consists of a channel with a compression-expansion ramp (Fig. 1c). The governing equations and boundary conditions are provided here for all physical problems considered in this study.

The physical problem considered for basic understanding of radiative interaction in supersonic flows is two-dimensional variable property laminar flow between two parallel plates. For this model, two-dimensional Navier-Stokes equations in fully conservative form are used to describe the flow field. These equations, in physical domain, can be written as [27,29]

$$\frac{\partial U}{\partial t} + \frac{\partial F}{\partial x} + \frac{\partial G}{\partial y} + H = 0 \tag{1}$$

where vectors U, F, G and H are written as

$$U = \begin{bmatrix} \rho \\ \rho u \\ \rho v \\ \rho E \\ \rho f_j \end{bmatrix}$$

$$F = \begin{bmatrix} \rho u \\ \rho u^2 + p + \tau_{xx} \\ \rho uv + \tau_{xy} \\ (\rho E + p)u + \tau_{xx}u + \tau_{xy}v + q_{cx} + q_{Rx} \\ \rho u f_j - \rho D \frac{\partial f_i}{\partial x} \end{bmatrix}$$

$$G = \begin{bmatrix} \rho v \\ \rho uv + \tau_{yx} \\ \rho u^2 + p + \tau_{yy} \\ (\rho E + p)v + \tau_{yy}v + \tau_{xy}u + q_{cy} + q_{Ry} \\ \rho v f_j - \rho D \frac{\partial f_i}{\partial y} \end{bmatrix}$$

$$H = \begin{bmatrix} 0 \\ 0 \\ 0 \\ 0 \\ -\dot{w}_j \end{bmatrix}$$

The viscous stress terms appearing in the definitions of F and G are given in [27]. The relations for conduction heat transfer in x and y directions are given by

$$q_{Cx} = -k\frac{\partial T}{\partial x}, \quad q_{Cy} = -k\frac{\partial T}{\partial y} \tag{2}$$

The terms q_{Rx} and q_{Ry} represent radiative fluxes in x and y directions, respectively; expressions for these are provided in the next section. The total energy flux in a given direction is given by the corresponding last term in the definitions of F or G. Consequently, this formulation involves all kinds of energy interaction including frictional (aerodynamic) heating. The coefficient of viscosity is evaluated by using the Sutherland's formula and the coefficient of thermal conductivity is calculated by using a constant value of the Prandtl number. The total internal energy E appearing in U, F, and G is given by

$$E = P/\rho + \frac{u^2 + v^2}{2} + \sum_{i=1}^{m} h_i f_i \tag{3}$$

Equation (1) can be used to obtain solutions for all kinds of compressible flows. However, boundary conditions and numerical procedures for different flows are quite different. For supersonic flows the inflow conditions are specified and outflow conditions are obtained by extrapolation. The boundary conditions used along the surfaces are u=0, v=0, $\partial P/\partial y = 0$, and $T=T_w$.

The governing equations and boundary conditions for the supersonic flow through a channel with a compression-expansion ramp is essentially the same as for the parallel plate geometry. However, a strong shock is produced at the compression corner and the flow becomes highly reacting from the beginning of the x_2–coordinate. (Fig. 1c).

The basic governing equations for chemically reacting compressible flow through a circular tube can be written as [29,30]

$$\frac{\partial U}{\partial t} + \frac{\partial F}{\partial x} + \frac{1}{y}\frac{\partial}{\partial y}(yG) = H/y \tag{4}$$

where x and y represent the streamwise and radial coordinates, respectively. In Fig. 1b, the radial coordinate is denoted by r. Thus, both r and y notations are used to represent the radial coordinate for the circular geometry. The definitions of vectors U, F, and G in Eq. (4) are same as given in Eq. (1) and vector H is expressed as

$$H = [0 \quad 0 \quad p + \tau_{\theta\theta} \quad 0 \quad y \quad \dot{w}_j] \tag{5}$$

For the circular tube geometry, the viscous terms appearing in Eq. (1) are given by

$$\tau_{xx} = -\lambda \left(\frac{\partial u}{\partial x} + \frac{\partial u}{\partial y} + \frac{u}{y} \right) - 2\mu \frac{\partial u}{\partial x} \tag{6a}$$

$$\tau_{yy} = -\lambda \left(\frac{\partial u}{\partial x} + \frac{\partial u}{\partial y} + \frac{v}{y} \right) - 2\mu \frac{\partial v}{\partial y} \tag{6b}$$

$$\tau_{xy} = -\mu \left(\frac{\partial u}{\partial y} + \frac{\partial v}{\partial x} \right) \tag{6c}$$

$$\tau_{\theta\theta} = -\lambda \left(\frac{\partial u}{\partial x} + \frac{\partial u}{\partial y} + \frac{v}{y} \right) - 2\mu \frac{v}{y} \tag{6d}$$

The boundary conditions for the circular tube geometry are similar to the parallel plate geometry.

Radiative Transfer Models

Evaluation of the energy equation presented in Eqs. (1) and (4) requires an appropriate expression for the net radiative flux in each direction. A suitable radiative transport model is needed to represent the true nature of participating species and transfer processes. In this section, a brief discussion of various absorption models is given and essential equations for the radiative flux are presented.

Absorption Models

Several models are available in the literature to represent the absorption-emission character-istics of molecular species. The total band absorptance of a vibration-rotation band is given by

$$A = \int_{-\infty}^{\infty} [1 - \exp(-\kappa_\omega X)d(\omega - \omega_o)] \tag{7}$$

where κ_ω is the volumetric absorption coefficient, ω is the wave number, ω_o is the wave number at the band center, $X = Py$ is the pressure path length, and the limits of integration are over the entire band pass. Various models are used to obtain the relation for A in Eq. (7).

The gray gas model is probably the simplest model to employ in radiative transfer analyses. In this model, the absorption coefficients is assumed to be independent of frequency, i. e., κ_ω is not a function of ω. A convenient model to represent the average absorption coefficient of a gray gas is the Planck mean absorption coefficient κ_p which is defined as [1]

$$\kappa_p = \int_o^\infty k_\omega \, e_{b\omega}(T)d\omega / e_b(T) \tag{8a}$$

For a multiband gaseous system, this is expressed as

$$\kappa_p = [P_j/(\sigma T^4)] \sum_i^n e_{\omega_i}(T)S_i(T) \tag{8b}$$

where P_j is the partial pressure of jth species in a gaseous mixture, $e_{\omega i}(T)$ is the Planck function evaluated at the ith band center, and $S_i(T)$ is the integrated band intensity of the ith band.

As defined in Eq. (8), κ_p is a property of the medium. When κ_p is evaluated at the temperature of the gas, it is actually a mean emission coefficient and it becomes equal to the actual mean absorption coefficient only for the conditions of equilibrium radiation field. For a nonuniform temperature field, the mean absorption coefficient used for the optically thin radiation is the modified Planck mean absorption coefficient which for black bounding surfaces is defined as [1,9]

$$\kappa_m(T, T_w) = \left[\int_o^\infty \kappa_\omega(T)e_{b\omega}(T_w)d\omega\right] / e_b(T_w) \tag{9a}$$

Note that κ_m is a function of both the gas temperature and the wall temperature. An approximate relation between κ_p and κ_m is available for infrared radiation as [1]

$$\kappa_m(T, T_w) = \kappa_p(T_w)(T_w/T) \tag{9b}$$

This expression is usually employed in gray gas radiative energy transfer analyses.

Several other models for the mean absorption coefficient are available in the literature [1,31]. Since these models account for detailed spectral information of molecular bands, this approach of radiative formulation is referred to as the "pseudo-gray formulation." The gray gas formulation for radiative transport is very useful in parametric studies.

There are several nongray models available in the literature to represent the absorption-emission characteristics of vibration-rotation bands. These are classified generally in four classes, (1) line-by-line (LBL) models, (2) narrow band models, (3) wide band models, and (4) band model correlations. A complete discussion on usefulness and application of these models is provided in [12, 13]. For many engineering applications, wide band model correlations provide quite accurate results. The most commonly used wide band model correlations are due to Edwards [5, 11] and Tien and Lowder [9]. The Tien and Lowder correlation for the total band absorptance is a continuous correlation and is given by the relation

$$\bar{A}(u,\beta) = A(u,\beta)/A_o = \ln\{uf(t)[(u+2)/(u+2f(t))]+1\} \tag{10}$$

where

$$f(t) = 2.94[1 - \exp(-2.60t)], t = \beta/2$$

and $u = SX/A_o$ is the nondimensional path length, $\beta = 2\pi\gamma/d$ is the line structure parameter, γ is the line half width, S is the integrated band intensity, and A_o is the band width parameter. Equation (10) provides accurate results for pressures higher than 0.5 atmosphere [12, 13].

Spectral properties and correlation quantities for various radiation participating species are available in [5, 9, 11]. These are useful in gray as well as nongray radiative formulations.

Radiative Flux Equations

For many engineering and astrophysical applications, the radiative transfer equations are formulated assuming one-dimensional planar systems. For diffuse nonreflecting boundaries and in absence of scattering, the expression for the spectral radiative flux in the normal direction is given by [1, 19]

$$
\begin{aligned}
q_{R\omega}(y) = e_{1\omega} - e_{2\omega} \\
+ \frac{3}{2} \int_0^y F_{1\omega}(z)\kappa_\omega \exp\left[-\frac{3}{2}\kappa_\omega(z - y)\right] dz \\
- \frac{3}{2} \int_y^L F_{2\omega}(z)\kappa_\omega \exp\left[-\frac{3}{2}\kappa_\omega(z - y)\right] dz
\end{aligned}
\tag{11}
$$

where

$$
F_\omega(z) = e_\omega(z) - e_{1\omega}, \quad F_{2\omega}(z) = e_2(z) - e_{2\omega}
$$

It should be pointed out that the exponential kernel approximation has been used in obtaining Eq. (11). The total radiative flux in a given direction is expressed as

$$
q_R = \int_0^\infty q_{R\omega}\, d\omega
\tag{12}
$$

A combination of Eqs. (11) and (12) provides a proper form of total radiative flux equation for obtaining nongray solutions of molecular species. Any convenient absorption model can be used to obtain nongray results.

For a gray medium, Eq. (11) reduces to a simpler form and upon differentiating the resulting equation twice, the integrals are eliminated and there is obtained a nonhomogeneous ordinary differential equation as [1, 16, 27]

$$
\frac{1}{\kappa^2} \frac{d^2 q_R(y)}{dy^2} - \frac{9}{4} q_R(y) = \frac{3}{\kappa} \frac{de(y)}{dy}
\tag{13}
$$

where $\kappa = \kappa_p$. Equation (13) is a second order differential equation and, therefore, requires two boundary conditions. For nonblack diffuse surfaces, these are given as

$$
\left(\frac{1}{\epsilon_1} - \frac{1}{2}\right)[q_R(y)]_{y=0} - \frac{1}{3\kappa}\left[\frac{dq_R}{dy}\right]_{y=0} = 0
\tag{14a}
$$

$$\left(\frac{1}{\epsilon_2} - \frac{1}{2}\right)[q_R(y)]_{y=L} - \frac{1}{3\kappa}\left[\frac{d_{q_R}}{dy}\right]_{y=L} = 0 \tag{14b}$$

Equation (13) along with boundary conditions can be used to obtain the energy equation for gray gas radiative interaction. For black walls and $T_1 = T_2$, the boundary conditions for Eq. (13) become

$$q_R(1/2) = 0, \frac{3}{2}q_R(0) = \frac{1}{\tau_o}(dq_R/d\xi)_{\xi=0} \quad , \quad \tau_o = \kappa L, \xi = y/L \tag{15}$$

For a black circular tube, the spectral radiative heat flux in the radial direction is given by the expression [17]

$$
\begin{aligned}
q_{R_\omega}(r) = \frac{4}{\pi} \int_0^{\pi/2} \Bigg\{ & \int_{r\sin\gamma}^r F_{\omega(r')}\kappa_\omega a\exp\left[-\frac{b\kappa_\omega}{\cos\gamma}(r-r')\right] dr' \\
& - \int_r^{r_o} F_\omega(r')\,\kappa_\omega a\exp\left[-\frac{b\kappa_\omega}{\cos\gamma}(r'-r)\right] dr \\
& + \int_{r\sin\gamma}^{r_o} F_\omega(r')\,\kappa_\omega a\exp\left[-\frac{b\kappa_\omega}{\cos\gamma}(r+r'-2r\sin\gamma)dr'\right] \Bigg\} d\gamma
\end{aligned}
\tag{16}
$$

where $F_\omega(r')=e_\omega(r') - e_\omega(T_w)$ and constants a and b have values of unity and 5/4, respectively. A combination of Eqs. (12) and (16) provides a convenient form of the total radiative flux for nongray analyses.

For a gray medium, the expression for the total radiative flux can be obtained from differential approximation as [1, 17]

$$\frac{d}{dr}\left[\frac{1}{r}\frac{d}{dr}(rq_R)\right] - \frac{9}{4}\kappa^2 q_R = 3\sigma\kappa\frac{dT^4}{dr} \tag{17}$$

For a black tube, the boundary conditions for Eq. (16) are found to be

$$\frac{3}{2}q_R(1) = -\frac{1}{\tau_o}\left[\frac{1}{\xi}\frac{d}{d\xi}(\xi q_R)\right]_{\xi=1} \quad , \quad q_R(0) = 0 \quad , \quad \tau_o = \kappa r_o, \xi = r/r_o \tag{18}$$

Equation (17) is used along with Eq. (18) for general one-dimensional gray gas formulation and analyses.

With certain modifications, the radiative flux equations presented in this section can also be used to investigate the radiative interactions in the flow direction. The procedure for doing this is provided in [27].

Chemistry and Thermodynamic Models

Chemical reaction rate expressions are usually determined by summing the contributions from each relevant reaction route (or path) to obtain the total rate of change of each species. Each path is governed by a law of mass action expression in which the rate constants can be determined from a temperature dependent Arrehenius expression. The reaction mechanism is expressed in a general form as

$$\sum_{j=1}^{ns} \gamma'_{ij} C_j \underset{k_{bi}}{\overset{k_{fi}}{\rightleftharpoons}} \sum_{j=1}^{ns} \gamma''_{ij} C_j, \quad i = 1, \text{nr} \tag{19}$$

where ns= number of species and nr= number of reactions. The chemistry source terms in Eqs. (1) and (4) are obtained, on a mass basis, by multiplying the molar changes and corresponding molecular weight as

$$\dot{w}_j = M_j C_j = M_j \sum_{i=1}^{nr} (\gamma''_{ij} - \gamma'_{ij}) \left[k_{f_i} \prod_{m=1}^{ns} C_m^{\gamma'_{im}} - k_{bi} \prod_{m=1}^{ns} C_m^{\gamma''_{im}} \right] \tag{20}$$

The reaction constants k_{f_i} and k_{b_i} appearing in Eqs. (19) and (20) are determined from an Arrhenius rate equation given by

$$k_{f_i} = A_i \, T^{Ni} \exp\left(-\frac{E_i}{RT}\right) \tag{21}$$

where

$$k_{b_i} = k_{f_i}/k_{eqi} \quad, \quad k_{eqi} = \left(\frac{1}{RT}\right)^{\Delta N} \exp\left(\frac{-\Delta G_{Ri}}{RT}\right)$$

The coefficients A, N, and E appearing in Eq. (21) are given in Table 1 and the Gibbs energy term ΔG_{Ri} is calculated as

$$\Delta G_{R_i} = \sum_{j=1}^{ns} \gamma''_{ij} g_i - \sum_{j=1}^{ns} \gamma_{ij} g_i \, , \quad j = 1, \text{nr} \tag{22}$$

where

$$\frac{g_j}{R} = A_j(T - \ln T) + \frac{B_j}{2} T^2 + \frac{C_j}{6} T^3$$
$$+ \frac{D_j}{12} T^4 + \frac{E_j}{20} T^5 + F_j + G_j T$$

The gas constant for the mixture is evaluated by a mass-weighted summation over all species as

$$\bar{R} = \sum_{j=1} f_j R_j \tag{23}$$

The equation of state for the mixture is written as

$$P = \rho \bar{R} T \tag{24}$$

Method of Solution

The governing equations are transformed from the physical domain (x, y) to a computational domain (ξ, η) using an algebraic grid generation technique similar to the one used by Smith and Weigel [32]. The grid spacing is kept uniform in the flow direction and compressed near the boundaries in the normal direction. The governing equations, Eqs. (1) and (4), are expressed respectively in the computational domain as

$$\frac{\partial \hat{U}}{\partial t} + \frac{\partial \hat{F}}{\partial \xi} + \frac{\partial \hat{G}}{\partial \eta} + \hat{H} = 0 \tag{25}$$

$$\frac{\partial \hat{U}}{\partial t} + \frac{\partial \hat{F}}{\partial \xi} + \frac{1}{\eta} \frac{\partial}{\partial \eta} \left(\eta \hat{G} \right) = \hat{H}/\eta \tag{26}$$

where

$$\hat{U} = UJ, \quad \hat{F} = Fy_\eta - G\, x_\eta, \quad \hat{G} = Gx_\xi - Fy_\xi,$$

$$\hat{H} = HJ, \quad J = x_\xi\, y_\eta - y_\xi\, x_\eta$$

The temporal descretization procedure for Eqs. (25) and (26) in given in [25-27]. Once this has been performed, the resulting system is spatially differenced using the explicit unsplit MacCormack predictor-corrector scheme [33]. This results in a spatially and temporally discrete, simultaneous system of equations at each grid point [34,35]. Each simultaneous system is solved using the Householder technique [36,37], and is marched in time until convergence is achieved.

The details of gray as well as nongray radiative flux formulations and solution procedure are available in [19,27]. For the gray gas model, the governing equations are discretized using a central difference scheme. The descretization of Eqs. (13) and (17) results, respectively, in

$$\left(\frac{2}{A_j}\right)q_{j-1} - \left[\frac{2}{B_j}\left(\frac{1}{C_j} + \frac{1}{\Delta y_j}\right) + \frac{9}{4}\kappa_j^2\right]q_j + \left(\frac{2}{A_j\beta_j}\right)q_{j+1} = \text{RHS} \tag{28}$$

$$\left(\frac{2}{A_j} + \frac{1}{2y_jC_j}\right)q_{j+1} - \left[\frac{2}{B_j}\left(\frac{1}{C_j} + \frac{1}{\Delta y_j}\right) + \frac{9}{4}\kappa_j^2\right]$$

$$+ \frac{1}{y^2} + \frac{1}{2y_jC_j} - \frac{1}{2y_j\Delta y_j}\right]q_j + \left(\frac{2}{A_j\beta_j} - \frac{2}{2y_j\Delta y_j}\right)q_{j-1} = \text{RHS} \tag{29}$$

where

$$A_j = \Delta y_j^2(1 + \beta_j), \quad \boldsymbol{\beta}_j = \Delta y_j(1 + \beta_j), \quad C_j = \beta_j\Delta y_j,$$

$$\text{RHS} = 1.5\kappa_j\left[\frac{e_{j+1} - e_j}{\beta_j\Delta y_j} + \frac{e_j - e_{j-1}}{\Delta y_j}\right], \quad \Delta y_j = y_j - y_{j-1}, \quad \beta_j = \frac{y_{j+1} - y_j}{y_j - y_{j-1}}$$

Equations (27) and (28) along with boundary conditions given by Eqs. (15) and (18) form tridiagonal systems of equations which can be solved efficiently by the Thomas algorithm.

In the nongray gas formulation, the divergence of the radiative flux is evaluated using a central differencing scheme and is treated as radiative source term in the energy equation. Since the radiative flux terms involves integral formulation, unlike other flux terms which are only in a differential form, it is uncoupled and treated separately.

Physical Conditions and Data Source

The physical conditions for which specific flowfield analyses and computations are needed are discussed in [21–28]. In this work selected parametric studies have been conducted for certain flow and physical conditions. Radiation participating species considered are H_2O, OH, and NO. Radiative properties of these species are available in [5, 9, 11-13]. Different amounts of these gases, in combination with air, are considered for parametric studies. Essential data for the chemistry model employed are obtained from Refs. 38–40 and these are provided in Table 1.

For basic studies, the physical dimensions considered for the channel are L=3 cm and L_x=10 cm, and for the circular tube they are L=D=3 cm and L_x= 10 cm. Certain results, however, were obtained also for other dimensions.

Results and Discussion

Based on the theory and computational procedure described in the previous sections, an existing computer code was modified to solve the two-dimensional Navier-Stokes equations for radiating supersonic laminar flows between two parallel black plates. A similar code was developed for radiating supersonic flows in a circular tube. In most cases, the radiative interaction was considered only in the normal direction. Extensive results have been obtained for pure H_2O, OH, and NO as homogeneous participating species, and for different mixtures of these species with air. Selected results are presented and discussed in this section.

For the parallel plate geometry (3 cm x 10 cm), a comparison of the divergence of radiative flux for general (nongray), gray, and their optically thin limit models is presented in Fig. 2 for two different y-locations (y=0.2 and 1.5 cm). The inflow conditions for this case are P_∞ = 1 atm, T_∞ = 1,700 K, M_∞ = 4.3, f_{H_2O} = 0.5, f_{O_2} = 0.1, and f_{N_2} = 0.4. The gray formulation is based on the modified Planck mean absorption coefficient which accounts for the detailed information on different molecular bands. The range of optical thickness calculated in [27] was found to be between 0.0003 and 0.4. Thus, for the physical model and inflow conditions considered, the radiative interaction is essentially in the optically thin range. No significant difference in results is observed for the two y-locations. This is a typical characteristic of the optically thin radiation [1,10]. The solution of the gray formulation requires about ten times less computational resources in comparison to the solution of the nongray formulation [27].

As mentioned earlier, the Planck mean absorption coefficient κ_p (or κ_m) is considered to be an optically thin radiation absorption coefficient, although it has been used in other optical ranges as well [1,9]. The appropriate absorption coefficient for the optically thick radiation is the Rosseland mean absorption coefficient κ_R. It has been pointed out in [1] that if the medium is

gray then $\kappa_R = \kappa_P = \kappa$; otherwise $\kappa_p > \kappa_R$. Thus, use of κ_p (or κ_m) in pseudo-gray gas formulation will provide maximum influence of radiative interaction. The κ_p values for H_2O, OH, and NO have been calculated from Eq. (8b) by employing radiative properties available in [5, 9, 11] and these are illustrated in Fig. (3). Figure 3a shows the results of 100% homogeneous species whereas results in Fig. 3b are for different mixtures. The results provide indication of radiative ability of different species at a given temperature. Values of κ_p for other species are available in [1, 9].

The results of supersonic entrance region flow between parallel plates are presented in Figs. 4–10 for different physical and inflow conditions. As mentioned earlier, the basic physical dimensions considered for the channel are L=3 cm and L_x=10 cm. In most cases, the inflow conditions considered are P_∞=1 atm, T_∞=1,700 K, U_∞=2574 m/s (M_∞=3.0) with varying amounts of radiation participating species in combination with air. Certain variations in physical and inflow conditions are also considered for parametric studies. The chemical reactions are not considered in obtaining the results of Figs. 4-10, and radiative flux results are presented only for the normal direction.

Results for radiative flux are illustrated in Figs. 4 and 5 as a function of the nondimensional y-coordinate. For P=1 atm, the results presented in Fig. 4 for different water vapor concentrations indicate that the radiative interaction increases slowly with an increase in the amount of the gas. The results for 50% H_2O are presented in Fig. 5 for two different pressures (P_∞=1 and 3 atm) and x-locations (x=5 and 10 cm). It is noted that the increase in pressure has dramatic effects on the radiative interaction.

For a mixture of 50% H_2O in air, the conduction and radiation heat transfer results are compared in Fig. 6 for P_∞=3 atm and for two different x-locations (x=5 and 10 cm). The results demonstrate that the conduction heat transfer is restricted to the region near the boundaries and does not change significantly from one x-location to another. The radiative interaction, however, is seen to be important everywhere in the channel, and this can have a significant influence on the entire flowfield.

Comparative results for 100% homogeneous species of H_2O, NO and OH are illustrated in Fig. 7 at the exit plane (x=10 cm). As would be expected, the radiative contribution of H_2O (with five bands) is significantly higher than NO and OH. Only the fundamental bands of NO and OH are considered in this study, and it is noted that NO is a better radiating gas in comparison to OH.

For a mixture of 25% H_2O in air, radiative flux for two different plate spacings (L=3 and 6 cm) are illustrated in Fig. 8 for two x-locations (x=5 and 10 cm). The rate of radiative transfer is a strong function of the amount of the participating species and the pressure path length, PL. consequently, the results for the larger plate spacing indicate significantly higher radiative interactions.

The effect of increased Mach number on the radiative transfer is illustrated in Fig. 9 for pure H_2O and for a mixture of 50% H_2O in air. The results shown are for the exit plane (x=10 cm). At higher Mach number, the boundary layer is relatively thinner and the temperature in the boundary layer is significantly higher. This, in turn, results in higher rate of radiative transfer.

For a mixture of 50% H_2O in air, comparative results for the parallel plate channel and the circular tube are presented in Fig. 10 for two x-locations (x=5 and 10 cm). The results for the circular tube in general, exhibit the same trend as for the parallel plate geometry. Since the circular geometry provides additional degrees of freedom for radiative interactions [17], the rate of radiative transfer is higher for the tube.

The influence of radiative interactions in chemically reacting supersonic internal flows was investigated by considering the physical model shown in Fig. 1c. The specific problem considered is the supersonic flow of premixed hydrogen and air in a channel with a compression corner on the lower boundary. The physical dimensions considered for obtaining results are L=2 cm, x_1= 1 cm, x_2=2 cm, $L_x=x_1+x_2$=3 cm, and α=10°. The inlet conditions, which are representative of the scramjet operating condition, are P=1 atm, T=900 K and M=4.0. The flow is ignited by the shock from the compression corner. The flowfield for this problem has been investigated by several researchers [21–28] where different chemistry models have been

used. Influence of radiative interactions was investigated in [25-27] by considering a simple two-step chemistry model. Recently [28], a comparative study of the flowfield was conducted by employing three chemistry models (see Table 1). It was found that significant amount of radiation participating species are produced by the 35-step chemistry model. The results presented in Figs. 3–10 provided essential information on radiative behavior of these species. Complete discussions on use of the three chemistry models with and without radiation are provided in [28]. Selected results are presented here to demonstrate the influence of radiative interactions.

The computed results for the 35–step chemistry model are presented in Figs. 11–14 with and without radiative interactions. The results were obtained by using a 31x31 grid; this was found to be an appropriate grid for the model. The variations in temperature, pressure, and species concentrations along the x-coordinate are shown for a y-location of 0.02 cm from the lower wall. The shock occurs at about $x/L_x=1/3$, and it is noted that the 35-step chemistry model predicts the ignition time accurately. The temperature is seen to increase uniformly along the channel (Fig. 11) and there is a significant increase in pressure after the shock (Fig. 12). Results of Figs. 13 and 14 show that significant amounts of radiation participating species H_2O and OH are produced after the shock. The effect of radiative interaction is to lower the amount of species production due to radiative transfer in the x-direction.

The results of radiative transfer by the three chemistry models are compared in Figs. 15 and 16 at y=0.02 cm. The results for the normal radiative flux presented in Fig. 15 demonstrate that radiative interactions increase rapidly after the shock. The three models are seen to predict the same general trend. The results of streamwise radiative flux illustrated in Fig. 16 show that the net q_{Rx} decreases towards the end of the channel. This is due to cancellation of fluxes in the positive and negative x-directions. It is noted that the net radiative transfer is in the negative x-direction. The 18-step and 35-step models are seen to predict significantly higher q_{Rx} than the 2–step model. This is because radiative heat transfer is a strong function of temperature, pressure and species concentration which are higher (in the positive x-direction) for the 18–step and 35–step models than the 2-step model.

Conclusions

Two-dimensional compressible Navier-Stokes equations have been used to investigate the influence of radiative energy transfer on the entrance region flow under supersonic flow conditions. Computational procedures have been developed to incorporate gray as well as nongray formulations for radiative flux in the general governing equations. Specific results have been obtained for different amounts of H_2O, OH and NO in combination with air. Results demonstrate that the radiative interaction increases with an increase in pressure, temperature and the amount of participating species. This can have a significant influence on the overall energy transfer in the system. Most energy, however, is transferred by convection in the flow direction. The radiative interactions in reacting flows have been investigated by considering the supersonic flow of premixed hydrogen and air in a channel with a compression corner at the lower boundary. Depending upon the chemistry model employed, the radiative interaction is seen to change significantly the temperature, pressure and species concentration in the flow direction.

Acknowledgments

References

1. Sparrow, E. M. and Cess, R. D., Radiation Heat Transfer, Brooks/Cole, Belmont, Calif., 1966 and 1970. New Augmented Edition, Hemisphere Publishing Corp., Washington, D.C., 1978.

2. Hottel, H. C. and Sarofim, A. F., Radiative Transfer, McGraw-Hill Book Co., New York, 1967.

3. Siegel, R. and Howell, J. R., Thermal Radiation Heat Transfer, McGraw-Hill Book Co., New York, 1971; Second Edition, 1981.

4. Ozisik, M. N., Radiative Transfer and Interaction with Conduction and Convection, John Wiley & Sons, Inc., New York, 1973.

5. Edwards, D. K., Radiation Heat Transfer Notes, Hemisphere Publishing Corporation, Washington, D.C., 1981.

6. Cess, R., "The Interation of Thermal Radiation with Conduction and Convection Heat Transfer," Advances in Heat Transfer, Vol. 1, Academic Press, New York, 1964.

7. Sparrow, M., "Radiation Heat Transfer between Surfaces," Advances in Heat Transfer, Vol. 2, Academic Press, New York, 1965.

8. Viskanta, R., "Radiation Transfer and Interaction of Convection with Radiation Heat Transfer," Advances in Heat Transfer, Vol. 3, Academic Press, New York, 1966.

9. Tien, C. L., "Thermal Radiation Properties of Gases," Advances in Heat Transfer, Vol. 5, Academic Press, New York, 1968.

10. Cess, R. and Tiwari, S. N., "Infrared Radiative Energy Transfer in Gases," Advances in Heat Transfer, Vol. 8, Academic Press, New York, 1972.

11. Edwards, D. K., "Molecular Gas Band Radiation," Advances in Heat Transfer, Vol. 12, Academic Press, New York, 1976.

12. Tiwari, S. N., "Band Models and Correlations for Infrared Radiation," Radiative Transfer and Thermal Control (Progress in Astronautics and Aeronautics), Vol. 49, American Institute of Aeronautics and Astronautics, New York, 1976.

13. Tiwari, S. N., "Models for Infrared Atmospheric Radiation," Advances in Geophysics, Vol. 20, Academic Press, New York, 1978.

14. Viskanta, R., "Radiation Heat Transfer," Fortschrift der Verfahrenstechnik, Vol. 22A, 1984, pp. 51–81.

15. Viskanta, R. and Menguc, M. P., "Radiation Heat Transfer in Combustion Systems," Progress in Energy Combustion Sciences, Vol. 13, 1987, pp. 97–160.

16. Cess, R. D. and Tiwari, S. N., "Heat Transfer to Laminar Flow of an Absorbing-Emitting Gas Between Parallel Plates," Heat and Mass Transfer-USSR, Vol. 1, May 1968, pp. 229-283.

17. Tiwari, S. N. and Cess, R. D., "Heat Transfer to Laminar Flow of Nongray Gases Through a Circular Tube," Applied Scientific Research, Vol. 25, No. 314, December 1971, pp. 155–170.

18. Tiwari, S. N., "Applications of Infrared Band Model Correlations to Nongray Radiation," International Journal of Heat and Mass Transfer, Vol. 20, No. 7, July 1977, pp. 741–751.

19. Tiwari, S. N., "Radiative Interaction in Transient Energy Transfer in Gaseous System," NASA CR-176644, December 1985.

20. Tiwari, S. N. and Singh, D. J., Interaction of Transient Radiation in Fully Developed Laminar Flow," AIAA Paper 86–1521, June 1987.

21. Kumar, A., "Numerical Simulation of Scramjet Inlet Flow Field," NASA TP-25117, May 1986.

22. Drummond, J. P., Hussaini, M. Y. and Zang, T. A., "Spectral Methods for Modelling Supersonic Chemically Reacting Flowfields," AIAA Journal, Vol. 24, No. 9, September 1986, pp. 1461–1467; also Drummond, J. P., "Numerical Simulation of a Supersonic Chemically Reacting Mixing Layers," Ph.D. Dissertation, George Washington University, May 1987.

23. Drummond, J. P., Rogers, R. C., and Hussaini, M. Y., "A Detailed Numerical Model of a Supersonic Reacting Mixing Layer," AIAA Paper No. 86-1427, June 1986.

24. Chitsomboon, T., Kumar, A., Drummond, J. P., and Tiwari, S. N., "Numerical Study of Supersonic Combustion Using a Finite-Rate Chemistry Model," AIAA Paper 86–0309, January 1986.

25. Mani, M., Tiwari, S. N., and Drummond, J. P., "Numerical Solution of Chemically Reacting and Radiating Flows," AIAA Paper 87–0324, January 1987.

26. Mani, M., Tiwari, S. N., and Drummond, J. P., "Investigation of Two-Dimensional Chemically Reacting and Radiative Supersonic Channel Flows," AIAA Paper 88–0462, January 1988.

27. Mani, M. And Tiwari, S. N., "Investigation of Supersonic Chemically Reacting and Radiating Channel Flow," NASA CR-182726, January 1988; also Ph.D. Dissertation by M. Mani, Old Dominion University, May 1988.

28. Chandrasekhar, R., Tiwari, S. N., and Drummond, J. P., "Radiative Interactions in a Hydrogen-Fueled Supersonic Combustor," AIAA Paper 91–0373, January 1991.

29. Anderson, D. A., Tannehil, J. C., and Pletcher, R. H., Computational Fluid Mechanics and Heat Transfer, Hemisphere Publishing Corporation, 1984.

30. Frankel, S. H., Drummond, J. P., and Hassan, H. A., "A Hybrid Reynolds Averaged/PDF Closure Model for Supersonic Turbulent Combustion," AIAA Paper 90–1573, 1990.

31. Patch, R., "Effective Absorption coefficient for Radiant Energy Transport in Nongray Nonscattering Gases," Journal of Quantitative Spectroscopy and Radiative Transfer, Vol. 7, No. 4, July/August 1967, pp. 611–637.

32. Smith, R. E. and Weigel, B. L., "Analytical and Approximation Boundary Fitted Coordinates System for Fluid Flow Simulation," AIAA Paper 80–0192, January 1980.

33. MacCormack, R. W., "The Effect of Viscosity in Hypervelocity Impact Cratering," AIAA Paper 69–354, May 1969.

34. Stalnaker, J. F., Robinson M. A., Spradley, L. W., Kurzius, S. C., and Theores, D., "Development of the General Interpolants Methods for the CYBER 200 Series of Computers," Report TR-0867354, Lockheed-Huntsville Research Engg. Center, Huntsville, Alabama, October 1983.

35. Bussing, T. R., and Murman, E. M., "A Finite Volume Method for the Calculation of Compressible Chemically Reacting Flows," AIAA Paper 85–0331, January 1985.

36. Wilkins, J. H., The Algebraic Eigenvalue Problem, Oxford University Press, Oxford, England, 1965, pp. 233–236.

37. Householder, A. S., The Theory of Matrices in Numerical Solution Analysis, Dover Publication, New York, 1964, pp. 122–140.

38. Rogers, R. C. and Schnexnayder, C. J., Jr. "Chemical Kinetic Analysis of Hydrogen-Air Ignition and Reaction Time," NASA TP-1856, 1981.

39. Rogers, R. C. and Chinitz, W., "Using a Global Hydrogen-Air Model in Turbulent Reacting Flow Calculations," AIAA Journal, Vol. 21, No. 4, April 1983.

40. Carpenter, M. H., "A Generalized Chemistry Version of SPARK," NASA CR-4196, December 1988.

Table 1. Hydrogen-Air Combustion Mechanism [40]

| REACTION	A(moles)	N(cm^3)	E(calories/gm-mole)
** following reactions constitute the 18-step model **			
(1) $O_2 + H_2 \leftrightarrow OH + OH$	1.70×10^{13}	0	48150
(2) $O_2 + H \leftrightarrow OH + O$	1.42×10^{14}	0	16400
(3) $H_2 + OH \leftrightarrow H_2O + H$	3.16×10^{7}	1.8	3030
(4) $H_2 + O \leftrightarrow OH + H$	2.07×10^{14}	0	13750
(5) $OH + OH \leftrightarrow H_2O + O$	5.50×10^{13}	0	7000
(6) $H + OH + M \leftrightarrow H_2O + M$	2.21×10^{22}	—2.0	0
(7) $H + H + M \leftrightarrow H_2 + M$	6.53×10^{17}	—1.0	0
(8) $H + O_2 + M \leftrightarrow HO_2 + M$	3.20×10^{18}	-1.0	0
(9) $OH + HO_2 \leftrightarrow O_2 + H_2O$	5.00×10^{13}	0	1000
(10) $H + HO_2 \leftrightarrow H_2 + O_2$	2.53×10^{13}	0	700
(11) $H + HO_2 \leftrightarrow OH + OH$	1.99×10^{14}	0	1800
(12) $O + HO_2 \leftrightarrow O_2 + OH$	5.00×10^{13}	0	1000
(13) $HO_2 + HO_2 \leftrightarrow O_2 + H_2O_2$	1.99×10^{12}	0	0
(14) $H_2 + HO_2 \leftrightarrow H + H_2O_2$	3.01×10^{11}	0	18700
(15) $OH + H_2O_2 \leftrightarrow H_2O + HO_2$	1.02×10^{13}	0	1900
(16) $H + H_2O_2 \leftrightarrow H_2O + OH$	5.00×10^{14}	0	10000
(17) $O + H_2O_2 \leftrightarrow OH + HO_2$	1.99×10^{13}	0	5900
(18) $H_2O_2 + M \leftrightarrow OH + OH + M$	1.21×10^{17}	0	45500
** remaining reactions complete the 35-step model **			
(19) $O_2 + M \leftrightarrow O + O + M$	2.75×10^{19}	—1.0	118700
(20) $N_2 + M \leftrightarrow N + N + M$	3.70×10^{21}	—1.6	225000
(21) $N + O_2 \leftrightarrow O + NO$	6.40×10^{9}	1.0	6300
(22) $N + NO \leftrightarrow O + N_2$	1.60×10^{13}	0	0
(23) $N + OH \leftrightarrow H + NO$	6.30×10^{11}	0.5	0
(24) $H + NO + M \leftrightarrow HNO + M$	5.40×10^{15}	0	—600
(25) $H + HNO \leftrightarrow H_2 + NO$	4.80×10^{12}	0	0
(26) $O + HNO \leftrightarrow OH + NO$	5.00×10^{11}	0.5	0
(27) $OH + HNO \leftrightarrow H_2O + NO$	3.60×10^{13}	0	0
(28) $HO_2 + HNO \leftrightarrow H_2O_2 + NO$	2.00×10^{12}	0	0
(29) $HO_2 + NO \leftrightarrow OH + NO_2$	3.43×10^{12}	0	—260
(30) $H + NO_2 \leftrightarrow OH + NO$	3.50×10^{14}	0	1500
(31) $O + NO_2 \leftrightarrow O_2 + NO$	1.00×10^{13}	0	600
(32) $NO_2 + M \leftrightarrow O + NO + M$	1.16×10^{16}	0	66000
(33) $M + OH + NO \leftrightarrow HNO_2 + M$	5.60×10^{15}	0	—1700
(34) $M + OH + NO_2 \leftrightarrow HNO_3 + M$	3.00×10^{15}	0	—3800
(35) $OH + HNO_2 \leftrightarrow H_2O + NO_2$	1.60×10^{12}	0	0
** following reactions constitute the global 2-step model [24, 27, 39] **			
(1″) $H_2 + O_2 \leftrightarrow 2 OH$	11.4×10^{47}	—10.0	4865
(2″) $2 OH + H_2 \leftrightarrow 2 H_2O$	2.50×10^{44}	—13.0	42500
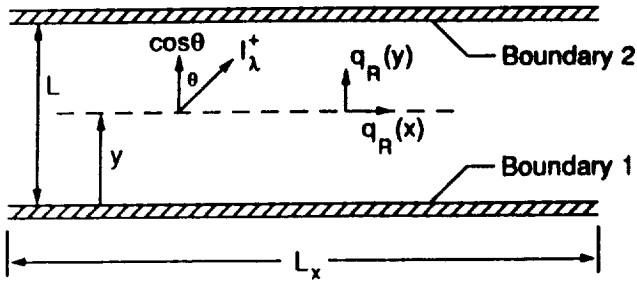
Fig. 1a   Radiating gas flow between parallel boundaries.
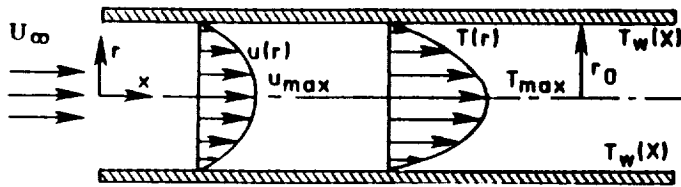

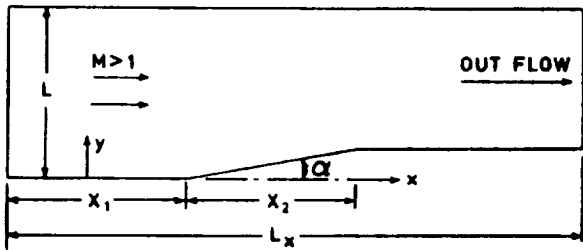Fig. 1b   Radiating gas flow within a circular tube.

Fig. 1c   Radiating gas flow in a channel with a compression-
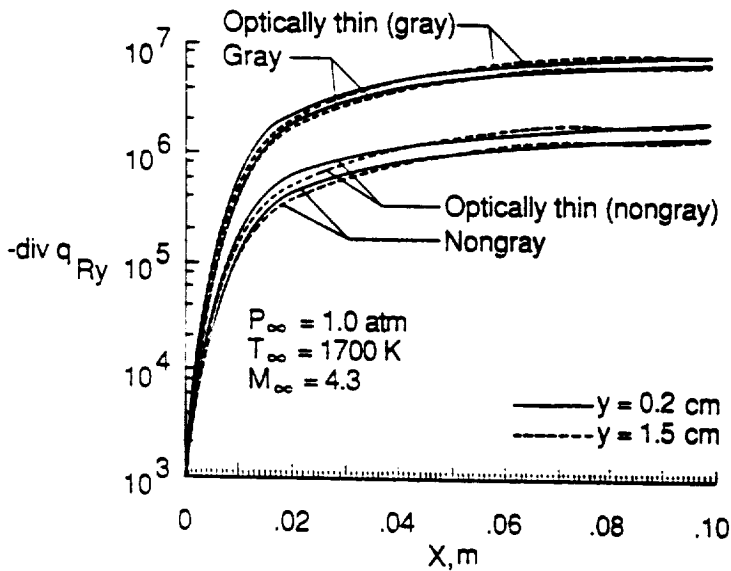expansion ramp.

Fig. 2   Divergence of radive flux along the channel for gray
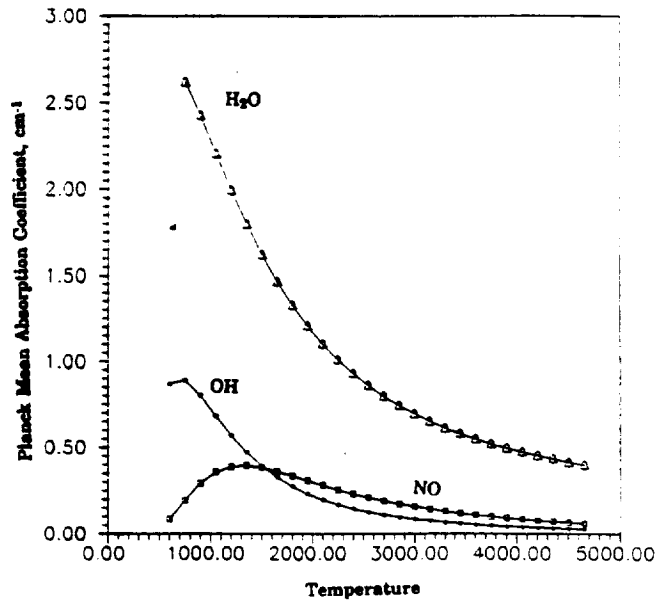and nongray models, M_∞ = 4.3.

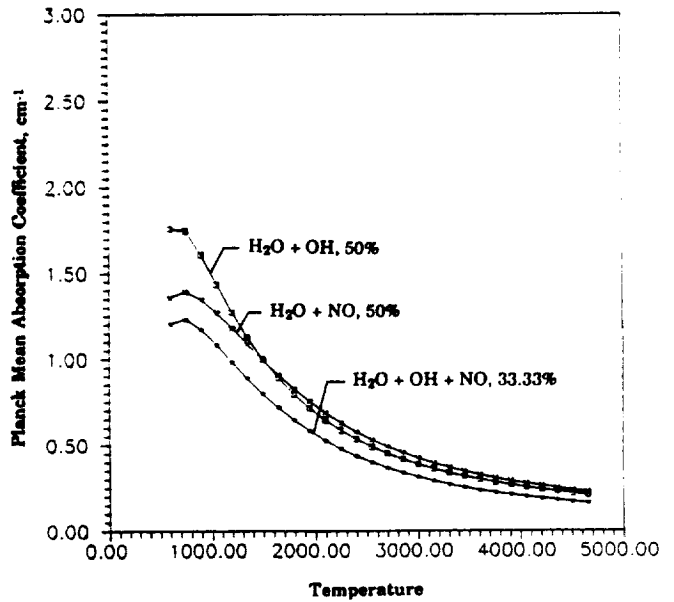Fig. 3a   Variation of the Planck-mean absorption coefficient
for H_2O, NO, and OH.

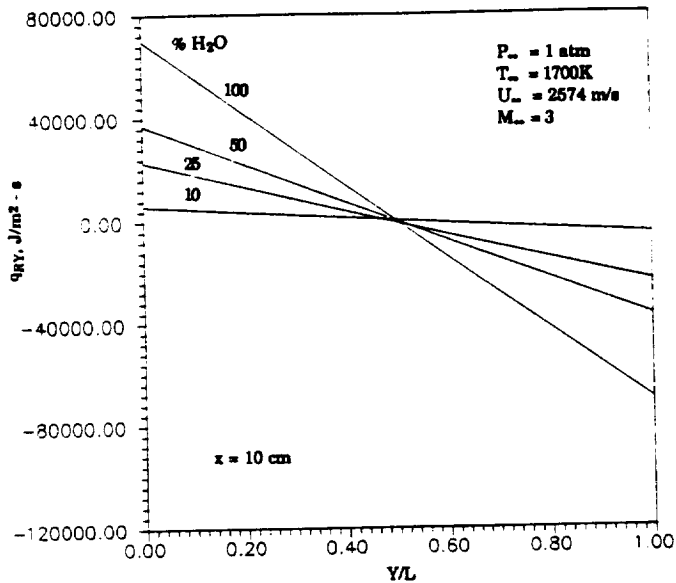Fig. 3b   Variation of the Planck-mean absorption coefficient for
different mixtures of H_2O, NO, and OH.

Fig. 4   Radiative flux vs. y at the channel exit, $M_\infty = 3.0$.
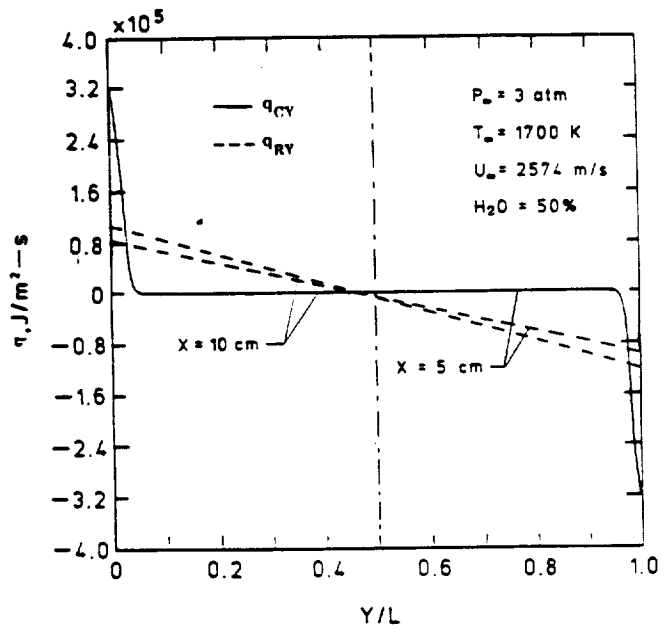
Fig. 6   Radiative and conductive fluxes vs. y for P = 3 atm, x = 5 and 10 cm, 50% H_2O, $M_\infty = 3.0$.
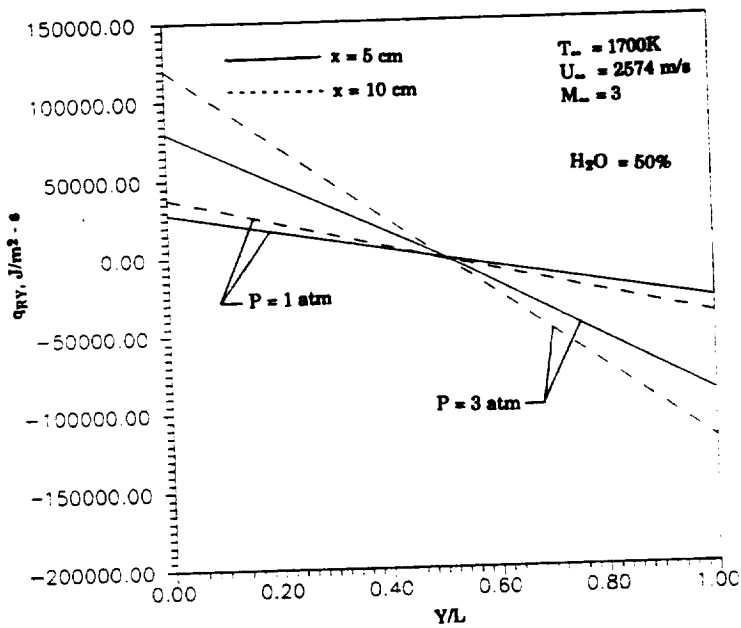
Fig. 5   Radiative flux vs. y for P = 1 and 3 atm, x = 5 and 10 cm, 50% H_2O, $M_\infty = 3.0$.
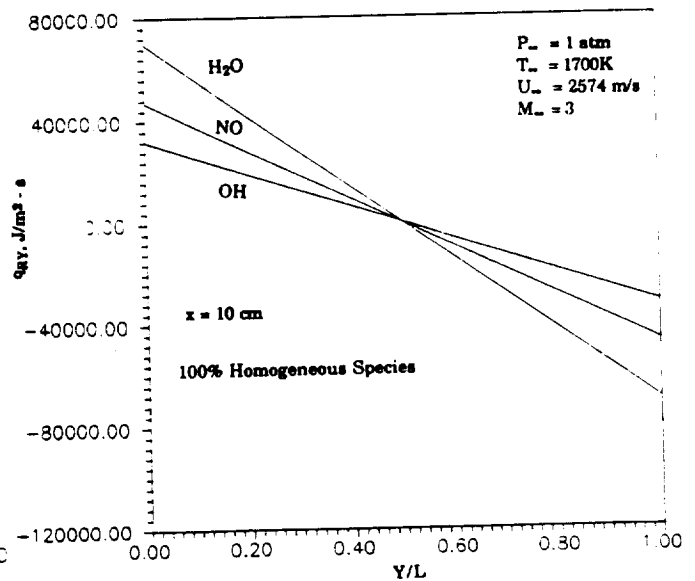
Fig. 7   Radiative flux vs. y for H_2O, NO, and HO. P = 1 atm, $M_\infty = 3.0$.

23
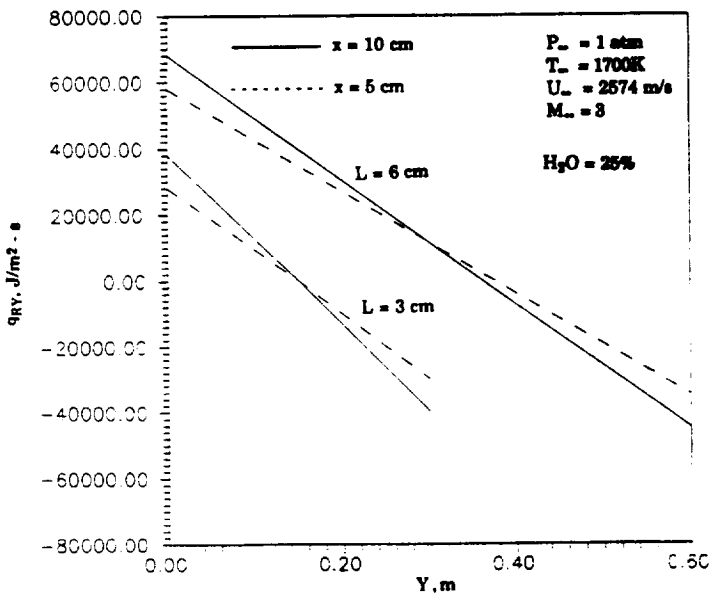
Fig. 8   Radiative flux vs. y for two different plate spacings (L = 3 and 6 cm) at x = 5 and 10 cm, M∞ = 3.0.
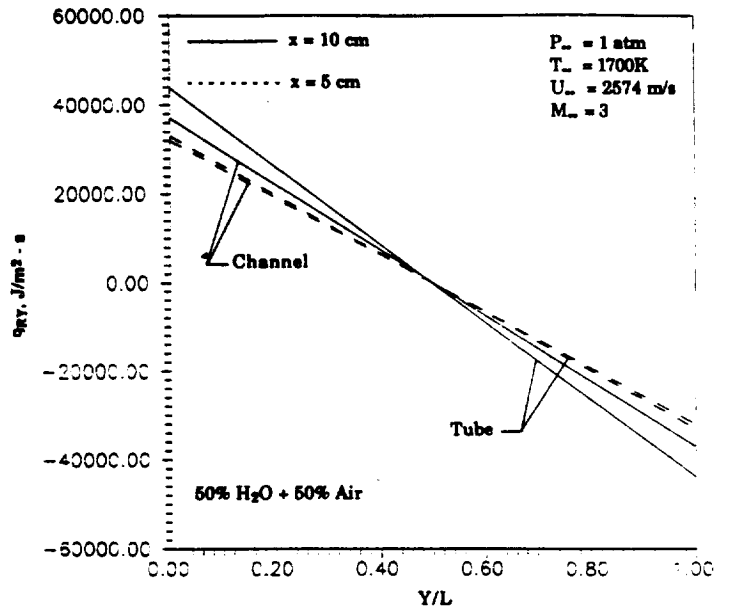
Fig. 10   Radiative flux vs. y for channel and tube (L = D = 3 cm) at x = 5 and 10 cm, 50% H₂O, M∞ = 3.0.
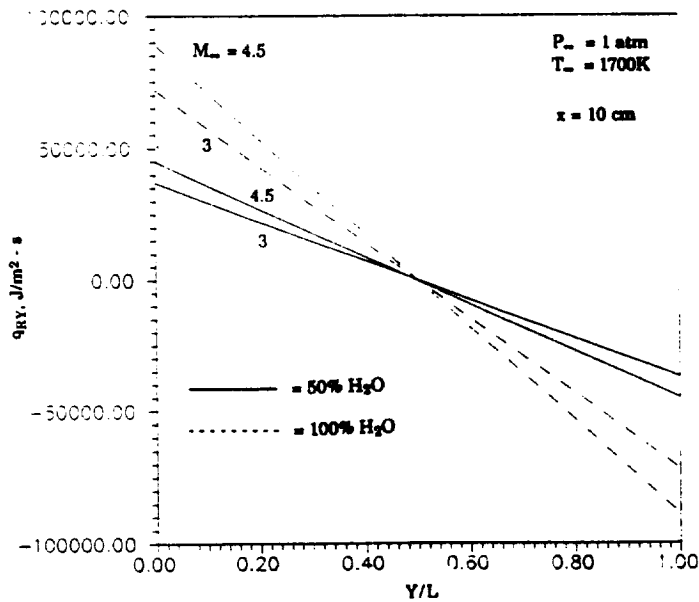
Fig. 9   Radiative flux vs. y for 50% and 100% H₂O, x = 10 cm, M∞ = 3.0 and 4.5.
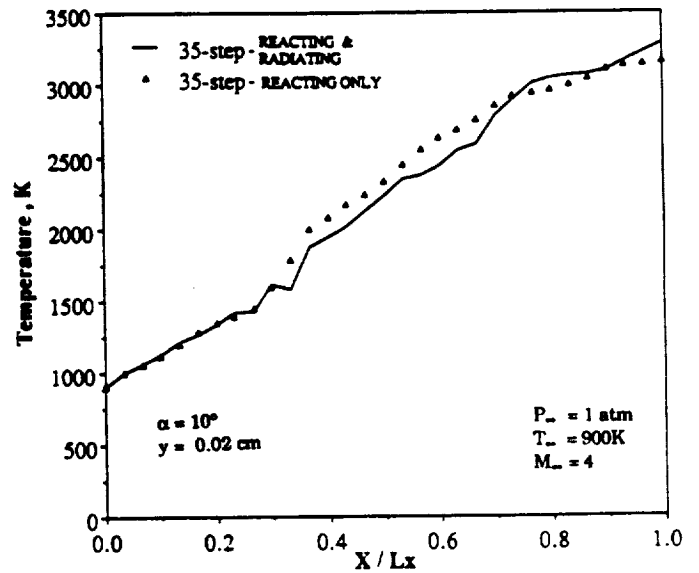
Fig. 11   Temperature variation with x for reacting, and reacting and radiating flows.
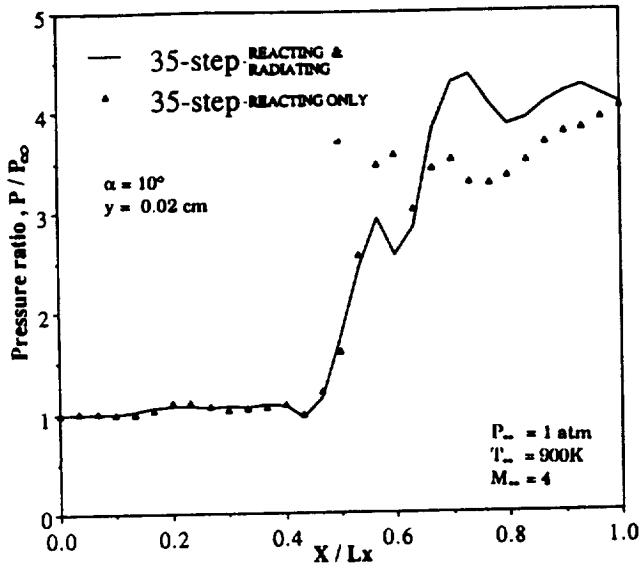
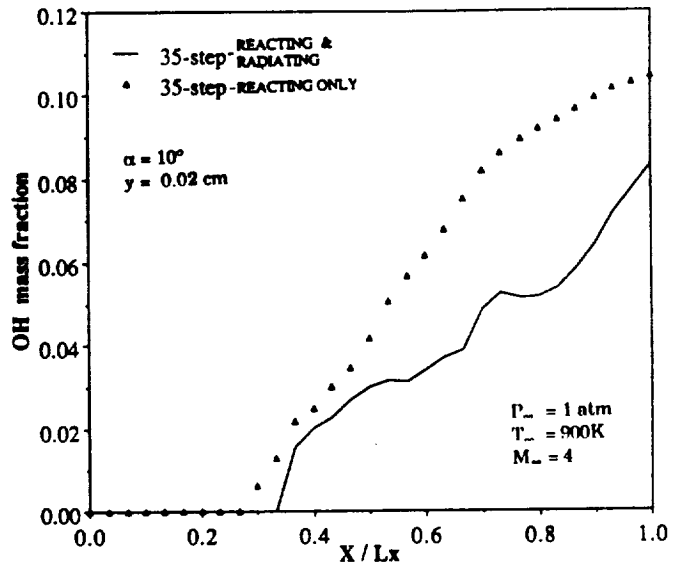Fig. 12   Pressure variation with x for reacting, and reacting and radiating flows.

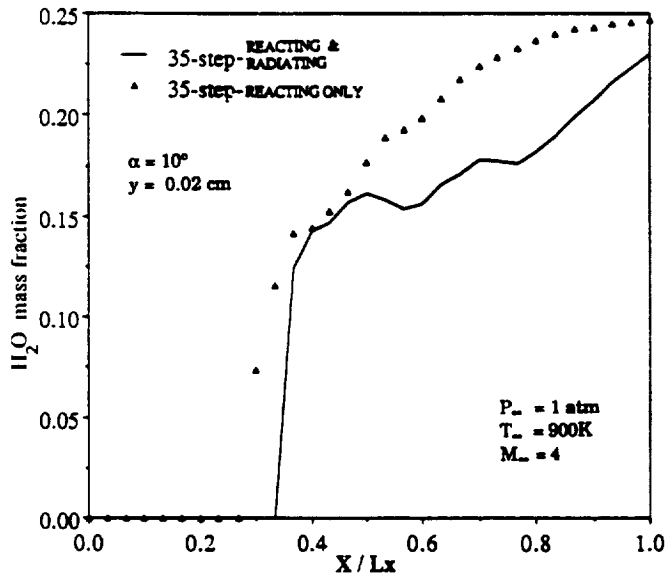Fig. 14   Variation of OH mass fraction with x for reacting, and reacting and radiating flows.

Fig. 13   Variation of H_2O mass fraction with x for reacting, and reacting and radiating flows.
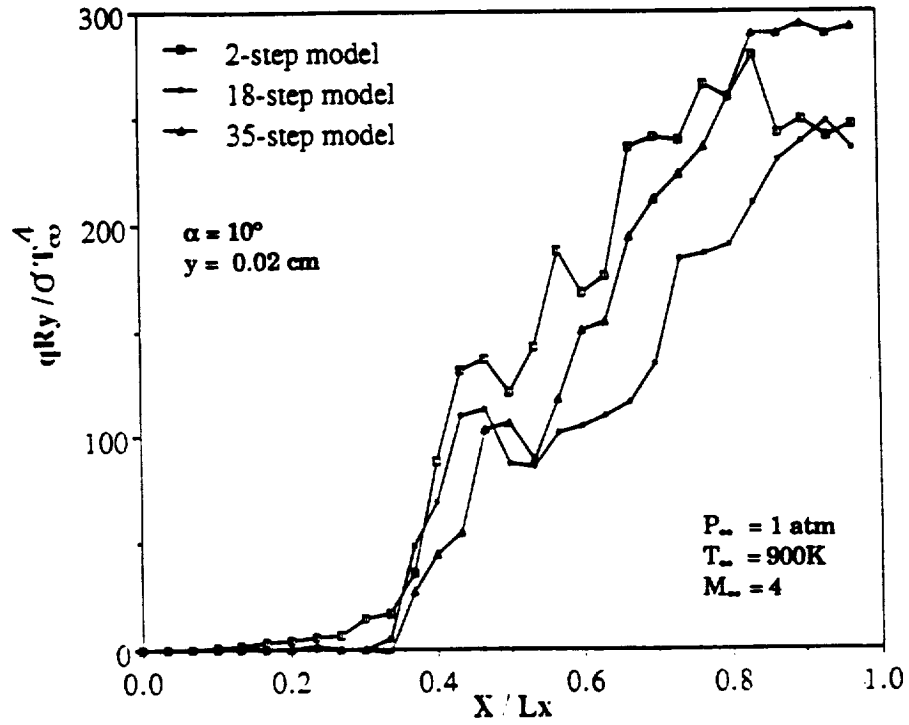
25

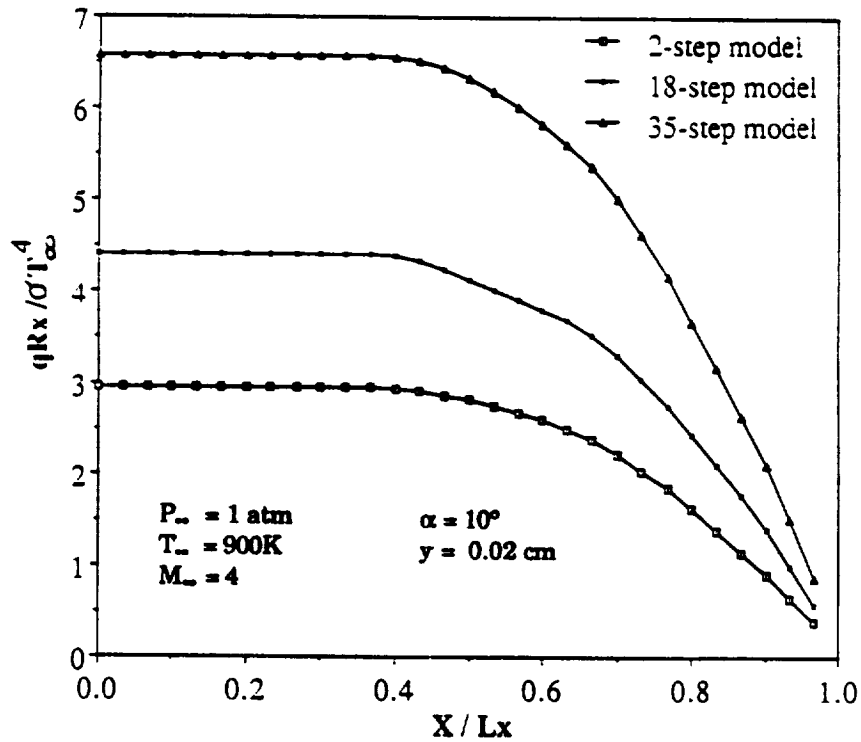**Fig. 15** Variation of normal radiative flux with x for three chemistry models.

Fig. 16 Variation of streamwise radiative flux with x for three chemistry models.